Studies of Silica-Hybrid Nanoparticles with targeting and photodynamic capabilities for the topical therapy of melanoma

THAM HUIJUN PHOEBE

Interdisciplinary Graduate School

NTU Institute for Health Technologies

(HealthTech NTU)

2018

Studies of Silica-Hybrid Nanoparticles with targeting and photodynamic capabilities for the topical therapy of melanoma

THAM HUIJUN PHOEBE

Interdisciplinary Graduate School

NTU Institute for Health Technologies

(HealthTech NTU)

A thesis submitted to the Nanyang Technological University in partial fulfilment

of the requirement for the degree of

Doctor of Philosophy

2018

Acknowledgements

To the following people, I would like to offer my sincere gratitude:

Prof. Subbu S. Venkatraman, A/P Zhao Yanli, A/P Ng Kee Woei and A/P Steven Thng for their supervision and time over these 4 years. Prof Zhao for giving me freedom to explore and work in his lab. Prof Subbu for always being very encouraging throughout. A special thanks to Prof Ng for guiding me through this journey for the past 7 years, and to Prof Thng, for making time to come to all the meetings and sharing his knowledge so freely. To A/P Xu Chenjie for collaborating in this project, and his guidance and advice all the way. Dr Xu Keming for guiding me through the basics of animal experimentation.

All past and present members of A/Prof Zhao Yanli's group who have helped me in one way or another. Dr Chen Hongzhong, Dr Xiang Huijing, Dr Zhao Lingzhi, Dr Xing Pengyao, Dr Sreejith, Dr Li Menghuan, Dr Tan Si Yu, Wei Qi, Fiona etc, for the helpful discussions and assistance. Mengjia for help in mice matters.

Fiona Sze for her generous help in coordinating administrative matters.

The staff of HealthTech and IGS office.

Technical personnel of School of Physical and Mathematical Sciences Division of Chemistry and Biological Chemistry (SPMS CBC), School of Materials Science and Engineering (MSE), and School of Biological Sciences Animal Research Facility (SBS-ARF) labs.

Interdisciplinary Graduate School for the scholarship and opportunity.

Family and friends, who have supported and are still supporting me.

Contents

List of Abbreviations

5-FU, 5-fluorouracil

ABDA, 9,10-anthracenediyl-bis(methylene)dimalonic acid

AIDS, acquired immune deficiency syndrome

AK, actinic keratosis

ALA, aminolevulinic acid

ANOVA, analysis of variance

APC, antigen presenting cel

ApH, acid phosphatase

ATP, adenosine triphosphate

BCC, basal cell carcinoma

BET, Brunauer-Emmett-Teller

BRAF, proto-oncogene B-Raf

CDK, cyclin-dependent kinase

Ce6, chlorin-e6

CI, combination index

c-KIT, proto-oncogene c-Kit

CLSM, confocal laser scanning microscopy

c-MET, mesenchymal–epithelial transition factor

CML, Chronic myeloid leukaemia

CTCF, Corrected Total Cell Fluorescence

CTLA-4, cytotoxic T-lymphocyte associated protein 4

DFT, Density Functional Theory

DLC, drug loading capacity

DLI, drug-light interval

DLS, dynamic light scattering

DMEM, Dulbecco's Medium Eagle's Media

DOX, doxorubicin

DPBF, 1,3-Diphenylisobenzofuran

DPPC, Dipalmitoylphosphatidylcholine

DTIC, dacarbazine

EA, elemental analysis

EE, entrapment efficiency

EGFR, epidermal growth factor receptor

EMA, European Medicines Agency

EPR, Enhanced Permeation and Retention

ERK, extracellular signal-regulated kinase

FBS, fetal bovine serum

FDA, Food and Drug Administration

FRET, Förster Resonance Energy Transfer

GM-CSF, Granulocyte-Macrophage Colony-Stimulating Factor

H&E, Hematoxylin and Eosin

HDF, human dermal fibroblast

HEK, human epidermal keratinocytes

HSV, herpes simplex virus

hTERT, human telomerase reverse transcriptase

ICG, indocyanine green

IFN-α, interferon alpha

IGF, insulin-like growth factor

IL-2, interleukin-2

ISC, intersystem crossing

IVIS, *in vivo* imaging system

KS, Kaposi's sarcoma

mAb, monoclonal antibody

MAL, methyl aminolevulinate

MAPK, Mitogen-activated protein kinase

MB, methylene blue

MCC, Merkel cell carcinoma

MEK, serine/tyrosine/threonine kinase

MN, microneedle

MRI, magnetic resonance imaging

MSN, mesoporous silica nanoparticle

m-THRC, temoporfin

MTT, 3-(4,5-Dimethylthiazol-2-yl)-2,5-Diphenyltetrazolium Bromide

MWCO, molecular weight cut-off

NF1, nuclear factor 1

NLC, nanostructured lipid carrier

NMSC, nonmelanoma skin cacner

PBS, phosphate buffered saline

Pc, pthalocyanine

PC4, silicon pthalocyanine

PD-1, programmed-death 1

PDGF, platelet-derived growth factor

PDT, photodynamic therapy

PEG, polyethylene glycol

PheoA, pheophorbide A

PI, propidium iodide

PI3K, phosphatidylinositol 3-kinase

PLA, polylactic acid

PLGA, polyl lactic-co-glycolic acid

PMO, periodic mesoporous organosilica

PPI, poly(propylene imine)

PS, photosensitizer

ROS, reactive oxygen species

RTK, receptor tyrosine kinase

SC, stratum corneum

SCC, squamous cell carcinoma

SiNc, silicon napthalocyanine

SLN, solid lipid nanoparticle

TDD, transdermal drug delivery

TEM, transmission electron microscopy

TGI, tumour growth inhibition

THPP, Meso-tetra(4-hydroxylphenyl)porphyrin

TNF-α, tumour necrosis factor alpha

TPZnPc, Tetra(4-carboxyphenoxy)-phthalocyaninatozinc(II)

TSPP, meso-tetra(4-sulfonatophenyl)porphine dihydrochloride

T-VEC, Talimogene laherparepvec

UCNP, upconversion nanoparticle

UV, ultraviolet

VEGF, vascular endothelial growth factor

WHO, World Health Organisation

XPS, X-Ray photoelectron spectroscopy

ZnPc, zinc pthalocyanine

List of Figures

List of Tables

Abstract

The topical treatment of skin cancer is a better alternative to systemic therapy. This is because of the accessibility of the cancerous tissue compared to deeper tissues. However, when it comes to melanoma, the topical treatment in clinics has been restricted by the limited penetration of drugs through the skin to the melanoma site. Of the possible modes of topical treatment, photodynamic therapy is the most promising, as it offers the added advantage of selectivity of therapy. However, for melanoma, photodynamic therapy is not yet used in clinics as the approved photosensitizers are unable to permeate deep enough into the skin, and the light wavelength used to activate them is not penetrative enough to reach the melanoma site. Furthermore, the photosensitizers that can absorb at longer wavelengths tend to be strongly hydrophobic and of high molecular weight, resulting in an inability to penetrate the skin barrier. Selectivity can be further improved by adding targeting ability to the particles. For melanoma, two small molecular inhibitors, Dabrafenib and Trametinib, have been identified as targeting chemotherapeutic drugs. These very promising inhibitors, however, suffer from several drawbacks, including their low bioavailability when systemically administered. A topical approach to deliver these inhibitors would be beneficial.

In order to solve the problems faced in the topical treatment of melanoma using photodynamic therapy and targeted therapy, this work explored the use of nanotechnology, in particular a class of materials called organic-inorganic hybrid mesoporous nanoparticles. This class of nanomaterials are an extension of the conventional mesoporous silica nanoparticles, in which the silica skeleton of the nanoparticle can be modified organically, giving the nanoparticle functional

abilities while freeing up the mesopores for additional drug loading. Such particles have not been explored for topical therapy previously.

The synthesis procedure and chemicals required were first optimised. Variables such as the TMOS to PC ratio and the inhibitor ratio were studied in terms of photodynamic efficiency, and optimized. Following which, the nanoparticle was characterised in depth using various techniques. It was shown to have a good singlet oxygen quantum yield of 0.42 and excellent photostability. Its small size and surface area enables more interaction of the generated ROS with intracellular biomolecules, improving overall efficacy of photodynamic therapy, and also the permeation through skin.

The final product (PcNP@Drug) was first tested *in vitro* against the melanoma cell lines ($BRAF^{V600E}$, $BRAF^{wt}$) and healthy skin cells. It was effective against $BRAF^{V600E}$ cells, proving its efficacy and specificity towards the targeted $BRAF^{V600E}$ cells, while not affecting the healthy or $BRAF^{wt}$ cells as much. The combination analysis was also conducted, and it was observed that photodynamic therapy and the two inhibitors worked synergistically together for the $BRAF^{V600E}$ mutant cells. Various assays such as live/dead, *in vitro* ROS generation assays were also conducted and it was shown that ROS can be generated in cells as well, and the cells could die.

Subsequently, the penetration ability of PcNP@Drug was tested on full-thickness porcine skin and was observed that with the use of microneedles, the penetration was much higher than without.. The microneedle approach to topical administration has the benefit of reducing drug build-up in the epidermis, and thus minimize damage to healthy cells. The PcNP@Drug nanoplatform was then

tested on living mice and it was proven that the nanosystem was able to not only permeate through into the melanoma subcutaneous growths, but the combined targeted therapy and photodynamic therapy was able to inhibit tumour growth. The results obtained in this study show that this PcNP@Drug nanosystem can be used as a topical method for treating the deeper-seated malignancies in skin, with reduced damage to healthy cells, especially in conjunction with the microneedle approach.

Chapter 1. Introduction

1.1 Background of cancer

Cancer refers to a family of diseases that results from abnormal cell growth which can potentially metastasize to other regions of the body. This is most often caused by genes that do not copy properly during normal cell division. This is known as mutation and it leads to the cell not being receptive to the normal chemical signals of the body and hence, growing uncontrollably. When sufficient mutations have occurred, the cell turns cancerous.[1]

According to the World Health Organisation (WHO), cancer is the second most frequent cause of death. Back in 2015, it caused the death of 8.8 million people in the world. This is equivalent to nearly 1 in 6 deaths being as a result of cancer.[2] In Singapore, cancer was responsible for 29.7% of all deaths in 2015, making it the prevailing cause of mortality.[3] The risk of developing cancer in a person's lifetime in Singapore is about 20 – 25%. Between 2011 – 2015, 64,341 cases of cancer were diagnosed in Singapore, 48.6% were males and 51.4% were females.[4] Skin cancer is on an increasing trend in Singapore, with 1,822 cases of skin cancer occurring in men and 1,404 in women yearly. It ranks 6th in male's cancers and 7th in female's cancers in Singapore. This accounts for 5.8% of the cancer incidence for males, and 4.2% for females.[4]

1.2 Rationale

In the world, over a million cases of malignant melanoma are detected each year.[5–8] This is equivalent to only 4% of all skin cancer incidence, yet it accounts for up to 79% of all its mortalities.[9] It is resistant to radiotherapy and chemotherapy[10], especially for chemotherapy, showing serious side effects due

to nonspecific targeting.[11] Surgical resection is ineffective in 20% of all cases too.[9] Interestingly, 60% of melanoma possess BRAF mutation[12], of which 90% are of the subtype $BRAF^{V600E}$.[13] Due to this relation, recently, targeted therapy was employed to improve the overall cure and survival rates of melanoma.[14]

Recently, the combined administration of Dabrafenib and Trametinib was given the approval by the Food and Drug Administration (FDA) for treating $BRAF^{V600E}$ unresectable melanoma.[15–18] Dabrafenib and Trametinib inhibit BRAF and the downstream MEK pathway, respectively.[10,15,19] In clinics, however, this combination is given in high dosages orally, but has low bioavailability and a range of potentially fatal side effects.[10]

Another promising mode of therapy is photodynamic therapy (PDT). It is currently used for superficial skin cancers, but its efficacy on deeper-seated skin cancers is still limited by the penetration of photosensitizers into the skin. Furthermore, PDT does not require the release of photosensitizers to take effect, unlike chemotherapy's mechanism.[20] It is thus possible and rational to covalently link photosensitizers in a mesoporous nanovehicle matrix, as this project addresses. This allows a high loading of photosensitizers, yet prevent their aggregation-induced quenching as they can be engineered to be spaced out, increasing the quantum yield of photosensitizers in the system.[21] Furthermore, the porous nanostructure facilitates the co-loading of therapeutic drugs.[22] In this project, Dabrafenib and Trametinib were co-encapsulated for the combination treatment of mutant melanoma, while pthalocyanine was covalently embedded within the skeleton of the nanoparticle.

As malignant melanoma originates from within the skin, topical administration is a sensible route of treatment. However, this has barely been

optimised. There exist huge knowledge disparities in the relationship between photodynamic response and treatment dosage conditions. Moreover, there are a few key limitations that have hindered the use of PDT to treat melanoma.

1.3 Objectives and hypothesis

The hypothesis of this PhD project is that suitably modified silica-hybrid nanoparticles can offer a platform for the selective and photodynamic therapy of melanoma.

This project introduces a platform that address the limitations of the topical treatment of photodynamic therapy (Scheme 1) in the treatment of melanoma with the following objectives:

- The first objective is to develop a drug-containing mesoporous organosilica nanocarrier that is pre-conjugated with large molecular weight photosensitizer (i.e. phthalocyanine) and load it with Dabrafenib and Trametinib.
- The second objective is to test its therapeutic efficacy on $BRAF^{V600E}$ melanoma versus $BRAF^{wt}$ (wildtype) and healthy skin cell lines.
- The third objective is to test its penetration through skin.
- And the last objective is to test this nanoplatform to *in vivo*, to investigate its capability of treating melanoma in a living body.

1.4 Scope

In this work, the photosensitizer (Pc-Si) was first synthesized in a three-step reaction pathway. Then, the ratio of silica precursors was optimised by testing their ROS production efficiency and the best outcome was chosen to synthesize PcNP subsequently. After which, the ratio of Dabrafenib to Trametinib loaded in PcNP was also optimised by testing their cell killing efficacy on $BRAF^{V600E}$ mutant melanoma cell lines (SKMEL-28 and A375)

versus $BRAF^{wt}$ melanoma (B16F10), healthy human epidermal keratinocytes (HEK) and dermal fibroblasts (HDF). The best ratio was chosen as the drug loading ratio to produce PcNP@Drug.

After the optimisation work, PcNP and PcNP@Drug nanoparticles were characterised using methods like Dynamic Light Scattering (DLS), zeta potential, Transmission Electron Microscopy (TEM), X-ray Photoelectron Spectroscopy (XPS), and its photostability, singlet oxygen quantum yield, nitrogen adsorption and desorption analysis and cumulative drug release kinetics was measured.

The therapeutic efficacy of the nanoparticles was then tested on the 5 cell lines under various experimental conditions. The synergistic effect was also analysed via Chou-Talalay combination index (CI). The intracellular uptake of the nanoparticles, the *in vitro* oxidative stress condition and live/dead assay was observed via confocal laser scanning microscopy (CLSM) as well. Caspase 3 activity assay was conducted to test the possible mechanism of cell death too.

3D tumour spheroid cultures were then generated to mimic tumour conditions and the nanoparticles were used to treat the spheroids. Skin penetration analysis were also carried out on full-thickness porcine skin and analysed with In Vivo Imaging System (IVIS) and CLSM to test the effect of nanoparticle conjugation of photosensitizer versus free photosensitizer, as well as the effect of using microneedle patches in the penetration.

Finally, *in vivo* animal studies were conducted to test the therapeutic efficacy of the nanoparticles in a living being.

1.5 Overview

This thesis is divided into 8 chapters:

The first chapter covers the background, rationale behind the project, and the scope of the work.

The second chapter covers the related literature about (1) skin cancer treatment options, (2) photodynamic therapy, its advantages, limitations and mechanisms, (3) targeted therapy and its different mechanisms, (4) nanoparticles used for administering photodynamic therapy and targeted therapy, and lastly (5) the skin as a topical delivery route and the methods of permeation possible.

The third chapter describes in detail the experimental methods and materials used in this work.

The results of this research work are documented in chapters 4, 5, 6 and 7 in detail and covers the material characterisation, cell culture experiments, skin penetration studies and *in vivo* pilot studies respectively.

Finally, the eighth chapter will give a summary of the study, its novelties, as well as the outlook and future recommendations of this work.

Chapter 2. Literature Review

2.1 Skin Cancer

Skin cancers are malignancies of keratinocytes, basal cells or melanocytes. They can originate from premalignant conditions such as actinic keratosis (AK), which are red scaly patches that mostly appear in areas chronically exposed to sun.[23] Skin cancers can be broadly divided into non-melanoma skin cancer (NMSC) and melanoma. NMSC mostly comprises of basal cell carcinoma (BCC) and squamous cell carcinoma (SCC). Other less common skin cancers include Merkel cell carcinoma (MCC), Kaposi sarcoma (KS) and cutaneous lymphoma.

2.1.1. Basal Cell Carcinoma (BCC)

BCC is the most frequently occurring skin cancer in Singapore, at least 3 times more prevalent than SCC in non-immunocompromised patients. It also accounts for about 60% of all skin cancers.[23] BCCs are made up of non-keratinizing cells obtained from the basale layer of the epidermis. It grows slowly and may continue growing for many years before patients seek treatment. It is a locally destructive malignancy, but it rarely metastasizes. The most distinctive presentation is the asymptomatic nodular lesion, which protrudes from the skin around it. It appears pearl-like and has telangiectatic vessels.[24]

2.1.2 Squamous Cell Carcinoma (SCC)

SCC is the next most prevalent type of skin malignancy in Singapore. It tends to occur in humans with chronic skin damage caused by the sun, past experiences of sunburns, arsenic exposure, and long term cutaneous

inflammation. SCC originates from the keratinizing cells of the skin and can present in different forms.[24] SCCs may arise from AK with thick adherent scales resulting from sun-damaged skin. This type of SCC rarely metastasizes but may be locally aggressive. The other form of SCC arises from normal skin or the lip. This form is known to be aggressive and can spread to regional lymph nodes.[25]

2.1.3 Melanoma

Melanoma originates from mutated melanocytes and behaves in a much more aggressive manner than BCCs and SCCs. It occurs predominantly in adults and is considered the most dangerous of all the types of skin cancers due to its ability to metastasise early.[6,26] There are several types of melanoma. The most frequently occurring type in Singapore is the acral lentiginous melanoma. It commonly appears on the palms, soles or under toenails or fingernails. This type of melanoma can originate from skin that appears normal or from an existing pigmented growth.[27] Other forms of melanoma cellular subtypes include superficial spreading, nodular, mucosal lentiginous, lentigo maligna, desmoplastic and verrucous. Cutaneous melanomas are subclassified into 3 major subtypes: BRAF mutants, RAS mutants, NF1 mutants and triple wild-type.[28] BRAF mutants account for the majority of all cutaneous melanomas,[12] followed by RAS (NRAS, HRAS and KRAS), triple wild-type and NF1 mutations.[24] The treatment options for these different classifications of melanoma vary and is explained in section 2.2 Skin cancer treatment.

2.1.4 Other types of skin cancers

2.1.4.1 Merkel Cell Carcinoma (MCC)

A much rarer type of skin cancer is the Merkel cell carcinoma (MCC). This type of skin cancer originates from the Merkel cells in the skin which are a kind of skin neuroendocrine cell found mainly at the base of the epidermis. MCC may be less common than BCC/SCC and melanoma but it is one of the most dangerous types, with a high inclination to metastasize to other parts of the body if not discovered early, and would thus be very tough to cure once it has spread.[29]

2.1.4.2 Kaposi Sarcoma (KS)

Kaposi sarcoma (KS) is an even rarer neoplasm of the skin that originates from the lymphatic endothelial cells and the lining of the blood vessels. It generally develops as multiple vascular cutaneous growths on the skin or mucosal surfaces. However, the tumours can also grow in other areas e.g. lymph nodes, lungs, or digestive tract.[30] KS, however, is the most prevalent malignancy in AIDS sufferers, and it also affects patients with drug-related or transplant-associated immunosuppression.[31]

2.1.4.3 Cutaneous Lymphoma

Cutaneous lymphoma is a distinct subgroup of non-Hodgkin's lymphoma. They mainly concern the skin, although they actually develop from the lymphocytes in blood. So, some people may consider it to be a form of skin cancer. However, cutaneous lymphoma may actually not only involve the skin, but also the blood, lymph nodes and other organs of the body. This disease is classified based on the type of lymphocyte involved (B-cell or T-cell) with the

T-cell type being more common than its B-cell counterpart, represented by red patches of scales or thick plaque of skin.[32]

2.1.5 Signal transduction pathway anomalies

In malignant melanoma, any changes in the receptor tyrosine kinases (RTKs) such as mesenchymal–epithelial transition factor (c-MET), EGF receptor (EGFR) and Kit receptor tyrosine kinase (c-KIT) will affect the subsequent signal transduction cascades.[33] For example, 28% of all melanoma cases that occurred in chronically sun-damaged skin were due to mutations in the KIT gene.[34]

In the case of EGFR, activation of it was identified in about half of all BCC cases and almost all the cutaneous SCCs. Overexpression of EGFR was detected in 73% of SCCs. The overexpression or overactivated EGFR binding in SCC led to SCC acquiring a more aggressive phenotype.[35] The dysregulation in the binding affects the downstream MAPK (mitogen-activated protein kinase) pathway and also affects chemotherapeutic drug resistance. Abnormal activation of BRAF and NRAS are one of the most important identified mutations in human cancers with NRAS mutations being found in 33% and 26% of primary and metastatic melanoma tumours respectively. KRAS mutations occur in a relatively low proportion (10%) of SCC, yet some studies have proven that HRAS mutations accounts for the high rate of SCC cases.[35] In this thesis, BRAF mutation will be the focus and is explained in detail.

2.1.6 BRAF pathway and mutation

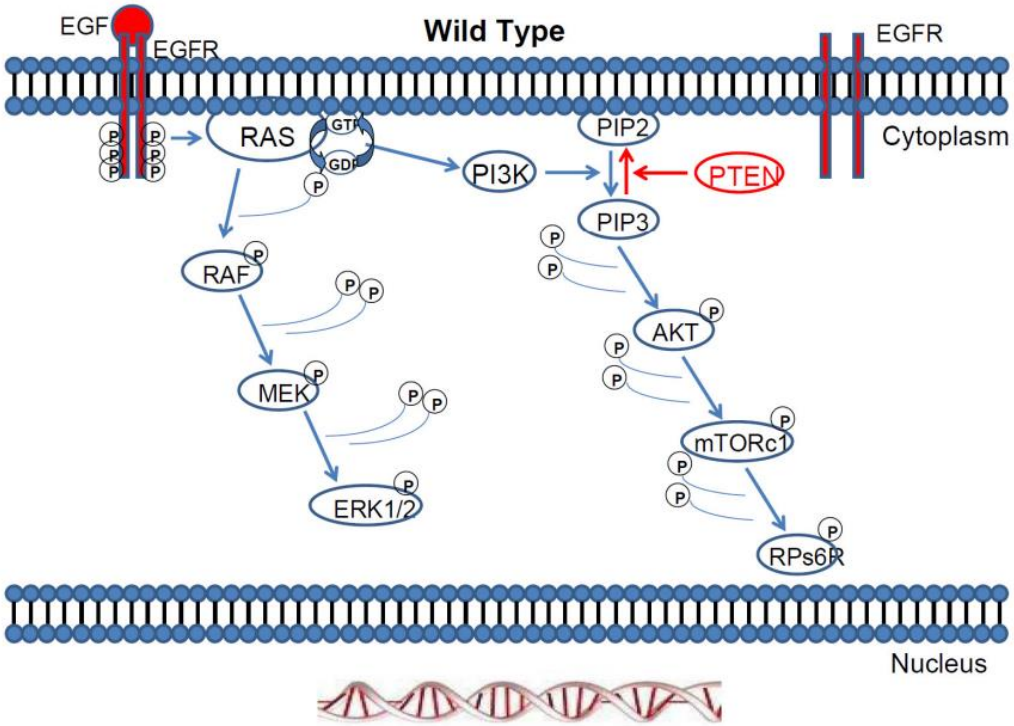

Figure 1. The MAPK pathway and the Ras/PI3K/PTEN/mTOR pathway. Reproduced from Oncotarget, CC BY, ref. 36.

The MAPK pathway is a cellular signalling pathway that passes extracellular signals to the cell nucleus that eventually controls the proliferation, differentiation, movement and apoptosis of cells.

Ras proteins are at the top of MAPK pathways and act as a molecular on/off switch. They comprise of 3 isoforms (HRAS, NRAS, KRAS). The Ras proteins are turned on when RTKs are activated by a ligand. This initiates the signalling cascade by Ras first recruiting and activating the proteins required to propagate growth factors and other signals, e.g. RAF and phosphatidylinositol 3-kinase (PI3K). The pathways of activation are illustrated in Figure 1.[36]

The RAF is a set of protein kinases which include ARAF, BRAF and CRAF. These kinases phosphorylates the hydroxyl group of serine or threonine. Protein

kinases are enzymes that phosphorylates amino acids, with the energy from adenosine triphosphate (ATP), hence regulating the activity of proteins. After this process is carried out, the protein undergoes a change in its conformation from the inactive to the active form and binds to RAF to activate it. The activated RAF protein subsequently phosphorylates MEK1 and MEK2 kinases. This, in turn, activates a third protein kinase known as extracellular signal-regulated kinase (ERK). The ERK kinase controls cellular functions such as gene expression and metabolism to manage the cell's reactions to extracellular signals, thus regulating cell proliferation, differentiation, and cell death.[33]

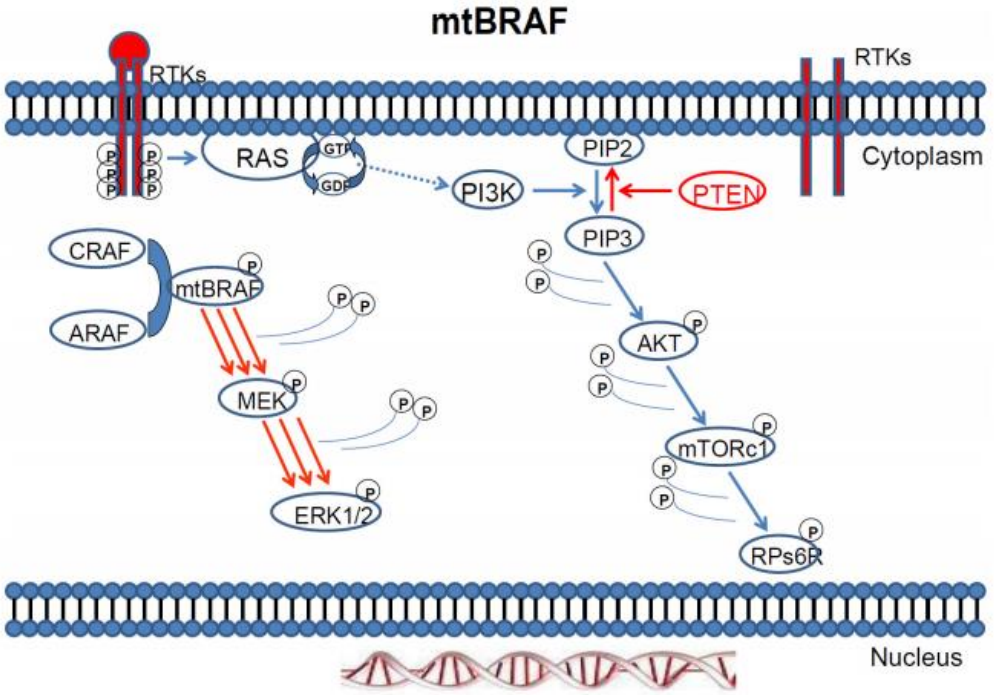

Figure 2. MAPK pathway activation in the presence of BRAF mutation. Reproduced from Oncotarget. CC BY, ref 36.

BRAF, one of the protein kinases in the RAF family, is responsible for a vast number of malignancies, including 70% of melanoma.[12,33] Figure 2 shows the effects of a mutation in BRAF.[36] Out of the possible BRAF mutations, $BRAF^{V600E}$ accounts for 80 – 90%.[37,38] $BRAF^{V600E}$ corresponds to a mutation

located in the activation section whereby the amino acid at the 600th position has been substituted from valine (V) to glutamic acid (E). This mutation leads to over-stimulation of ERK signaling, increasing the unwanted growth and survival of cancer cells as the overstimulation provides for the maintenance ability of cancerous cells.[12,39] Mutations in BRAF are also responsible for the angiogenesis to tumour tissues as it causes the overstimulation of the vascular endothelial growth factor (VEGF) generation.[40] Alone, $BRAF^{V600E}$ mutation shows a 137-fold increase in the transformation and the oncogenic activity compared to $BRAF^{wt}$.[12] BRAF mutations are also commonly identified in cancers with no other mutations in the other genes (NRAS, KIT, or other genes).[41,42]

2.2 Skin cancer treatment

2.2.1 Surgery

The primary treatment of skin cancers is usually surgery as it is often a curative means in treating most skin cancers. In the case of treating melanoma, surgical excision is still the gold standard and primary modality. Malignant melanomas that are still localised at the site of origin are highly curable.[43]

2.2.1.1 Excision

Surgery can be done in various ways. The easiest would be simple excision which can be conducted to remove the growth and a bit of the skin and tissue around it. Shave excisions can also be done in which the lesion is shaved off. Wide excisions are mostly done for melanomas or MCCs. This is carried out by removing the skin tumour and a wider perimeter of healthy tissue.[44]

2.2.1.2 Curettage or electrodessication

Another method of surgical treatment is curettage or electrodessication. This can be done on well-differentiated and defined small BCCs/SCCs (less than 1 cm big). This is done by scraping the cancerous region with a curette (an elongated tool that has a sharp loop on a side). Subsequently, an electric current is passed through an electrode to destroy any remnant cancerous cells and reduce bleeding. This method leaves scarring.[44,45]

2.2.1.3 Mohs surgery

Another option of surgery is called Mohs surgery. This is used when the extent of cancer is unknown, or when there is a high risk or recurrence after treatment, or when the cancer occurs near the eye or other critical regions, where the goal would be to preserve as much healthy skin as possible. Mohs surgery is done first by removing the top layer of the skin that contains the tumour. The removed sample is checked under the microscope. If cancer cells are still detected in the removed sample, another layer of the skin is scraped off, and this process is repeated until no more cancerous cells are detected in the removed sample.[44]

Adverse reactions of skin cancer surgery depend on the extent of surgical procedure required. Side effects include pain, bruising/swelling, bleeding, or scarring, and at times, disfigurement. Nerve damage, numbness, infections, fatigue or even lymphedema may also happen.

Although surgery is usually the primary mode used to treat skin cancers, newer technologies which target major cellular receptors or stimulate the body's

immune system have proven successful in reducing morbidity considerably, and increased the quality of patients' lives.[6]

2.2.2 Radiotherapy

Radiotherapy is another option to treat BCCs, SCCs and melanoma. Radiotherapy requires the use of energetic X-rays or another kind of radiation to destroy and shrink tumours, alleviate symptoms for improved quality of life in palliative therapy, and/or control their development. It is used for cancer that has recurred, if cancer cells remain after surgery, or if the cancer grows in regions that make surgical removal tough.[46] Palliative radiation therapy may alleviate symptoms as well, even for melanoma which is rather radiation resistant. Some studies have demonstrated that the tumour shrank with radiation therapy in patients with multiple brain, bone metastases and spinal cord compression.[47,48]

There are two different kinds of radiotherapy modes. The first is internal radiation therapy. In this mode, a radioactive substance is enclosed within needles, wires, or catheters and positioned directly into or near the cancer site. The second mode is external radiation therapy, which is often used to treat melanoma. In this mode, a machine sends radiation toward the cancer from outside of the body.

Radiotherapy used for SCC treatment have been proven to give good cosmetic results, leaving only minimal hypopigmentation or telangiectatic vessels at the site of application.[46] However, radiotherapy is typically very damaging to the body and causes skin changes, fatigue and nausea, etc.[49]

2.2.3 Targeted therapy

Another form of treatment for skin cancer is targeted therapy. Targeted therapy seeks out specific characteristics in cancer cells such as gene mutations or proteins. Targeted therapy drugs attach to cancer cells to kill them with minimal side effects.[50] They can be classified into two categories. One of which is the class of signal transduction inhibitors. These inhibitors prevent signals from passing between the molecules within a cell, which prevents the proliferation and survival of cancer cells. For example, angiogenesis inhibitors, which have been used to treat melanoma, obstruct the creation of new blood vessels.[51,52] The second category of targeted therapy drugs is through the use of monoclonal antibodies. Signal transduction inhibitors will be covered in detail in section and monoclonal antibodies in section 2.4.3 Monoclonal antibodies (mAbs)

2.2.4 Immunotherapy

Immunotherapy is a promising form of treatment that assists a patient's immune response in identifying and attacking cancer cells. This method can treat melanoma and some BCCs and SCCs. It is usually given to advanced melanoma patients, for tumours that cannot be treated by surgery, or if the cancer has metastasized. Immunotherapy makes use of checkpoint inhibitors or cytokines.[53]

Checkpoint inhibitors are one of such possible immunotherapy drugs that target the signalling proteins that allow cancer cells to disguise themselves as healthy cells. The first pathway, PD-1 (programmed-death 1), is a major pathway which mediates the T-cell response to pathogens. Blocking this pathway activates T-cells, while expanding and enhancing effector functions. Nivolumab (Opdivo®)

and Pembrolizumab (Keytruda®) are PD-1 checkpoint inhibitors that have also been approved to treat melanoma.[54]

The activation of T-cells starts from the initial stimulation from T-cell receptors, and following which, T-cells are active after the CD28 receptor on their surface interacts with CD80/CD86 molecules located on the surface of antigen-presenting cells (APC). CTLA-4 (cytotoxic T-lymphocyte associated protein 4) will appear on the surface of active T-cells. CTLA-4 also recognises CD80/CD86 molecules of APCs but have a much better affinity to them compared to the CD28 on T-cells. Therefore, APCs prefer to bind to the CTLA-4 receptors, rather than to CD28, inhibiting T-cells from functioning. Anti-CTLA-4 antibodies have been formulated to bind with CTLA-4, allowing APCs to bind with CD28, countering the inhibition of T-cells, thus allowing the T-cells to fight the cancer cells.[53,55] These anti-CTLA-4 antibodies have also been reported to function by getting rid of the regulatory T-cells that also have the CTLA-4 receptor.[56] For example, Ipilimumab (Yervoy®) is one of such anti-CTLA-4 antibodies that prevents the inhibition of T-cell activation when bound to CTLA-4. This antibody has been approved by the FDA since 2011 and two clinical trials have proven its potential against melanoma.[57,58]

Cytokines on the other hand, are another class of immunotherapy drug that use molecules to help regulate immune activity. The drugs alpha-interferon (IFN-α) and interleukin-2 (IL-2) are cytokines that are used to treat certain cases of advanced melanoma.[59] IFN-α and IL-2 stimulate the rapid activity and growth of immune cells to attack cancer cells quickly. Immunotherapy is thus a promising form of treatment and an option to treat melanoma and some BCCs and SCCs. It

is usually given to advanced melanoma patients, for tumours that cannot be surgically treated, or if the cancer has spread. Interferons may be intra-tumourally injected when surgery is impossible, though proven not to be as effective.[60] Research and preliminary clinical results recommend the simultaneous blocking of both CTLA-4 and PD-1, as it was found to be more effective than individual blocking. This study is currently in clinical trial stage III.[61]

A relatively new means of treatment for melanoma is through the usage of a genetically modified oncolytic virus (Talimogene laherparepvec, T-VEC) for patients with stage IV unresectable melanoma.[62] This therapy programs live viruses by attenuation or by using the native form of the herpes simplex virus type 1 (HSV1) in local injections into various forms of unresectable skin lesions in patients with recurrent melanoma. The genetically modified T-VEC virus replicates inside the tumours, resulting in lysis and subsequently generating granulocyte-macrophage colony-stimulating factor (GM-CSF). The introduced T-VEC virus and the generated GM-CSF trigger the body's immune response, selectively killing melanoma cells. However, drawbacks of this mode of treatment include the possibility of a herpetic infection so this method should not be used in immunocompromised patients or on pregnant patients. [62,63]

2.2.5 Chemotherapy

Chemotherapy utilises drugs that slow or halt the further growth of rapidly growing cancer cells in the body. Systemic chemotherapy may be recommended for patients with advanced skin cancers that has metastasized to the lymph nodes or other sites, while topical chemotherapy would be for more superficial and localised skin cancers.

To treat SCC by chemotherapy, the intravenous administration of cisplatin[64,65], doxorubicin (DOX), 5-fluorouracil (5-FU) and other drugs can be prescribed to slow the development of SCC and relieve symptoms. BCC very seldomly reaches an advanced stage to warrant systematic chemotherapy, although there are anecdotal reports on its usage in literature.[66] Alternatively, targeted therapy drugs are used to treat advanced BCCs as in section 2.2.3 Targeted therapy

Chemotherapy for melanoma include drugs like DTIC (dacarbazine). However, in recent clinical trials comparing DTIC and targeted drugs (vemurafenib and ipilimumab), DTIC was proven inferior.[57] Temozolomide, an oral alkylating chemo-drug, has also been trialled.[67] Chemotherapy may result in hair loss, vomiting, nausea, diarrhoea, fatigue, constipation and mouth sores.

2.2.6 Lymph node management

Mapping of the lymph nodes and sentinel lymph node biopsies test if there is any spreading of melanomas to neighbouring lymph nodes in those with large-sized primary tumours (1- 4 mm). The mapping and biopsies help analyse which patients will benefit from adjuvant therapy and which patients will not.[68,69] Complete lymph node dissection is considered for clinical trials if the patient qualifies, which may help increase survival rates.[70]

2.2.7 Local treatment methods

Sometimes, nonsurgical forms of therapy are used to remove or destroy localised skin cancer cells to treat early-stage BCCs and SCCs. Such local treatments include photodynamic therapy, topical chemotherapy, immune response modifiers or cryotherapy.

2.2.7.1 Photodynamic therapy

Photodynamic therapy (PDT) uses a photosensitizer in combination with a suitable source of light to kill cancer cells. It is a relatively new treatment option for skin malignancies and is used to treat superficial BCCs and AKs, or premalignant lesions that have potential to develop into SCCs if left untreated. In clinics, PDT uses a photosensitizer, like aminolevulinic acid (Levulan®), which is applied directly to the tumour. Up to 18 hours later, the treated area is irradiated with blue light to trigger the photosensitizer's action, releasing toxic reactive oxygen species (ROS) which kills cancer cells on the skin. PDT has also been shown success in treating NMSC and precancerous growths, both alone or in combination with topical immunomodulators.[6] This mode of treatment is explained in detail in section 2.3 Photodynamic Therapy (PDT).

2.2.7.2 Topical chemotherapy

Topical chemotherapy requires the employment of drugs in the cream or liquid formulations (such as fluorouracil, temozolomide or dacarbazine) to be administered straight to the growth to kill unwanted cells. It is a great way to treat superficial BCCs, early SCCs or AKs. The drug typically only affects the cells it reaches and cannot penetrate deeply into the skin. Fluorouracil (Efudex, Carac, and Fluoroplex) is the most common drug used. As the drugs are unable to penetrate through the skin and into the body, the side effects of systemic chemotherapy are avoided. However, drawbacks include inflammation, substantial skin toxicity and discomfort as well as sensitization to the sun may occur. Also, given the superficial nature of the effects of topical treatment, the cancer cells in the dermis layer which are invisible to the eye may still remain,

making both patient and doctor think that the procedure succeeded when in actual fact, it was not complete.[24]

2.2.7.3 Immune response modifiers

Localised immunotherapy in skin cancer treatment makes use of creams which are put on the diseased areas directly to trigger the patient's immune response to fight the disease. Some BCCs and SCCs are susceptible to it.

Immune response modifier utilises a cream, imiquimod (Zyclara®, Aldara®) to treat AKs or superficial BCCs. Imiquimod, which is designed to trigger the immune system to attack diseased cells, works by stimulating the body to produce interferon, a natural protein that fights foreign invaders and cancer cells. This means that the immune system gets activated to attack cancer cells.[71] Imiquimod may be FDA-approved to treat superficial BCCs, but it is not always recommended for the initial monotherapy of BCC. It is usually used in patients with small lesions (smaller than 2 cm^2 in area) in low-risk sites who are not eligible for other more established therapies.[72] Similar to all topical treatments, this method may cause serious skin reactions or flu symptoms in some.

2.2.7.4 Cryotherapy

Cryotherapy is used mostly for AKs, small BCCs and SCCs. It is considered for those with conditions that do not allow the conventional kinds of surgery.[73] Liquid nitrogen is applied directly on the tumour to freeze the cancer cells. When the frozen area thaws, it swells, blisters and forms a crust. This treatment will leave a scar and the new skin will become paler in colour.[60] It is not recommended for people with abnormal cold tolerance, platelet deficiency

disorders, or tumours near nerves. Side effects of cryosurgery include edema, scarring, or motor and sensory neuropathy.[24]

2.2.7.5 Laser treatment

For this method of treatment, laser light is applied to vapourize cancer cells. It is mostly used for AKs, Bowen's disease, and very superficial BCCs. The efficacy of this method of treatment versus the standard methods is not known yet and it is rarely used.[60]

2.2.8 Palliative local therapy

Melanoma that has already migrated to lymphatic regions of the body may be palliated by regional lymphadenectomy. If it has metastasized to the lung, brain or bone, resection may be useful with possible prolonged survival.[47,48] Radiotherapy may also be used as mentioned in section 2.2.2 Radiotherapy.

2.3 Photodynamic Therapy (PDT)

2.2.1 Mechanism of PDT

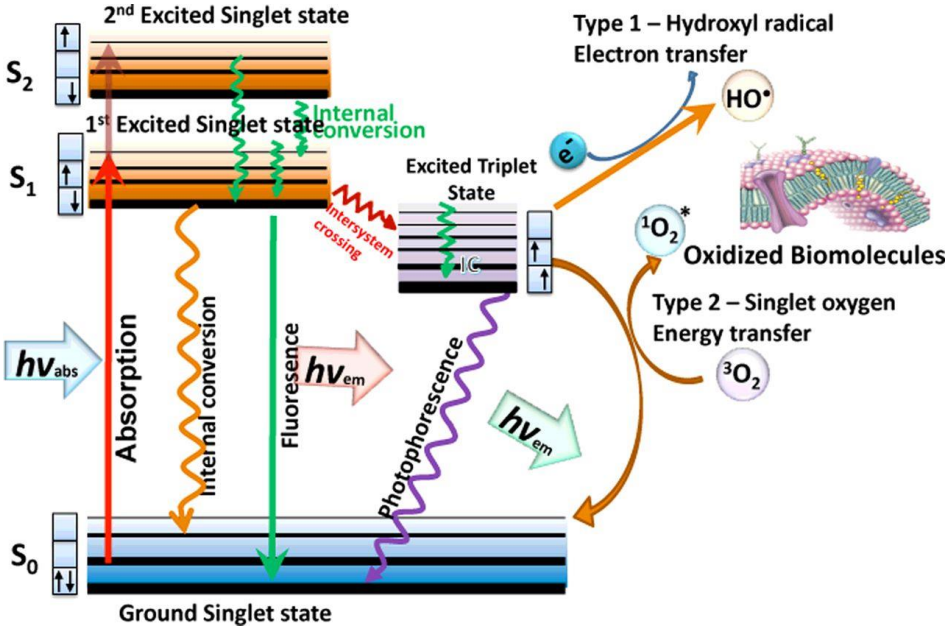

Figure 3: Jablonski diagram. Reproduced from Portland Press, open access. Ref 76.

PDT works by simultaneously employing three non-toxic components: molecular oxygen present in cells and blood, a photosensitizer, and light of a suitable wavelength. Alone, these components, have no toxic effects on the biological system. Upon irradiation with light ($h\nu_{abs}$), the electron transfers from ground state, low-energy singlet state (S_0) to an excited higher energy singlet state (S_1). In this state, the electron can either lose its energy ($h\nu_{em}$) by giving off a photon and produce fluorescence, or go through internal conversion, a form of non-radiative decay, which generates heat. However, photosensitizers tend to undergo intersystem crossing (ISC) from S_1 and become an excited triplet state (T_1). This flips the spin of the electron with higher energy, which leads to an excited triplet state with a long lifetime. Following which, two types of reactions can proceed:

- Type I reaction: the photosensitizer's triplet state reacts with a molecule or cell membrane and transfers an electron or hydrogen to form radicals. These in turn react with oxygen, forming ROS, for example, hydrogen peroxide (H_2O_2), superoxide radical anion ($O_2^{\bullet-}$), or hydroxyl radical ($HO^{\bullet}$).
- Type II reaction: the triplet state of the photosensitizer reacts with oxygen, transferring energy directly and form singlet oxygen ($^1O_2$) in this process. The photosensitizer in the ground state is then regenerated. $^1O_2$ is a highly reactive ROS and also the more likely path of reaction due to the relative simplicity compared to type I reactions.[74]

Type II reactions tend to occur in highly oxygenated environments whereas Type 1 tend to occur in hypoxic environments.[75] The ROS generated can damage majority of all molecules in the body.[76]

Figure 3 shows the mechanism of producing singlet oxygen.[76] After production of singlet oxygen, the photosensitizer is mostly regenerated. Energy transfer can keep occurring and hence singlet oxygen can be produced non-stop.

The ideal photosensitizer is one that preferentially accumulates within the tumour tissue but clears quickly from normal tissue. It has to be of pure quality and good stability with a certain degree of hydrophilicity, for it to travel to the tumour tissue, and also some lipophilicity, for it to translocate across the cell membrane of tumour tissue. In addition, an ideal photosensitizer must possess low dark toxicity, good quantum yields of triplet state formation and relatively long triplet state lifetime. Above all, the photosensitizer has to absorb strongly in the near infrared region, within the biological window (700 – 1000 nm) whereby light can penetrate the skin more deeply.[77,78] Majority of all photosensitizers are hydrophobic, causing them to aggregate in aqueous medium, self-quench and lose their efficiency, or even increase the risk of embolism.[78] The difficulty in formulating a photosensitizer has led scientists to research on delivering existing photosensitizers instead.

For systemic PDT treatment, a photosensitizer is administered into the blood circulation intravenously. It gets taken up by all the cells in the body. However, photosensitizers tend to stay in cancer cells for a longer duration relative to the healthy cells. Up to 72 hours post-administration, when most of the photosensitizer has been cleared from healthy cells but still present in cancer cells, the tumour region is shone with light in the wavelength that the photosensitizer absorbs at. The photosensitizing agent in the tumour absorbs the irradiated light and generates singlet oxygen and other forms of ROS through the process described in Figure 3, which destroys cancer cells in its vicinity.[79]

Although it used to be considered desirable for the interval between drug administration and irradiation (drug–light interval, DLI) to be as long as possible so that the photosensitizer has sufficient time to remain concentrated in tumours but clear from normal tissues, many studies have reported the tumour response to be markedly better at shorter DLI (minutes or hours). At this shorter DLI, some of the photosensitizer is still present in the blood vessels joining to the tumour, thereby producing substantial vascular damage.[80,81]

Some research studies have suggested that inflammatory response due to necrotic cell death from PDT is important as it helps stimulate the immune system. Other reports have suggested that the PDT treatments that produce more apoptosis but less necrosis and inflammation, are suitable for applications where swelling is undesirable, such as in brain tumours. Previous findings have claimed that PDT-induced apoptosis is highly immunogenic and can stimulate anti-tumour immunity.[82]

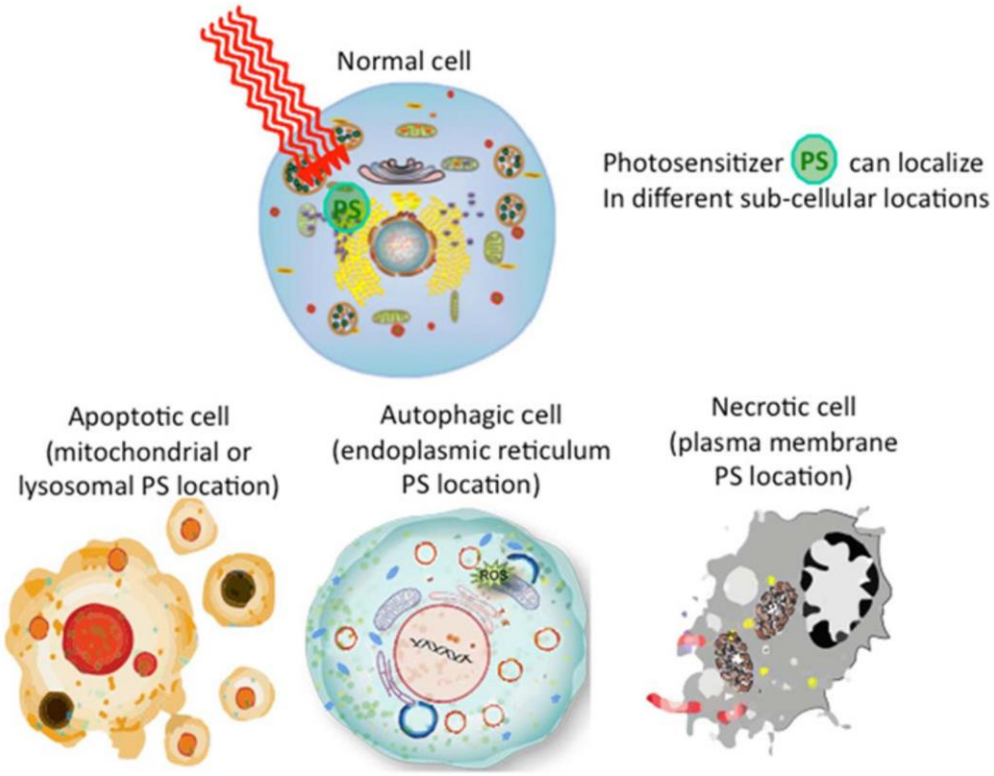

Figure 4. Cell death mechanisms. Reproduced from Portland press, open access Ref. 79.

Singlet oxygen causes cellular oxidative damage and hence apoptosis or necrosis. Singlet oxygen, being extremely reactive, has a lifetime that lasts for less than 3.5 µs, which means it can only diffuse 0.01 to 0.02 µm during this period of time.[83] The extent of PDT is thus only limited to its immediate surroundings. PDT can kill cells in three different mechanisms (Figure 4).[79] It is thought that the eventual location of the photosensitizer in different subcellular organelles (mitochondria, lysosomes, plasma membrane, etc.) plays an important role in the dominating cell death mechanism. Furthermore, it has even been claimed that the location affects the cell death efficacy more than the quantum yield of the photosensitizer, with the mitochondrial subcellular location proving the most effective in the study done by Oliveira *et al*.[81] Other factors such as the overall PDT dose (photosensitizer concentration × light fluence) and DLI also

play a role. Overall it is accepted that apoptosis is the principal modality of cell death when cells are treated with PDT *in vitro*.[79]

2.3.2 Advantages of PDT

Photodynamic therapy (PDT) is a viable alternative to the traditional cancer therapies such as chemotherapy, radiotherapy and surgery. Clinical studies have shown that PDT has the potential to cure early stage tumours and prolong the life of people with inoperable cancers.[74,83–86] It is less invasive than surgery, yet highly localised, with the precise and selective damage of cancer tissues achievable as opposed to chemotherapy.[74,83–88] This spares the extracellular tissues, allowing regeneration of normal tissues after treatment, as opposed to surgical intervention. PDT also enables minimal dark cytotoxicity with negligible systemic effects.[6,77,89] Compared to radiotherapy, PDT can be repeated and minimum scarring can also be achieved.[85] As skin is the most superficial organ, it is much more important than the rest of the body, that the treatment of skin malignancy to not only be successful, but has to have excellent functional and cosmetic outcomes. As PDT possesses these favourable characteristics, it has been intensively studied to make it an alternative to the conventional modes of treatment such as radiation, surgery or chemotherapy.[11] Furthermore, compared to the recuperation period and hospitalisation involved when patients undergo chemotherapy or radiotherapy, PDT is often done as an outpatient treatment for superficial sites.[86] PDT can also induce immunity against tumours, enabling it as a long-term cancer control. Immunologic effects including the production of IL-1β, IL-2, tumour necrosis factor-alpha (TNF-α), and GM-CSF, thus stimulating the body to attack cancer cells.[74,83,90] PDT generally do not cause unwanted DNA damage, mutations, and carcinogenesis.[91] Besides destroying cells directly by

ROS action, PDT may also shrink tumours in another way which is to damage blood vessels in the tumour, blocking important nutrients from reaching the cancer.[92] All these makes PDT a viable treatment in combination with others, giving it the potential to be integrated into mainstream cancer treatment.

2.3.3 Limitations of PDT

However, limitations of PDT exist. For example, most photosensitizers absorb at wavelengths of light that are unable penetrate any more than 1 cm of tissue. Because of this, PDT is usually used to only treat superficial tumours, those that are located just beneath the skin surface, or those occurring on the lining of organs.[93] PDT is not useful for treating large tumours, for the same reason that the required light is unable to go deep into the tumour.[88,93,94] Intravenously administered photosensitizers unfortunately result in prolonged durations of skin photosensitivity, causing patients to have to avoid sunlight.[88] As the lifetime of ROS is very short, it makes PDT only effective to its immediate surroundings, so it typically is not employed for metastasized cancer.[94] These limitations of PDT do not really affect the treatment of skin cancer compared to other regions of the body, making PDT a sensible candidate for treating skin cancer, which tends to be localised and superficial relative to deep-seated organs.

Despite the minimal limitations of PDT to treat cancers and the encouraging characteristics compared to conventional treatments, the FDA and the European Medicines Agency (EMA) have only approved four photosensitizers to treat a few cancers.[88] Porfimer sodium (Photofrin®) was the first to be approved to treat Barret's Oesophagus, lung cancer or obstructive oesophageal cancer. However, its poor purity, bad tissue selectivity, poor absorption and tissue penetration of light results in elevated dosages being

required, thereby having prolonged circulation times and photosensitivity for longer durations.[95] The second EMA-approved photosensitizer is temoporfin (Foscan® or mTHPC) for advanced head and neck SCCs. Temoporfin can absorb at a longer wavelength and has a shorter circulation time, therefore having a better pharmacological profile than Photofrin®. Two kinds of aminolaevulinic acid (ALA) are authorized for dermatological usage. ALA and its methyl derivative MAL are used to treat AKs, Bowen's disease, superficial and nodular BCCs. These ALA formulations have a good safety profile due to their local or topical administration. However, their limited tissue penetration renders them only usable for superficial lesions.[88] Therefore, PDT for skin cancers is limited in terms of penetration to deeper seated malignancies such as melanoma and nodular SCCs.

2.4 Targeted therapy

2.4.1 Cell signalling pathways

When cancer starts to grow or progress further, healthy cells are altered in various ways. These include the ability to proliferate without activation by growth-promoting or inhibitory signals, to occupy neighbouring tissues and metastasize to other regions of the body, to escape signals or mechanisms that limit cell proliferation, e.g. apoptosis and replicative senescence. These behaviours are due to mutations in the cellular signalling pathways which otherwise control cell proliferation, motility, and survival in healthy cells. Many of the proteins involved in the mutations of cellular signalling pathways are possible targets for cancer therapy.[96] Just last year, a new pathway that promotes and supports cancer cell growth was discovered.[97]

Figure 5 represents an example of the cell signalling pathways involved when colorectal cancer grows and demonstrates the complex mechanisms behind mutations in cell signalling pathways.[98] It also demonstrates the various avenues that scientists can take advantage of in order to inhibit downstream pathways. This mode of therapy is known as targeted therapy.

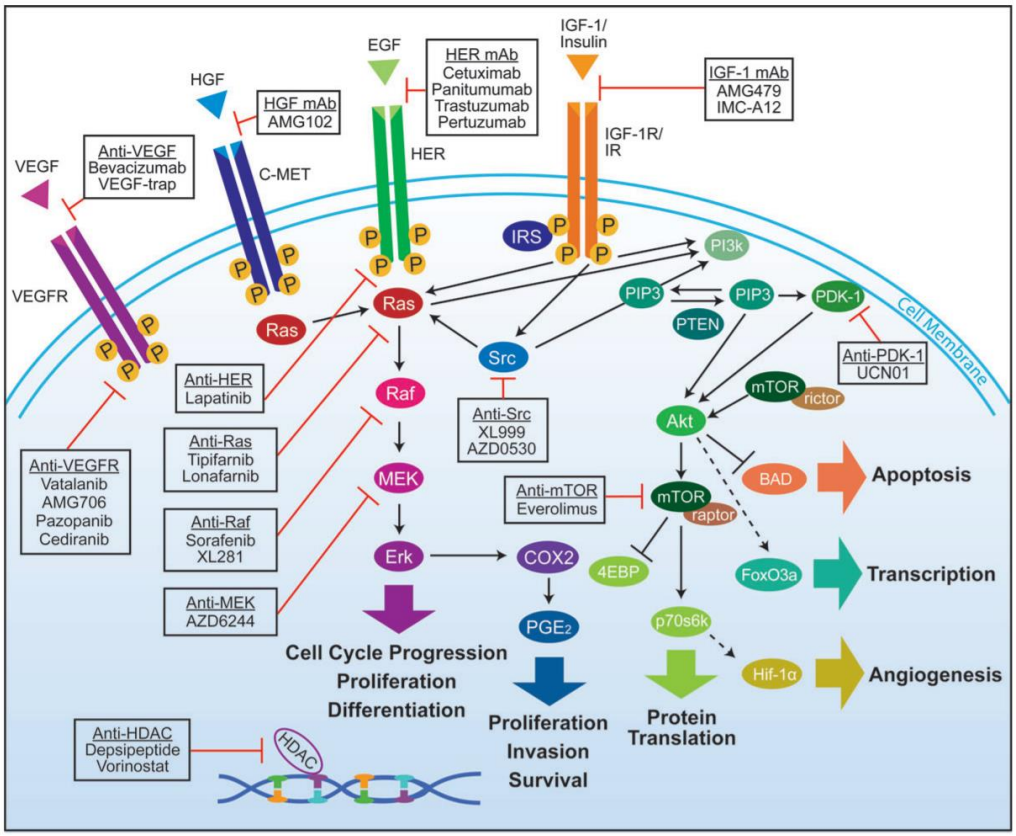

Figure 5. Summary of the signalling pathways involved in the growth of colorectal cancer. Reproduced with permission from Oxford press. Ref. 98

2.4.2 Mechanism of targeted therapy

Targeted therapy is the mode of delivery of therapeutic agents to specific genes or proteins that are related to the cancer cells or which promotes cancer progression. The efficacy of targeted therapy depends on the targeted action of drugs and not causing adverse effects. This mode of therapy is frequently administered in conjunction with other forms of conventional cancer treatments.

Researchers have developed drugs that specifically prevent proliferation, regulate cell cycles or induce cell death by apoptosis or autophagy of cancer cells. This mode of therapy involves the use of monoclonal antibodies or small molecular inhibitor drugs.[96] Most targeted therapeutic drugs are small molecules inhibitors or monoclonal antibodies (mAbs). Small-molecule compounds are usually formulated for targets present inside cancer cells as they can penetrate the cell membrane and disrupt the enzymatic activity of the target protein. MAbs are comparatively large and unable to penetrate through the cell membrane. Hence, they are used to only target unique antigens such as transmembrane receptors or extracellular growth factors present on the cell surface.

Targeted therapy differs from conventional chemotherapy in that they only affect specific molecular targets associated with cancer, while chemotherapeutic agents act on rapidly growing normal or cancerous cells. Targeted therapies are designed, or specifically selected to interact only with their chosen target, whereas chemotherapy drugs are chosen or developed to kill any cell. Targeted therapies are known to be cytostatic, in which tumour cell proliferation is halted, whereas chemotherapy agents are cytotoxic, in which tumour cells are killed.

2.4.3 Monoclonal antibodies (mAbs)

MAbs are designed on a similar basis as small molecular inhibitors, i.e., identifying characteristics of cancer cells that results from genetic defects. Antibodies are a part of the body's immunity. When the body encounters an antigen entering the body, it makes antibodies in response. These antibodies attach themselves onto the antigen to mark it, so that the immune system is able to identify the mark and get rid of the antigen. Scientists analyse special unique antigens on the surface of cancer cells, compare them with healthy cells and then

determine which protein will specifically bind to the targeted antigen but not to normal cells. Then, scientists create a new special antibody to do that job, resulting in treatment being non-immunogenic, cancer-specific, good biodegradability, with lowered toxicity to healthy cells.[99,100] These mAbs result in signalling proliferation arrests, apoptosis, cytokine receptors being blocked, in order to block cancer cells from receiving the growth signals necessary for their survival. They can also prevent tumour cell from interacting with the extracellular matrix which will minimise potential for metastasis. MAbs also cause tumour cells to be recognisable by immune cells, thus enabling them to be used as immunogens, starting adaptive immune responses against cancer cells. Another way mAbs can be used is by targeting important events that occur in tumour microenvironment. For example, VEGFs block angiogenesis, starving tumours of their growth supply while also preventing any escape of cells.[101]

2.4.4 Small molecule inhibitors

Small-molecule inhibitors or signal transduction inhibitors are being actively researched on in the new generation of cancer therapeutics. Till now, about 80 inhibitors have reached some stage of clinical trials.[102] Kinase activity dysfunction is a key mechanism by which cancer cells are different from healthy ones in terms of survival and proliferation.[102] Roughly 30 kinases inhibitors have advanced to at least a Phase I clinical trial level, making them one of the most extensively studied categories of drug targets.[103] This is because kinases have very important parts to play in the stages leading to malignancy growth and survival. These deregulated kinases are oncogenic, oblivious to the normal mechanisms that regulate genetic mutation or translocation of normal cells.[102] This behaviour of not listening to normal regulatory mechanisms becomes the

reason why the cancer cells can survive and proliferate. This behaviour is known as oncogene addiction, and this causes cancer cells to be especially vulnerable to relevantly matching kinase inhibitors.[104,105] In spite of the highly conservative conformation of the site that binds to ATP, high selectivity small molecules inhibitors with acceptable pharmacological behaviours can be developed.[106,107]

Furthermore, in almost every one of the 518 kinases present in the human gene system, the cellular signalling process is started by a phosphotransfer chain of reaction. This suggests that inhibiting kinase activities can evoke some form of physiological responses. When it comes to healthy cells, inhibiting their kinase activity can often be tolerated. This opportune therapeutic window allows tumour cells to be selectively killed. For example, dasatinib, an inhibitor newly approved to treat imatinib-resistant chronic myeloid leukaemia, inhibits all members of the Src kinase family, yet it displays a better pharmaceutical safety profile compared to chemotherapy.[108–110] Many other researches have also discovered numerous kinases bearing mutations, and these are currently being functionally analysed and characterized.[111,112]

Till now, some of the most up-and-coming anti-cancer agents are protein tyrosine kinase inhibitors with credits to the work done some 10 – 15 years back. These studies identified and categorised very key compound categories, e.g. quinazolines and tyrphostins, which are able to inhibit these kinases.[113–115]

Hedgehog pathway inhibitors vismodegib (Erivedge®) and sonidegib (Odomzo®) are used to treat NMSC.[116] They target the hedgehog pathway, a signalling mechanism imperative to healthy cell growth in the development of

foetuses. This pathway normally goes dormant in adulthood, but sometimes it gets reactivated by cancer cells, hence tumours continue growing.

Vemurafenib (Zelboraf®), Dabrafenib (Tafinlar®) and Trametinib (Mekinist®) are examples of small molecular drugs approved to treat melanoma.[15] Dabrafenib is a small molecule selective BRAF inhibitor, orally taken and approved in 2013 for unresectable/metastatic $BRAF^{V600E}$ melanoma. Trametinib is also an orally administered inhibitor but it selectively inhibits the downstream MEK1/2 pathway instead. It is also an FDA approved inhibitor in 2013 for $BRAF^{V600E/K}$ mutations. In a clinical trial involving patients with stage III $BRAF^{V600E/K}$ melanoma, Dabrafenib (150 mg twice daily) and Trametinib (2 mg once daily) combination was proven superior to the placebo medication.[117,118] This clinical trial resulted in Dabrafenib and Trametinib being given together to combat Dabrafenib resistance or the reactivation of the MAPK cellular pathway. Another BRAF/MEK inhibitor combination is Cobimetinib as the MEK inhibitor approved in 2015 to be combined with Vemurafenib.[119]

Sometimes, melanoma may occur due to mutations or amplifications in c-KIT pathway. Of which, certain c-KIT inhibitors have been found to be effective in phase II and III studies. These inhibitors include imatinib mesylate.[120–122] Multikinase inhibitors such as sorafenib have also been explored. Sorafenib is known to inhibit both VEGF and MAPK pathway. However, two clinical trials of paclitaxel and carboplatin with or without the simultaneous sorafenib have shown to be not any better against chemotherapy.[19,123]

Extracellular growth factors trigger the activation of the MAPK pathway, normally required for healthy cells to grow. However, when this pathway is

activated uncontrollably or without external stimulus by growth factors, it causes cancer. This can be due to the overexpression of particular RTKs or due to mutation to its permanently active forms. For instance, many epithelial cancers (e.g. lung) overexpress the EGFR. Ras is mutated to the active oncogene form in a quarter of all human cancers, and RAF is discovered to be an oncogene. Therefore, developing drugs that target the protein kinases in the MAPK pathway has been of great interest in the scientific community.[103]

Another approach in developing these inhibitor drugs with wide specificities is established on the idea of preventing the blood from reaching the malignant site, through the prevention of angiogenesis. Angiogenesis is driven after being stimulated by platelet-derived growth factor (PDGF), vascular endothelial growth factor (VEGF) etc. Two antiangiogenetic inhibitors (sorafenib and sunitinib) have been approved by the FDA.[124]

Cyclin-dependent protein kinases (CDKs) are key to the proliferation of cells. This fact has accelerated the advancement in finding this CDK inhibitors to restrict the growth of tumours. For example, Palbociclib (Ibrance,)[125], Ribociclib (Kisqali®)[126] and Abemaciclib (Verzenio)[127] are FDA-approved CDK4/6 inhibitors for certain forms of breast cancer.

Although there has been a slew of inhibitors developed over the years and have shown very promising results in pre-clinical and clinical settings, researchers and doctors still struggle to treat solid tumours using these modalities alone. Besides, acquired resistance to the administered inhibitors has also been known to occur.[128] Long-term administration is very frequently required to achieve a favourable therapeutic outcome, resulting in toxicity issues in the long

run. However, just like conventional chemotherapy, in comparison to administering 'free' inhibitors in the body, small molecule inhibitors encapsulated within nanoparticles are known to cause much fewer side effects.[107]

2.5 Nanoparticles for drug delivery

Nanomaterials as drug carriers are promising as they have large surface areas capable of being modified to possess various desired biochemical properties, can be made hydrophilic, capable of penetrating deep into tissues and can also be easily internalised by cells.[129]

When nanoparticles are used to deliver drugs, a key advantage is the possibility of loading the nanoparticles with high concentrations of the drugs. As nanovehicles fetch a large amount of drug around the body, they can also favourably manipulate the pharmacokinetic profile and biodistribution of the drugs they deliver.[130] Delivering drugs in nanocarriers offers many benefits over just administering the free drugs as they are. The advantages include the ability to augment the therapeutic effects of the individual drug, as they can be manipulated to control the sustained/triggered release behaviour of the drug. They can also target the diseased sites either through the EPR phenomenon or through active targeting strategies like using ligands to recognise tumour-associated markers. Moreover, nanocarriers also increase the drug's stability and helps prolong the circulation time in the body by protecting the drug from premature elimination or degradation by phagocytic cells. Because of these distinct advantages, nanotechnology's use as a novel platform for cancer theranostics has been scrutinized and investigated.[83]

Numerous drug vehicles have been utilised in the pursuit of drug delivery, e.g., organic carriers like dendrimers, solid lipid nanoparticles, nanogels,

polymeric micelles and vesicles, or inorganic ones like simple spheres, porous or hollow nanoparticles like nanotubes, nanocages, gold nanoparticles, mesoporous silica nanoparticles (MSNs) etc. (Figure 6).[131–133] There have been a few drug delivery systems that are clinically allowed to be used for cancer therapy while many more are presently undergoing clinical trials or preclinical evaluations.

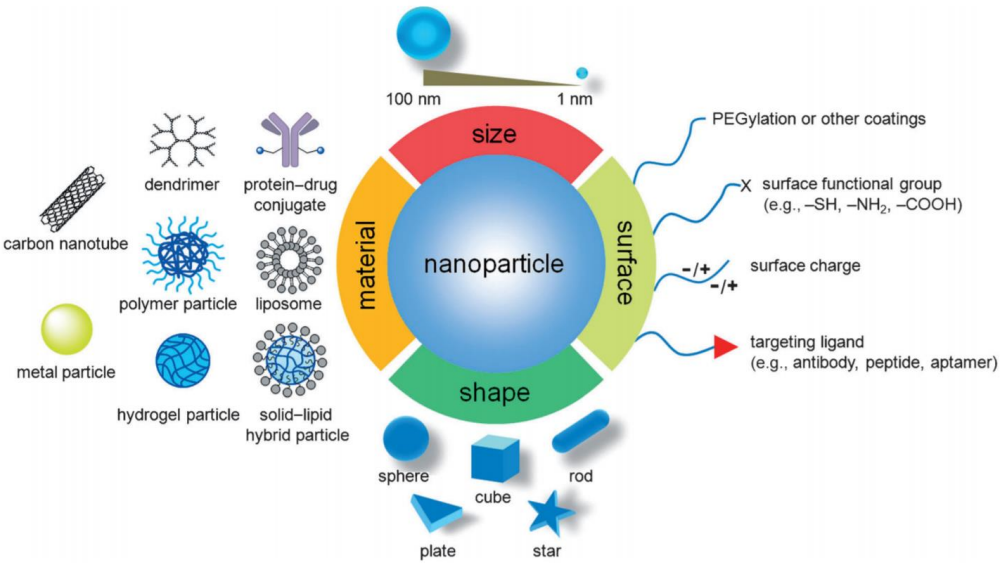

Figure 6. A chart of the nanoparticles already investigated as possible drug delivery vehicles in cancer therapy, with their biophysicochemical properties. Reproduced in permission from Wiley. (Ref: 4353420494719). Ref. 133.

2.5.1 Nanoparticles for PDT

Recent PDT progress has mostly been limited to combination with other treatment techniques and the delivery of photosensitizers. Using nanoparticles to deliver photosensitizing agents will allow the enhancement of PDT efficiency, the increase of circulation time through systemic delivery, the co-delivery of two and more drugs, etc.[134]

When it comes to skin cancer therapy, the two FDA-approved ALA derivatives (5-ALA and MAL), when given in high enough concentrations induce production of protoporphyrin IX, which is a naturally occurring photosensitizer,

in skin cells.[135] Both ALA and MAL are known to have bad penetration abilities through the skin with only 0.26% of applied MAL penetrating in 24 h. MAL acts faster than ALA, 3 h compared to 4–6 h but MAL does not come cheap either, with it costing USD 225/gram, ten times the price of ALA.[136] Furthermore, an Australian clinical trial determined that 19% of patients do not respond favourably to treatment.[137] Enhancing photosensitizer application could greatly improve response and cure rates, hence pushing down therapy costs. One way to improve the therapeutic efficacy of photosensitizers would be through the use of nanoparticles due to the advantages mentioned above. Nanoparticles are broadly classified into two categories: inorganic nanoparticles and organic nanoparticles and they are summarised in Figure 6.[133]

2.5.1.1 Inorganic nanoparticles

Using inorganic materials as a delivery vehicle for photosensitizers has several advantages in that they are more easily synthesized, more stable, easily functionalisable, have good size control and can achieve monodispersity.[138] Inorganic nanoparticles are normally formed via precipitation of inorganic salts, which link together within a 3D matrix, either through covalent bonds, metallic bonds or other forms of interaction.

Silica nanoparticles

Silica nanoparticles are advantageous compared to organic carriers due to their controllable sizes, shapes, porosities, and monodispersity. They are soluble in water, with exceptional stability, and are generally regarded as safe by the US FDA.[139] They are also known to be heat-resistant, non-metallic solids made of both metallic and non-metallic compounds. They are chemically unreactive, hence do not interact with other molecules present in the body. Their synthesis

can be easily controlled, allowing precise manipulation over their morphology. Mesoporous silica nanoparticles (MSNs) is a subclass of silica nanoparticles which has uniform mesoporosity (2 – 20 nm pore diameters) and lets small molecules be entrapped within their pores or covalently attached to the surface.[140]

Ma *et al* utilised hollow MSNs to load photosensitizers such as 5-ALA to cure B16F10 melanoma.[141] Rizzi *et al* have managed to treat melanoma using verteporfin conjugated MSNs.[142]

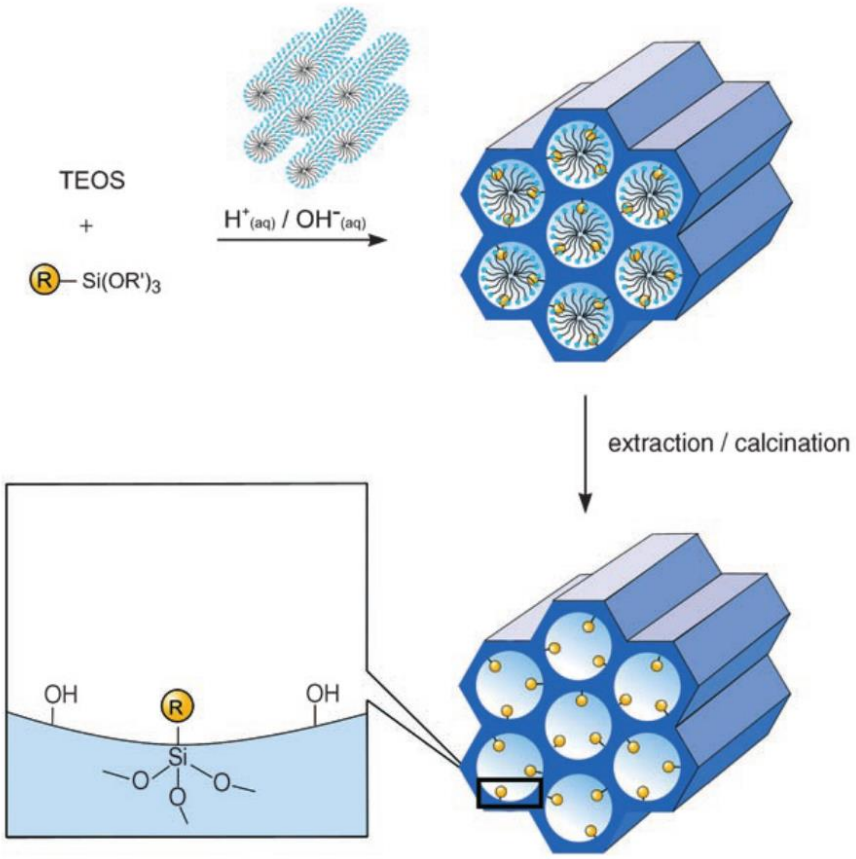

Figure 7. Co-condensation method for organically modifying MSN phases in a direct synthesis. R=organic group. Reproduced with permission from Wiley. Ref. 143

Another rather new class of silica nanomaterials for PDT applications is the class of organic-inorganic hybrid porous nanomaterials or more loosely known as periodic mesoporous organosilica (PMOs).[143,144] These nanomaterials

are formed using the silica precursor such as TEOS or TMOS, together with a mono/bridged organoalkoxysilane using a templating agent[144], and its formation is illustrated in Figure 7.[143] Croissant *et al* have co-condensed a tetra-trialkoxysilylated photosensitizer with bis-(triethoxysilyl)phenylene and ethylene for two-photon PDT.[145] Jimenez *et al* have also synthesized a similar nanodiamond-PMO hybrid using 1,2-bis(triethoxysilyl)ethylene and TEOS for two-photon PDT treatment of cancer.[146] This type of organically-modified MSNs, provide the nanoparticle with additional functions within the framework and is very useful for drug delivery.

Gold-based nanoparticles

Gold-based nanoparticles with diverse sizes, shapes and homogeneous size distribution have fascinatingly different properties. Gold-based nanoparticles can be used as delivery vehicles, and they may be split into two categories: active or passive. This classification they fall under depends on the job they carry out in cancer therapy.[147] Passive gold nanoparticles do not greatly influence the efficiency of the photosensitizer in the PDT treatment and mainly serve as the vehicle to transport photosensitizers by immobilizing them on their surface or within the nanostructure.[148] Bare solid gold nanospheres have been used for most part of this type of passive gold nanoparticles delivery. For example, Haimov *et al* used solid gold nanospheres just as a delivery vehicle for meso-tetrahydroxyphenylchlorin to treat cancer cells.[149] On the other hand, active gold nanoparticles can efficiently absorb light and enhance the photosensitization of the photosensitizer, thereby increasing ROS generation. Examples of active gold nanoparticulate vehicles are the plasmonically active ones like gold nanorods[150], shells[151], cages[152] etc. For example, Srivatsan *et al* trapped a pheophorbide-based

photosensitizer in a polyethylene glycol (PEG monolayer surrounding gold nanocages, and used the gold nanocage to improve the PDT performance against cancer cells.[153]

Magnetic nanoparticles

Magnetic nanoparticles have an added advantage of being able to be aimed towards a specific target with the assistance of an external magnetic field, and subsequently being localised in tumour tissue. Another advantage of magnetic nanoparticles is their innate ability as contrast enhancement in magnetic resonance imaging (MRI). A few magnetic nanoparticles that are being explored for PDT are the iron oxide (Fe_3O_4)[154,155] and cobalt iron oxide ($CoFe_2O_4$).[156]

Upconversion nanoparticles (UCNPs)

The use of upconversion nanoparticles (UCNPs) is one of the latest strategies to deliver photosensitizers.[157,158] For example, Punjabi *et al* synthesized red-emitting α-$NaYF_4$:Yb(80%),Er(2%)@CaF_2 UCNPs and connected it to ALA via pH-sensitive hydrazone linkage and proved that the PDT effect was effective up to a depth penetration of 1.2 cm, and able to cure subcutaneously injected 4T1 tumours *in vivo*.[159]

Quantum dots (QDs)

Quantum dots have also been used as multifunctional nanocarriers for the delivery of photosensitizers in PDT as they naturally have a controllable optical properties, high quantum yields of emission, and easy surface modification.[160–162] QDs are also excellent donors in the fluorescence resonance energy transfer (FRET) process.[163] Samia *et al* have shown that the PDT effect of silicon pthalocyanine (PC4) can be improved when conjugated with a CdSe quantum

dot.[164] Tsay *et al* have also shown the possibility of loading Chlorin-e6 and Rose Bengal on CdSe/CdS/ZnS quantum dots.[165] An iridium-based photosensitizer,[166] silica phthalocyanine[164] and meso-tetra(4-sulfonatophenyl)porphine dihydrochloride (TSPP)[167] have been successfully delivered on quantum dots.

2.5.1.2 Organic nanoparticles

Organic nanoparticles are conceptually different from inorganic NPs in terms of the way they are synthesized. Majority of organic nanoparticles are formed when various organic moieties are guided together to self-assemble or bonded chemically. Other than dendrimers and some polymeric nanoparticles, the synthesis of organic nanoparticles first requires organic moieties that self-assemble three-dimensionally. Sometimes, the interaction among organic molecules are weak, like in the case of micelles and vesicles. However, a basic aspect of organic nanoparticles is their rather simple ways of encapsulating drugs, including photosensitizers. This, together with the fact that the molecules used for the fabrication of the organic nanoparticles can be biodegradable, makes organic nanoparticles promising systems for theranostic applications.[168]

Polymeric nanoparticles

Polymeric micelles are the smallest possible organic nanoparticle. Meso-tetra(4-hydroxylphenyl)porphyrin (THPP),[169] zinc phthalocyanine (ZnPc),[170] Indocyanine Green (ICG),[171] and hypericin[172] were delivered in polyesters such as polylactic acid (PLA) and poly lactic-co-glycolic acid (PLGA). Hydrophobic solketal-substituted phthalocyanine ($Si(sol)_2Pc$) photosensitiser has been loaded into such micelles for killing of B16F10 and 14C cell lines.[173] Pheophorbide A have also been encapsulated within a polymeric micelle to treat colon cancer.[174]

Liposomes

Liposomes are organic nanoparticles formed from lipids by a self-assembly procedure, separating its aqueous core from the external aqueous surroundings by a lipid bilayer. As a result of this arrangement, liposomes adopt spherical shapes to reduce its overall entropy. As such, both hydrophilic and hydrophobic drugs may be loaded separately but simultaneously inside the lipid bilayer and the aqueous core within the liposome. These liposomal carriers have been used to deliver Chlorin-e6 effectively with a "turn-on" switch using liposomes.[175] Liu *et al* has also used liposomes to encapsulate methylene blue (MB) using DPPC.[176] Tetra(4-carboxyphenoxy)-phthalocyaninatozinc(II) (TPZnPc) was self-assembled within the core of a liposome to enhance PDT.[177] Kim *et al* utilised liposomes for ZnPc delivery.[178] Liposomes have been reported to encapsulate 5-aminolevulinic (ALA) or temoporfin (m-THRC) in the topical treatment of skin cancers.[179,180] Unfortunately, limitations exist such as biocompatibility, low stability, low drug loading, and lack of effective drug-photosensitizer combination.[181]

Dendrimers

Dendrimers are polymers and are composed of repeating units called monomers. All bonds branch out radially from a centre atom to which monomers are attached in a regular manner, layer by layer, and each layer is called a 'generation'. The architecture and properties of dendrimers depend on the generation. Low generation-dendrimers are smaller molecules characterized by an open and asymmetric shape, whereas higher generation-dendrimers become globular and densely packed at the periphery. This specific structure makes dendrimers good drug delivery systems. Drugs can be attached to dendrimers on the core or the surface, or at any depth of the molecule in a covalent manner.[182]

Taratula *et al* did a hydrophobic modification on pthalocyanine (Pc), encouraging the physical trapping of the modified Pc within a generation 4 polypropylenimine (G4 PPI) dendrimer for PDT.[183] The same group had also bound silicon naphthalocyanine (SiNc) into a nanoparticulate system by encapsulating SiNc within the hydrophobic region of a PPI G5 dendrimer. They subsequently modified the surface with PEG, rendering the photosensitizer with aqueous stability, preserving its PDT properties.[184] Jang *et al* synthesized polymeric micelles by utilising the electrostatic interaction of a negatively charged dendrimer Pc and poly(ethylene glycol)-poly(L-lysine) block copolymers, and proved it effective for PDT.[185]

Other organic nanoparticles

Other forms of organic nanoparticles include nanocapsules and nanogels. Gluth *et al* encapsulated ICG in nanocapsules which has anti-EGFR ligands bound them to treat middle ear mucosa cells and cholesteatoma-derived keratinocytes. ICG was subsequently activated by 810 nm light for PDT.[186] Bae *et al* generated polysaccharide-derived nanogels from pullulan/folate-pheophorbide-a (PheoA) conjugates to improve the phototoxicity of PDT.[187]

2.5.2 Nanoparticles for delivery of targeted therapy agents

2.5.2.1 Nanoparticles used in delivery of monoclonal antibodies (mAbs)

In the past twenty years of so, therapeutic antibodies have proven promising in treating a whole spectrum of diseases. However, the utilisation of antibody-based therapy implies multiple administrations and a high cost of antibody production, resulting in costly therapy. Another disadvantage inherent to antibody-based therapy is the limited stability of mAbs and the low level of tissue penetration. The use of nanocarriers in delivering mAbs is an alternative

to minimize some of these limitations, with the possibility of lowering antibody dosing while promoting an overall decrease in toxicity and cost along with improved efficacy. It also presents a suitable alternative to increase mAb stability by shielding the loaded mAbs from lysosomal compartments, preventing degradation and hence better bioavailability.[188–190] Furthermore, if intracellular components (e.g. intracellular enzymes, oncogenic proteins, transcription factors) are to be targeted, nanoencapsulation may aid in the internalisation of mAbs into the cells.[191,192] It also reduces unwanted systemic antibody exposure, thus avoiding toxicity on off-target organs. The formulation of nanoparticles can be tailored to offer sustained release of the mAbs, allowing for the plasma concentration of therapeutic antibodies to be kept within a therapeutic range[189], and offering added protection from enzymatic degradation.[193] Therefore, therapies using antibodies incorporated into nanoparticles are less likely to be inefficient or toxic.[193]

Srinivasan and co-workers synthesized self-associated mAb nanoparticles, and showed the preferential internalisation by non-small lung cancer cells relative to healthy cells as cancer cells do not have, or have dysfunctional tight junctions, hence increased the permeability of the cancer cell membrane.[100] Son *et al* have optimised the formulation and stability of a mAb (3D8 scFv) into biodegradable PLGA nanoparticles.[194] Gao *et al* used the erythrocyte membrane to coat anti-hTERT (human telomerase reverse transcriptase) mAb nanoparticles proving that nanoencapsulation can enhance cancer cell uptake as hTERT is only present in the cytoplasm of cells and not on the cell surface.[195]

Most literature using nanoparticles to deliver mAbs use them as targeting ligands to deliver the other therapeutic payloads into the cells. Cui *et al* tagged a

polyethyleimine (PEI) and PLA nanoparticulate system with herceptin (a HER-2 antibody) to deliver DOX to breast cancer cells with overexpressed HER2 receptor. They proved that herceptin helped improve efficacy of DOX through its targeting ability.[196] Dinauer *et al* conjugated a biotinylated anti-CD3 antibody specific to lymphocytic cells to the exterior of gelatine nanoparticles and proved that receptor-mediated endocytosis enhanced cellular uptake of the antibody.[197]

2.5.2.2 Nanoparticles for delivery of small molecule inhibitors

The bulk of the attempts at utilising nanotechnology for cancer therapeutics have been concentrated almost entirely on delivering cytotoxic drugs for the improvement of therapeutic efficacies. Little attention has been paid to kinase inhibitors, which may also have significant drawbacks in terms of their therapeutic efficacy when delivered in its free state, such as the poor bioavailability of orally administered inhibitors.[10,128]

Very recently, many researches have started trying to deliver these small molecule inhibitors using nanoparticles. Marslin *et al* used PLGA nanoparticles to load erlotinib and showed that there was significantly reduced sub-acute toxicity in rats than when 'free' erlotinib was administered in its pure form.[198] Spring *et al* formulated a photoactivatable liposome that was composed of a liposome doped with a benzoporphyrin derivative within the lipid bilayer. Then, they encapsulated a multikinase inhibitor cabozatinib (XL184)-containing nanoparticle within the aqueous core.[199] Chenna *et al* designed a polymeric nanosystem using PLGA and PEG to encapsulate HPI-1, a Hedgehog pathway inhibitor, and have successfully inhibited the growth of a Smo-mutant medulloblastoma allograft. Kuruppu *et al* used apoferritin to deliver the EGFR inhibitor Gefitinib to inhibit cancer cell growth.[200] Similarly, Trummer *et al*

developed a nanoliposome formulation containing a high amount of gefitinib.[201] Sakkar *et al* used gold nanoparticles within micellar amphiphilic block copolymer networks to load the dual tyrosine kinase inhibitor ZD6474 and have achieved successful tissue- and site-specific delivery.[202] Mizrachi *et al* enhanced the effectiveness of PI3Ka inhibitors for head and neck SCCs by encapsulating BYL719, the inhibitor, into P-selectin-targeted nanoparticles. Although they used a sevenfold lower dose of BYL719 compared with oral administration, a superior efficacy was demonstrated.[203] Ashton *et al* developed an Accurin polymeric nanoparticle by an ion pairing mechanism that encapsulated AZD2811 (Aurora B kinase inhibitor). Accurins increase the accumulation at tumour sites and demonstrated a sustained release of the drug. The formulated nanosystem enhanced the therapeutic effect in various tumour models even at half the dose of the water-soluble prodrug of AZD2811.[128]

Cancer cells may very quickly develop resistance against kinase inhibitors most often by activating alternative pathways or further mutations at the target site.[107] For example, it has been shown that using kinase inhibitors that inhibit the EGFR pathway may result in inhibitor resistance, subsequently activating the insulin-like growth factor 1 (IGF-1R) pathway instead. In summary, numerous kinase inhibitors when used singly, have demonstrated less favourable physicochemical properties, decreasing their therapeutic potential.[204] As a result, kinase inhibitors are often combined with other drugs, and have shown great synergetic potential. There are certain combinations that improve therapeutic efficacy by influencing cancer tissue to be susceptible to chemotherapy. For instance, Basu *et al* formulated nanovehicles loaded with PD98059 (MAPK inhibitor) to predispose the MAPK-sensitive cancer cells to chemotherapy. They

then combined this nanosystem with cisplatin and proved that there was a significant tumour growth disparity compared to cisplatin or PD98059 treatment alone. This obvious synergistic behaviour was proven *in vivo* as well.[128]

Au *et al* designed a diblock copolymer nanoparticle which releases the cell signalling inhibitor wortmannin (Wtmn) and the drug docetaxel (Dtxl) in sequential order. The nanoparticles were used for chemoradiotherapy and it was observed that Wtmn improved the response rate of Dtxl and enhanced radiotherapy's effect in prostate and lung cancer cells *in vitro*.[205] Morton *et al* encapsulated erlotinib and doxorubicin in a folate-coated liposome and have optimised the best sequence of release of the drugs as well.[206]

2.6 The skin

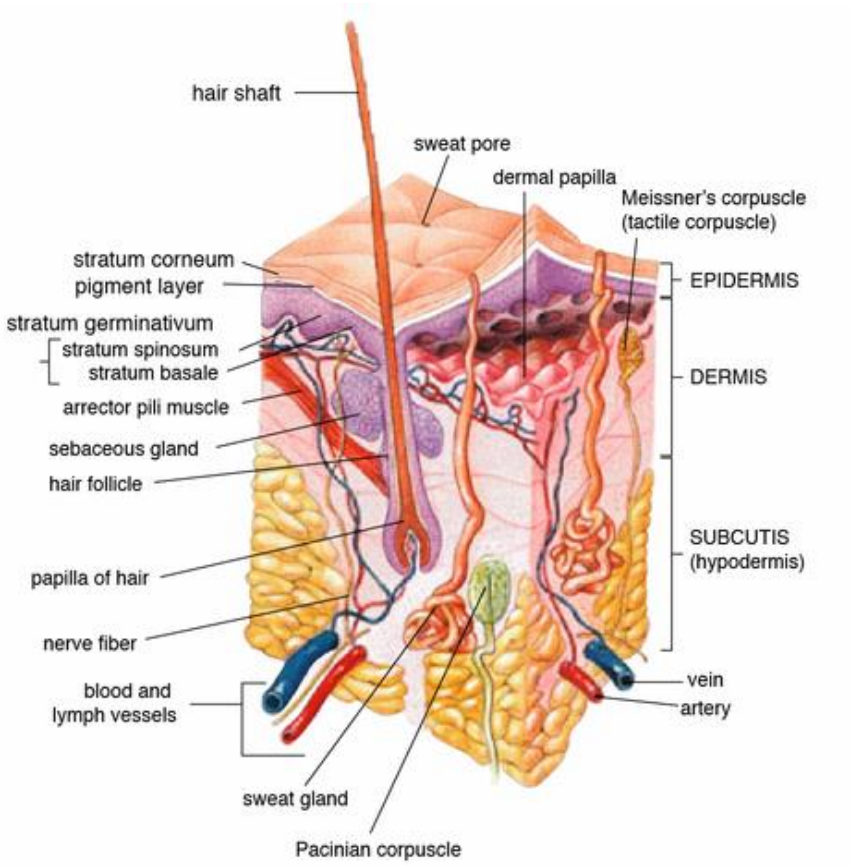

Figure 8. Anatomy of human skin. Reproduced from Wikipedia. Ref 207.

The skin is the biggest organ of the whole body, accounting for 16% by mass and is made up of two main layers, illustrated in Figure 8.[207] The dermis which is located at the bottom, contains an assortment of cells, blood vessels, nerves, and lymphatic cells contained within a compact matrix of connective tissue. This layer acts as the anchor for various cutaneous structures, e.g. nerves, hair follicles, sebaceous and sweat glands. It houses fibroblasts and immune cells that contribute to the physiological responses in the skin too.[208,209]

The basement membrane is the layer that separates the dermis from the layer above it: epidermis. The epidermis is made up of layers of stratified keratinocytes, securely joined to one another by desmosomes and tight junctions. The epidermis layer is in direct contact with the external environment, so it acts as the physiochemical barrier against environmental factors such as UV and pathogens.[208,210] The keratinocytes are developed after stem cells located in the stratum basale go through cell division, and as they move to the skin's surface, they will differentiate in a controlled manner to finally become corneocytes, or stratum corneum (SC) cells. Corneocytes are tightly-linked undamaged but dead cells which make up the main barrier of the epidermis. These corneocytes are covered in proteins with the outermost protection being lipid-based, and finally covered by an extracellular lipid network.[209,211] The SC is usually the one that limits the rate of permeation of drugs that want to pass through the skin.[212]

2.6.1 The skin as a drug delivery pathway

To attain great PDT effectiveness, it is crucial to deliver highly potent photosensitizers to the disease site. Traditionally, systemic administration of photosensitizers through intravenous injections has been used in clinical practice. However, such a drug administration approach would result in whole-body

distribution of the sensitizers, and require much higher amount of photosensitizers to be administered[136], as well as modifying the photosensitizers to circulate longer in the bloodstream.

An alternative pathway of drug administration is through the skin. This allows a sustained drug delivery into the bloodstream, reducing adverse reactions of parenteral and oral administration methods. Optimizing drug penetration into the body can be controlled by the loading of different concentrations of topical products or the surface area of the administration patch. This is a great approach as the delivery kinetics can be controlled with more flexibility.[213,214]

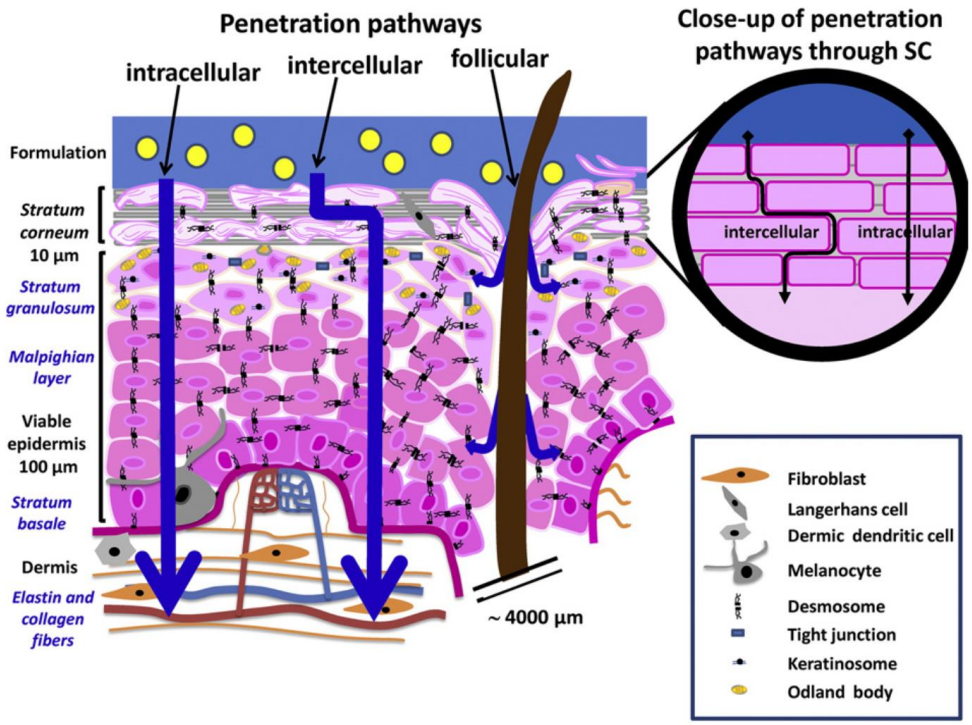

Figure 9. A rough illustration of the 3 pathways of penetration: intracellular, intercellular and follicular. Top right inset: close-up of SC showing the intracellular & intercellular pathway. Reproduced with permission from Elsevier. Ref. 214.

There are three major ways for a substance to enter the skin and reach the viable epidermis as illustrated in Figure 9.[214] These four methods are: (i) through

hair follicles; (ii) intracellular mechanisms; and (iii) intercellular mechanismsFigure 9. A rough illustration of the 3 pathways of penetration: intracellular, intercellular and follicular. Top right inset: close-up of SC showing the intracellular & intercellular pathway. Reproduced with permission from Elsevier. The easiest way for substances to get into the skin would be via the follicular route. Unfortunately, the hair follicles only occupy 0.1% of all superficial area of the skin and this follicular method works only in the short term.[212]

2.6.2 Topical delivery for PDT

Transdermal drug delivery (TDD) is an appealing means to administer drugs, given its non- or minimally-invasive nature, high patient compliance, and direct route of entry bypassing the gastrointestinal or liver metabolism.[215,216] The terms "transdermal" and "topical" delivery are frequently used interchangeably, however, a major difference exists between the two terms. Topical medications are designed to take effect at the application site and does not cause considerably high drug concentrations in the bloodstream or other tissues and thus have lesser side effects. Transdermal medications penetrate through the skin or mucosal membranes into the body. They are meant to take effect in other parts of the body located elsewhere from the application site. As the skin is superficial, the topical route of administration is especially attractive for skin diseases (*i.e.* skin cancer). Therefore, it is unsurprising to see the combination of topical delivery of photosensitizers and PDT for treating superficial BCCs and AKs.[6]

Topical PDT has various advantages in addition to those mentioned in section 2.3.2 Advantages of PDT, such as their non-invasive, selective treatment approach and requiring no surgical intervention. It is also done outpatient while allowing the possibility of frequent repeatable treatment procedures. It is known

to have good cosmesis, making it superior to certain standard therapies. Disadvantages, however, include factors like patients having to be present at hospital as it has to be administered by trained personnel with specific facilities. The DLI may be unfavourable to patients as well. There may be pain associated with the treatment, which will depend on the area of treatment required and the treatment region.[217]

The nanoparticles used in the topical delivery of photosensitizers can broadly be classified in terms of lipid-based (liposomes, niosomes, ethosomes, transethosomes, SLNs, NLCs), emulsions as well as others.

Examples of liposome-based carriers include the studies conducted by Oh *et al*[180] and Pierre *et al*.[179] They fabricated 5-ALA loaded liposomes and investigated their topical penetration into mouse skin. Dragicevic-Curic *et al* encapsulated the highly hydrophobic photosensitizer temoporfin into anionic, neutral and cationic flexible liposomes and tested their skin penetration study on human skin explants using Franz diffusion cells.[218] Fadel *et al* entrapped ICG within transfersomes, and proved them to permeate skin well to treat BCC.[219] Niosomal formulations include the study conducted by Bragagni *et al* who also loaded 5-ALA and tested on pig skin.[220] Garg *et al* encapsulated methoxsalen (8-MOP, a psolaren based derivative that induces melanin production on exposure of the skin tissues to ultraviolet light, inside ethosomes and claimed it possible to treat vitiligo.[221] Zhang *et al* had also used ethosomes containing 5-ALA in the treatment of hypertrophic scars.[222] Praca *et al* developed nanodispersions of monoolein-based liquid crystalline phases with $ZnPcSO_4$ dispersed and tested its ability to enhance $ZnPcSO_4$ uptake by the skin.[223] This same group also developed a microemulsion containing canola oil:surfactant:polypropylene-

glycol/water to deliver the same $ZnPcSO_4$ photosensitizer.[224] Shi *et al* developed a double emulsion solvent evaporation method to formulate PLGA nanoparticles with ALA loaded inside and claimed a promising topical delivery method to treat SCC.[225] Zhang *et al* also developed nanoemulsions incorporating 5-ALA and MAL in both soybean oil/squalene/water formulations. They demonstrated the increase in flux through porcine skin.[226] Qidwai *et al* synthesized a nanostructured lipid carrier (NLC) to deliver 5-ALA topically to treat BCC.[227]

Other forms of delivery vehicles for topical PDT include those developed by Beack *et al* who used carbon dots conjugated to chlorin-e6 and hyaluronic acid in order to permeate skin and treat melanoma.[228]

2.6.3 Method of skin penetration

There have been some various nanoparticle formulations to deliver photosensitizers but these formulations lack the topical penetration ability because hydrophilic ones and macromolecules (>500 Da) cannot diffuse past the compact lipid-rich network of the SC.[229] Penetration enhancers were explored to improve this barrier and the methods can be divided into chemical or physical.

2.6.3.1 Chemical penetration methods

Potential chemical permeability enhancers include glycols and alcohols. Short chain alcohols enhance the penetration of polar molecules. They extract or increase the fluidity of the lipids in the stratum corneum[230] as well as by interacting with the proteins in the stratum corneum.[231]

Urea and cyclic urea derivatives, amides, azone and its deratives, amino acids and their esters and pyrrolidones can be used to enhance permeability through skin. For example, azone's main mode of mechanism is to fluidize the intercellular lipids of the stratum corneum.[232]

Many fatty acids and their derivative esters have been investigated for skin permeation enhancement. Saturated fatty acids were proven to be inferior than the unsaturated ones in the permeation enhancement through skin.[233] Some mechanisms for which fatty acids work include the barrier disruption, the increases in partitioning and solubility of the drug inside the carrier, better solvent penetration, and barrier disruption.[234]

Terpenes, the fundamental makeup of volatile oils, are used to enhance transdermal permeation of both hydrophobic and hydrophilic drugs. The mechanism of action is by disrupting intercellular lipid layers.[235,236] They are often used in cosmetic and pharmaceutical products.

Metabolic or biochemical enhancers disrupt metabolic events, resulting in better permeability through skin. This can happen either by inhibiting the synthesis of SC lipids or boosting the metabolism of the lipids already present, and this controls the skin barrier function.[237]

2.6.3.2 Physical penetration methods

Recent improvements in engineering have made possible the physical enhancement of a diverse range of drugs using novel techniques. These technologies include iontophoresis[238], sonophoresis[239], microneedle technology[240], and electroporation.[241]

Uniform standardized microneedles can be manufactured using new technologies. These microneedles are strong enough to create pores that can be tailored to penetrate to various controllable depths of the skin. These created pores expedite the quick absorption of drugs into the skin, including large molecular weighted drugs. The first generation of the microneedle patches consisted of solid needles manufactured directly using silicon by plasma or wet-

etching methods. The drugs are coated on the outside of the microneedles. The use of microneedles was observed to improve the penetration of calcein (623 Da) through the skin by 1000 times after the microneedle patch was lodged in the skin for a second, and the permeation increased 25000 times after one hour of microneedle application. Insulin (5800 Da) and bovine serum albumin (64000 Da) were shown to permeate to a much greater extent (10000 times). The next generation of microneedle patches had hollow metal or silicon needles, which allowed them to be filled with drug solution. Most importantly, using microneedles to create pores in the skin had virtually eliminated any pain compared to administering by hypodermic needles.[242]

Sonophoresis technology is at least 40 years old and it is an ultrasound method within the frequency range of 0.5 - 3 MHz to boost the drug penetration through the skin. The key imperative of this method is that the skin barrier function takes a few hours to recover. It has been proven that this method is only modestly useful in improving the penetration of drugs through the skin. Another way of physically improving drug permeation is through the use of cavitation. Cavitation ultrasonically induces the generation of gas cavities within a sonicated medium. At high frequencies, gas cavities created are small and nucleate within the SC layer, disrupting the ordered structure and increasing permeation.[243]

Iontophoresis requires the application of an electrical current to "push" drugs across the skin. This technique allows the control of the delivery of drugs and is useful in increasing the speed of the transport of differently charged molecule across the skin barrier. The ions penetrate through the skin using paths with the lowest impedance.[244]

Electroporation requires the employment of micro- or millisecond electrical pulses (100-1000 V/cm) to create deep-reaching pores in the SC. Once these defects are present, drugs can quickly be transported across the skin.[245]

Chapter 3. Experimental materials and methodologies

3.1 Materials

The chemicals, solvents and cell culture reagents and equipment used in this study are tabulated in Table 1,

Table 2, Table 3 and Table 4 respectively.

Table 1. Table of chemicals used.

Chemical name	**Abbrev.**	**Company**
Tetramethoxysilane (98%)	TMOS	J & K Scientific
2-methoxy(polyethyleneoxy)-propyl)trimethoxysilane tech-90	PEG-Si	Gelest Inc.
3-(Triethoxysilyl)propylisocyanate (95%)	TESPIC	Sigma Aldrich
Ammonium molybdate	$Mo_7(NH_4)_6O_{24}$	Sigma Aldrich
4-nitrophthalic anhydride	-	Sigma Aldrich
Urea	-	Sigma Aldrich
Hexadecyltrimethylammonium bromide	CTAB	Sigma Aldrich
Triethanolamine	TEOA	Sigma Aldrich
Acetic acid	-	Sigma Aldrich
(3-(4,5-Dimethylthiazol-2-yl)-2,5-Diphenyltetrazolium Bromide)	MTT	Tokyo Chemical Industries
1,3-diphenylisobenzofuran	DPBF	Sigma Aldrich
9,10-anthracenediyl-bis(methylene) dimalonic acid	ABDA	Sigma Aldrich
Tetranitro-zinc-phthalocyanine	$Pc\text{-}4NO_2$	-
Tetraamino-zinc-pthalocyanine	$Pc\text{-}4NH_2$	-
Silylated-pthalocyanine	Pc-Si	-
Dabrafenib Mesylate (GSK-2118436B)	Dabrafenib	ActiveBioChem
Trametinib (GSK-1120212, JTP-74057)	Trametinib	ActiveBioChem

Table 2. Table of solvents used.

Solvent name	**Abbrev.**	**Company**
Nitrobenzene	-	Sigma Aldrich
Toluene	-	Sigma Aldrich
Ethyl acetate	EA	Sigma Aldrich
Ethanol	EtOH	Sigma Aldrich
Methanol	MeOH	Sigma Aldrich
Diethyl Ether	-	Sigma Aldrich
Hexane	-	Sigma Aldrich
Dimethyl sulfoxide	DMSO	Sigma Aldrich
Dimethylformamide	DMF	Sigma Aldrich

Table 3. Table of cell culture reagents used.

Cell culture reagent	**Abbrev.**	**Company**
Phosphate Buffered Saline	PBS	Biowest
Dulbecco's Modified Eagle's Medium	DMEM	Biowest
Fetal Bovine Serum	FBS	Biowest
Penicillin Streptomycin	PS	Biowest
Trypsin	-	Life Technologies
EpiGRO™ Human Epidermal Basal Medium	-	Merck
EpiGRO Human Keratinocyte Supplement Kit	-	Merck
Roswell Park Memorial Institute-1640 medium	RPMI-1640	Biowest
Image-IT® LIVE Green Reactive Oxygen Species Detection Kit	-	Thermo Fisher
Calcein AM	-	Life Technologies
Propidium Iodide	PI	Life Technologies
Caspase 3 Assay Kit (Colorimetric)	-	Abcam

p-Nitrophenyl phosphate	pNPP	Alfa Aesar
Sodium acetate	NaAc	Sigma Aldrich
Triton X-100	-	Sigma Aldrich
Sodium hydroxide	NaOH	Sigma Aldirch
Formaldehyde	-	Sigma Aldrich
Matrigel	-	Corning

Table 4. List of equipment and brand used.

Equipment/procedure	**Brand/model**
TEM	JEOL JEM 1400
UV	Shimadzu UV-VIS-NIR 3600
Fluorescence	Shimadzu RF5301PC
XPS	SPECS Phoibos 100; monochromatic Mg X-ray source
DLS	Malvern Zetasizer Z
Nitrogen adsorption/desorption	Quantachrome Instruments Autosorb-iQ
Cell viability assay	Tecan Infinite M200
Elemental Analysis	EuroEA CHNS-O Analyzer, EuroVector
CLSM	Carl Zeiss LSM800
Temperature measurements	FLIR infrared camera thermometer
Pig skin penetration analysis	IVIS SpectrumCT Pre-Clinical In Vivo Imaging System
H&E/Optical microscopy	Life Technologies EVOS microscope/ Olympus

3.2 Synthesis of chemical compounds

3.2.1 Synthesis of tetranitro-zinc-pthalocyanine (Pc-4NO_2)

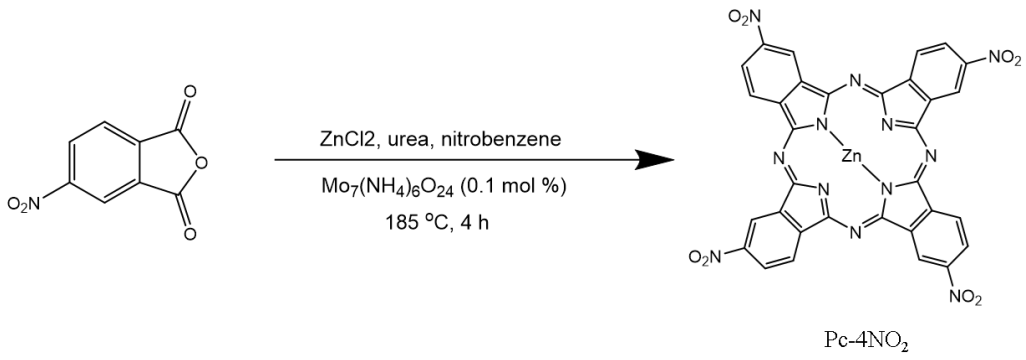

Scheme 1. Synthesis of Pc-4NO_2

Tetranitro-zinc-pthalocyanine (Pc-4NO_2) was synthesized according to published procedures.[246] Ammonium molybdate (6.5 mg, 0.005 mmol) was added to 4-nitrophthalic anhydride (1.0 g, 5 mmol), urea (1.5 g, 25 mmol), and zinc chloride (191 mg, 1.3 mmol) dissolved in nitrobenzene (7.5 mL). The mixture was stirred at 185°C under nitrogen protection. 4 hours later, the mixture was allowed to cool and then toluene (40 mL) was added. The precipitate was centrifuged down and washed with toluene, water, MeOH/ether (1:9) and EA/hexane (2:1), and then subsequently allowed to air-dry to obtain a dark green solid (1.0 g, 98%).

3.2.2 Synthesis of tetraamino-zinc-pthalocyanine (Pc-4NH_2)

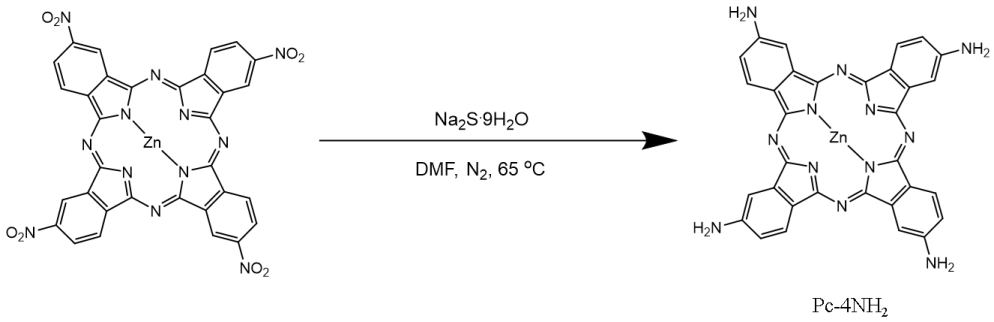

Scheme 2. Synthesis of Pc-4NH_2.

Tetraamino-zinc-phthalocyanine (Pc-4NH_2) was prepared according to published procedures.[246] Sodium sulfide nonahydrate (3.7 g, 15.5 mmol) was added to a solution of Pc-4NO_2 (0.95 g, 1.25 mmol) dissolved in DMF (25 mL). The mixture was heated and stirred at 60^o C under nitrogen protection. 1.5 hours later, the reaction mixture was allowed to cool down to room temperature, and iced water (75 mL) was added. The precipitate that followed was centrifuged down, washed repeatedly with MeOH/ether (1:9) and EA and subsequently air-dried to obtain a dark green solid (0.6 g, 75%).

3.2.3 Synthesis of silylated-pthalocyanine (Pc-Si)

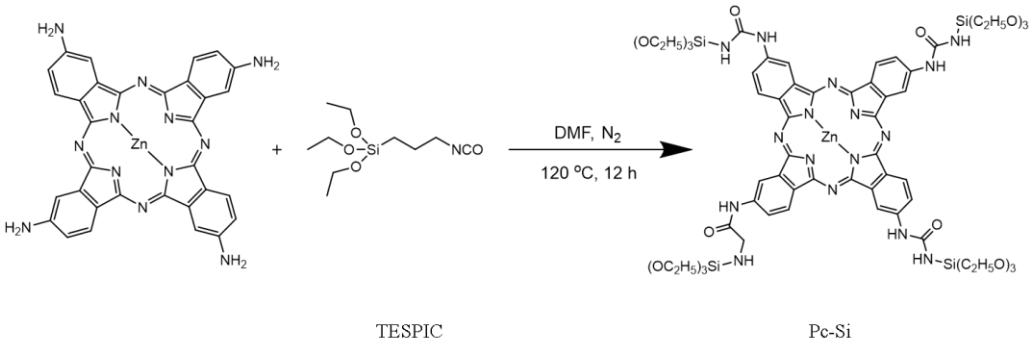

Scheme 3. Synthesis of Pc-Si.

Pc-Si was synthesized in a procedure similar to our previous work. Briefly, Pc-4NH_2 (9.0 mg) was weighed and transferred to a three-necked flask. Anhydrous DMF (5 mL) was added to dissolve Pc-4NH_2. 3-(Triethoxysilyl)propyl isocyanate (13.8 µL) was dissolved in anhydrous DMF (0.1 mL) and injected into the flask. The reaction was refluxed overnight at 120 ^{o}C under nitrogen gas flow. The resulting Pc-Si solution was directly used for synthesis of PcNP (Scheme 3**Error! Reference source not found.**).

3.3 Synthesis of nanoparticles

3.3.1 Optimisation and synthesis of PcNP

The amount of Pc to be incorporated was first optimized by synthesizing a series of PcNPs with TMOS to Pc ratios equivalent to100, 270, 500, and 1000:1. The synthesized PcNP was subjected to elemental analysis to find out the actual amount of Pc incorporated in the nanoparticle by its nitrogen weight percentage. The efficiency of Pc incorporation was calculated according to the formula below.

$$Efficiency = \frac{Actual\ Pc}{Theoretical\ Pc}\ x\ 100\%. \qquad \text{eq (1)}$$

This is the synthesis procedure for making PcNPs with TMOS:Pc ratio of 270:1. CTAB (1.0 g) was dissolved in H_2O (120 mL). Triethanolamine (420 µL, 1:1 w/w in water) was added and this solution was stirred vigorously for half an hour at 80 ^oC to form micelles. TMOS (160 µL) and Pc-Si (800 µL) was initially mixed evenly and then added dropwise into the CTAB solution under vigorous stirring. The reaction was allowed to proceed for 2 hours. Subsequently, the temperature was lowered to 50 ^oC and 400 µL of a 2-methoxy (polyethyleneoxy)-propyl) trimethoxysilane solution (1 g/mL in ethanol) was added dropwise. The reaction was left to proceed overnight for complete reaction. The next day, the mixture was dialysed against 10% v/v acetic acid/absolute ethanol solution for 3 days to remove unreacted silane precursors and CTAB, then 2 days against DMSO to remove unreacted Pc-Si (MWCO 12,000). Lastly, it was dialysed against water and freeze-dried.

3.3.2 Synthesis of PcNP@Drug

Dabrafenib (2 mg/mL) and Trametinib (2 mg/mL) in DMSO stock solutions were added to 1 mg of PcNP which was dispersed in DMSO, to obtain

a final ratio of 1 mg/mL drug loading solution. Various concentrations (1, 2, 5 and 10 mg/mL) were prepared in a similar way. The drug loading was carried out for 24 hours with continuous stirring after which the nanoparticles were washed with vast amounts of ethanol and water to remove excess drug and DMSO. The product, PcNP@Drug was collected by centrifugation at 9000 rpm, 45 minutes.

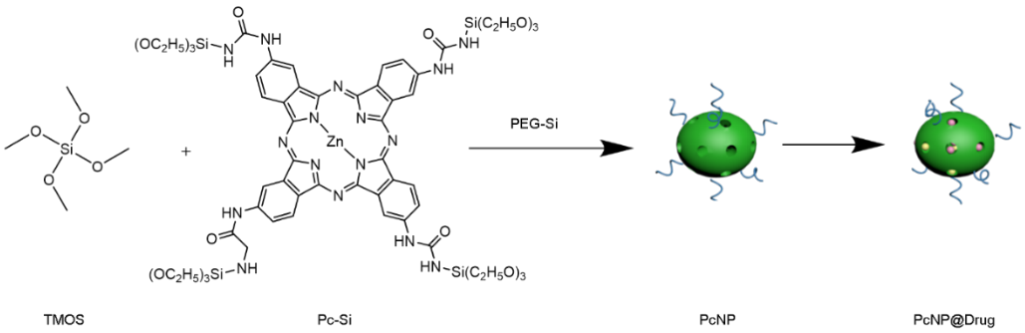

Scheme 4. Synthesis scheme of PcNP and PcNP@Drug.

3.4 Determination of drug loading content (DLC) and encapsulation efficiency (EE)

DLC and EE were calculated against a calibration curve with 1:1 v/v mixture of Dabrafenib and Trametinib.

$$DLC = \frac{drug_0 - drug_{supernatant}}{mass\ of\ PcNP@Drug} x\ 100\% \qquad \text{eq (2)}$$

$$EE = \frac{drug_0 - drug_{supernatant}}{drug_0} x100\% \qquad \text{eq (3)}$$

where $drug_0$ stands for initial mass of drug in loading solution, and $drug_{supernatant}$ stands for the mass of drug in supernatant after the loading.

3.5 Cumulative Drug release

PcNP@Drug (2 mg) was dispersed in PBS (2 mL) at pH 7.4 and 5 each. The nanovehicle was stirred continuously for 48 hours. At certain time intervals,

a portion of the solution was aliquoted out and centrifuged at 14800 rpm to obtain the supernatant, of which was put into a 96-well plate. Fresh PBS with the same volume was placed back into the release solution. The absorbance of the supernatant at different times were analyzed using a microplate reader, and the drug release kinetics was calculated against the calibration curve of Dabrafenib and Trametinib mixture.

3.6 Singlet oxygen quantum yield (ϕΔ) determination

The singlet oxygen quantum yield of PcNP was measured by chemical means using DPBF as the singlet oxygen trap with reference to MB. The optical density of PcNP and MB solutions at 730 nm was first ensured to be similar. The baseline was adjusted to the absorbance spectrum of PcNP. The PcNP solution (750 µL) was added to the DPBF solution (50 µL, 2.5 mM), and the combined solution was irradiated with 730 nm, 1 W/cm^2 laser. The absorbance of DPBF was measured regularly over a 10-minute period. The same procedure was repeated for MB with DPBF. The absorbance values at 428 nm were recorded against time, and the curves were fitted using first order exponential fitting to obtain the time to decay (t) data. The singlet oxygen quantum yield of PcNP was calculated according to the formula

$$\Phi_{\Delta(PcNP)} = \Phi_{\Delta(MB)} \, x \, \frac{t_{MB}}{t_{PcNP}}, \qquad \text{eq (4)}$$

where $\Phi_{\Delta(PcNP)}$ stands for singlet oxygen quantum yield of PcNP, $\phi_{\Delta(MB)}$ is singlet oxygen quantum yield of MB and set at 0.52 was obtained online, t_{MB} is the time to decay for MB and t_{PcNP} is the time to decay for PcNP.

3.7 Photostability measurements

The PcNP solution and Pc-Si solution were prepared such that their optical density at 730 nm was similar. Both solutions were subjected to 730 nm, 1 W/cm^2 laser irradiation for 50 minutes, and corresponding absorbance spectra were recorded every few minutes. The optical density at 722 nm was then plotted against time.

3.8 2D Cell Culture

BRAF^{V600E} human melanoma strains used include A375 and SKMEL-28. The BRAF wildtype strain used was mouse-derived melanoma B16F10. Normal human dermal fibroblasts (HDF) and human epidermal keratinocytes (HEK) were also used as controls. All cell lines were obtained from ATCC. A375, B16F10 and HDF cell lines were cultured in DMEM supplemented with 10% FBS and 1% PS. SKMEL-28 cells were cultured in RPMI-1640 supplemented with 10% FBS and 1% PS. HEK were cultured in EpiGRO^{TM} Basal Medium that was supplemented with EpiGRO^{TM} Human Keratinocyte Supplement Kit.

3.8.1 Cell viability assay

Cells were seeded in a 96-well plate and incubated overnight. Solutions of different ratios and concentrations of Dabrafenib to Trametinib were prepared up to 10 µL. Similarly, 10 µL of each drug solution was added to 90 µL of fresh media. After incubation for 24 hours, the cell viability was tested via MTT assay.

3.8.1.2 In vitro synergism calculation

The quantitative analysis of the synergism between various treatment methods was conducted using the combination index (CI) theorem by Chou-Talalay.[247] The effect of drug combinations could either be additive (CI = 1),

synergistic (CI < 1), or antagonistic (CI > 1). CI was calculated using CompuSyn software.[248]

3.8.1.3 Caspase 3 activity

Caspase 3 was detected using a Caspase 3 Assay Kit (Colorimetric) from Abcam and was conducted according to manufacturer's instructions.

3.8.2 Confocal laser scanning microscopy (CLSM)

3.8.2.1 In vitro oxidative stress detection

The *in vitro* oxidative stress was analyzed using the Image-IT® LIVE Green Reactive Oxygen Species Detection Kit from Thermo Fisher according to manufacturer's instructions. SKMEL-28 cells were seeded in a 12-well plate. PcNP was added at a final concentration of 25 µg/mL. After incubation for 12 hours, the cells were labelled with carboxy-H_2DCFDA for 10 minutes and washed with PBS. The cells corresponding to the PcNP+hv treatment were irradiated with 730 nm, 0.75 W/cm^2 laser for 20 minutes. A positive control using ROS production inducer tert-Butyl hydroperoxide (TBHP) was added to a final concentration of 1 µM and incubated for 15 minutes. After the treatment, the cell nuclei were labeled with Hoechst 33342 (1 µM). Coverslips were then washed with PBS, fixed and mounted onto microscopy glass slides for imaging by CLSM. Carboxy-H_2DCFDA $\lambda_{ex/em}$: 488/529 nm, Hoechst 33342 $\lambda_{ex/em}$: 350/461 nm.

3.8.2.2 Live/dead confocal assay

Calcein AM and PI were bought from Life Technologies. SKMEL-28 cells were seeded in µ-Slide 4-Well Glass Bottom and left to adhere overnight. Prior to the addition of nanovehicle, the cells were starved by using serum-free media. PcNP and PcNP@Drug were added to a final concentration of 10 µg/mL. After

the incubation for 4 hours, the cells corresponding to the PcNP@Drug+hv treatment and PcNP+hv treatment were irradiated with 730 nm, 0.5 W/cm^2 laser for 20 minutes each. Subsequently, the cells were left to incubate for additional 16 hours. To stain the cells, the culture media were removed, and a mixture of Calcein AM and PI was added into each well to stain the cells. Cells were incubated at 37 ^{o}C for 15 minutes. Tthe cells were rinsed with PBS twice and prepared for confocal imaging. Calcein $\lambda_{ex/em}$: 485/535 nm, PI $\lambda_{ex/em}$: 530/620 nm.

3.9 3D Cell Culture

3.9.1 Generation of tumour spheroids

3D tumour spheroids were generated by using hanging drop method. 8000 A375 cells were dispersed in complete media (35 µL with 1% Matrigel) and carefully pipetted on the lid of a cell culture dish in a spaced-out manner. The lid was carefully inverted over the dish that was filled with PBS (15 mL) to prevent the droplet evaporation. Spheroids were allowed to aggregate and grow for 2 weeks to achieve a diameter of 400 µm. After which, the treatment was started. Every 2 days, droplet media (5 µL) were removed and replaced with fresh media. PcNP@Drug or PcNP was added accordingly and incubated for 24 hours before irradiating with 730 nm laser every 2 days. Spheroid volume was calculated using the formula:

$$V = \frac{4}{3}\pi r^3 \qquad \text{eq (5)}$$

where r is radius of spheroid.

3.9.2 Acid phosphatase cell viability assay

Acid phosphatase buffer (ApH buffer) was first prepared by adding 0.1 M NaAc with 0.1% v/v Triton X-100. Droplets of spheroids were carefully washed

with ApH buffer before transferring 50 µL of spheroids to a 96-well plate. The ApH buffer was added to make up to 100 µL. p-Nitrophenyl phosphate (pNPP, 10 µL, 2 mg/mL) was added to each well, followed by the incubation at 37 ^{o}C for 3 hours. After which, NaOH solution (10 µL, 1 M) was added to quench the reaction. The absorbance was read at 405 nm with the reference at 630 nm.

3.10 *Ex vivo* porcine skin penetration studies

Fresh full-thickness porcine skin was obtained from a local wholesaler and cut into 1 cm by 1 cm pieces. The subcutaneous fats were gently stripped from the porcine skin. Any remaining skin was kept frozen at -20 ^{o}C and used as soon as possible. A pyramidal stainless-steel MN consisting of 100 needles in a 10x10 array with a height of ~500 µm, tip radius of 5 µm, pitch of ~700 µm and a base width of ~300 µm was obtained from Micropoint Technologies Pte Ltd (Singapore). To prove the efficacy of using MN patch on the penetration of skin, skins were split into 4 groups. PcNP solutions at 20 mg/mL concentrations was compared against free Pc (equivalent to the concentration of Pc in PcNP at 20 mg/mL). The penetration of PcNP was tested after two durations: 10 minutes and 1 hour. The penetration was conducted with and without the help of the MN patch. Briefly, if required, the skin was pierced with the MN patch under a force of about 4 N for 10 seconds before its removal. PcNP or free Pc solution (40 µL) was added to the skin. After 10 minutes or 1 hour, the PcNP or free Pc solution was gently removed using a micropipette, and the skin was rinsed 3 times with PBS (50 µL) to remove any excess. PBS, PcNP solution (20 mg/mL), and free Pc solution as controls added onto the skins were not removed away. The fluorescence intensity of the adsorbed Pc was measured using the IVIS machine, where $\lambda_{ex/em}$ is 640/700-760 nm. The autofluorescence of the porcine skin was

removed using a function in the instrument's software (Living Image). To calculate the percentage of PcNP that penetrated into the skin, the intensity reading for each skin was normalized against that of PBS and PcNP positive control. In the case of free Pc penetration, this percentage was calculated by normalizing the readings against that of PBS and free Pc positive control.

Fresh full-thickness porcine skin that was penetrated with 20 mg/mL PcNP for 10 minutes and 1 hour with or without MN were fixed in 4% paraformaldehyde, embedded in paraffin block, sectioned longitudinally, and mounted on glass slides that reduce autofluorescence. The sections were imaged on CLSM, λ_{ex}: 488 + 561 nm, λ_{em}: 565 – 700 nm. Quantification was based on the corrected total cell fluorescence (CTCF) formula:

$$CTCF = Int\ den - (A\ x\ Fl_{background}) \qquad \text{eq (6)}$$

where Int den is integrated density, A is area of interest and $Fl_{background}$ is the mean fluorescence of background, which were calculated using the software ImageJ.

3.11 *In vivo* pilot studies

3.11.1 A375 Xenograft

Female homozygous CrTac:NCr-Foxn1nu NCr nude mice (4 weeks old) were used. A375 cells were cultured in T175 flasks and harvested once confluence was reached. Cells were mixed in Matrigel at a 1:1 v/v ratio. 4 x 10^6 cells (200 µL) were injected subcutaneously into the flank of each mouse.

The care and use of laboratory mice were done according to the Institutional Animal Care and Use Committee (IACUC) at Nanyang Technological University, Singapore.

3.11.2 *In vivo* efficacy of PcNP@Drug

When tumours were established in the mice, the treatment was started. The nanovehicle (PcNP or PcNP@Drug) treatment was conducted on days 1, 3, 7 and 10. The laser treatment was conducted the day after the nanovehicle treatment, *i.e.*, days 2, 4, 8 and 11. The nanovehicle treatment was comprised of anaesthetizing the mouse, followed by 30 seconds of the MN application, and addition of PcNP solution (40 µL of 50 mg/mL in 3% sodium carboxymethylcellulose). The procedure of laser treatment includes the anesthesia and irradiation by 730 nm, 2W laser at a height of 15 cm. For the drug group, the laser treatment was not carried out. The tumour volume was measured regularly and calculated using the formula: volume = 0.5 x L x W^2, where L is the longest length of the tumour, and W is the width of the tumour. The relative tumour volume was calculated by the formula: relative tumour volume = (volume of tumour on day n/volume of tumour on day 1) x 100%.

The tumour growth inhibition ratios were calculated according to the formula

$$\%TGI = \frac{V_c - V_t}{V_{c-V_0}} x100 \qquad \text{eq (7)}$$

where V_c stands for median volume of tumour in the control group at day 16 of the experiment, V_t stands for median volume of tumour in experimental group at day 16 of the experiment, and V_0 stands for median volume of tumour in control group at the start of the experiment.

3.11.3 Histology analysis of tumours

On day 18 post-administration, the mice were euthanized by CO_2 inhalation. After which, the tumours were carefully extracted out, and fixed with 4%

formaldehyde. The tumours were embedded in paraffin block, sectioned, stained with H&E, and mounted on glass slides.

3.11.4 Statistical Analysis

Data are all expressed according to mean ± S.E.M (standard error of mean). Statistical difference between two sets of data was determined by one-way ANOVA and $p < 0.05$ was considered to be statistically significant.

Chapter 4. Nanoparticle Characterisation

Phthalocyanine (Pc) functionalized with four silicate units (Pc-Si) was first synthesized using a similar method reported in literature.[249,150] Pc can be excited by far-red light that is able to penetrate into the dermis of the skin, where melanoma infiltrates. Pc-bonded mesoporous organosilica (PcNP) was then synthesized using Pc-Si via silane co-condensation and hydrolysis. Hexadecyltrimethylammonium bromide (CTAB) was used as the structure-directing agent to form micelles in the presence of triethanolamine (TEOA), a basic catalyst.[250] Tetramethyl orthosilicate (TMOS) was chosen as inorganic silica source over commonly used tetraethyl orthosilicate (TEOS) because of its higher water solubility. This method results in a hastened but controlled completion of the hydrolysis process, allowing the formations of uniform small particles suitable for topical delivery.[251] The two precursors, TMOS and Pc-Si, were added dropwise under vigorous stirring. Subsequently, 2-methoxy (polyethyleneoxy)-propyl) trimethoxysilane (PEG-Si) was added to quench any further particle growth and provide hydrophilicity to the resultant PcNP. The PcNP was then purified via dialysis. Small inhibitor drugs, Dabrafenib and Trametinib, in a carefully optimized ratio, were loaded into the PcNP pores to obtain drug-loaded PcNP@Drug. When mice were treated with PcNP@Drug which were delivered after application of an MN patch, PcNP@Drug could produce reactive oxygen species (ROS) *in vivo* under NIR light irradiation. In addition, the release of the loaded drugs could inhibit mutant BRAF and subsequent MEK pathways of cancer cells.

4.1 Optimisation of silica precursor ratio (TMOS:Pc)

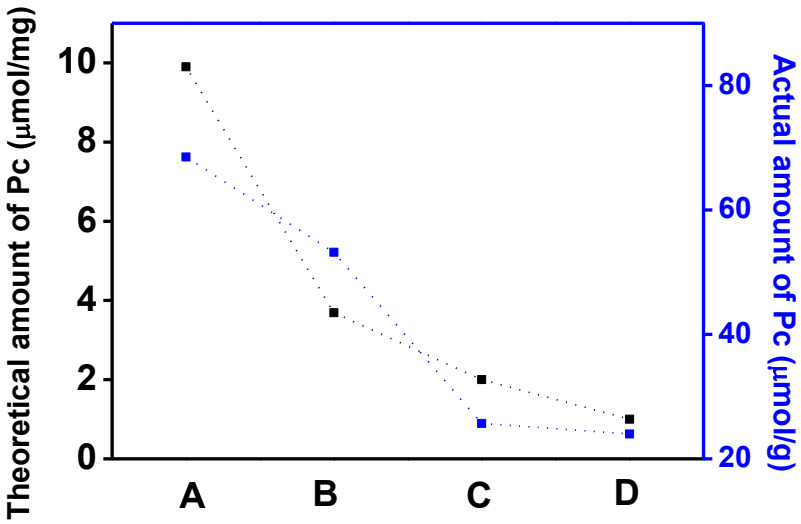

Figure 10. Optimisation of ratio of TMOS to Pc. Actual amount of Pc loaded in nanoparticle (right axis) as corresponding to the theoretical amount determined by EA.

Table 5. Tabulation of the theoretical Pc and actual loaded Pc and their corresponding efficiency.

Sample	TMOS:Pc	Theoretical Pc (µmol/mg)	Actual Pc (µmol/g)	Efficiency (%)
A	100	9.90	68.5	0.69
B	270	3.69	53.2	1.44
C	500	2.00	25.7	1.29
D	1000	1.00	24.2	2.42

Determination of actual amount of photosensitizer incorporated in PcNP

When photosensitizers aggregate, strong π–π stacking may cause their ROS-generating ability to be hindered due to quenching of their excited state.[252] It is thus important for photosensitizers to remain in their molecular state as much as possible. Therefore, in order to find out the optimum concentration of Pc to be included in each nanoparticle that would give the best photodynamic therapy

effects, different TMOS to Pc molar ratios (100, 270, 500, and 1000:1) were used and denoted as A, B, C and D, respectively.

It was observed that when the TMOS:Pc ratio decreased further, nanoparticles failed to form because of the large amount of hydrophobic and large molecular weighted Pc-Si used. When the TMOS:Pc ratio increased, nanoparticles were observed to have formed in a uniform manner by TEM.

After the nanoparticles were synthesized, purified and dried, the Pc content was analyzed by elemental analysis and calculated according to the nitrogen weight percentage. The actual Pc content versus the theoretical maximum Pc content was plotted in Figure 10. The efficiency of incorporating Pc into PcNP was calculated according to eq (1) and tabulated in Table 5.

Determination of optimum amount of photosensitizer to incorporate inside PcNP

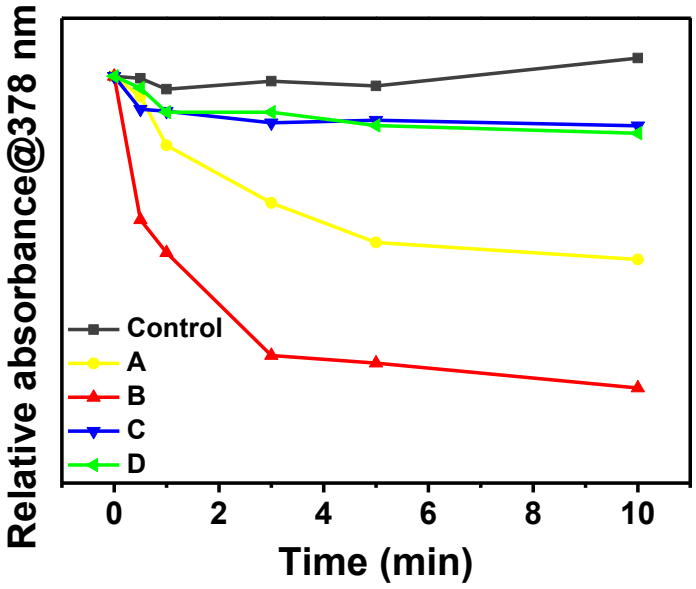

Figure 11. Optimisation of TMOS:Pc ratio. The singlet oxygen production efficiency tested using ABDA chemical ROS.

To determine the optimum concentration of Pc in PcNP, we employed a chemical ROS trapping method using ABDA as the trap agent. The absorbance of ABDA decreases as it reacts with ROS irreversibly to form an endoperoxide.[253] It was observed that nanoparticles C and D quenched the absorbance of ABDA only slightly with respect to the control, while nanoparticle B gave the most obvious quenching effect. Nanoparticle A, having the most Pc incorporated, was expected to produce the most ROS and hence most quenching of ABDA. However, nanoparticle A showed only intermediate quenching effect most probably due to the abovementioned aggregation-induced quenching. The relative drop in absorbance was plotted in Figure 11. It was proven that the TMOS:Pc ratio used in the synthesis of nanoparticle B (270:1) was the optimum and was used for the subsequent synthesis of the nanoparticle (PcNP).

4.2 TEM images, DLS and zeta potential of PcNP and PcNP@Drug

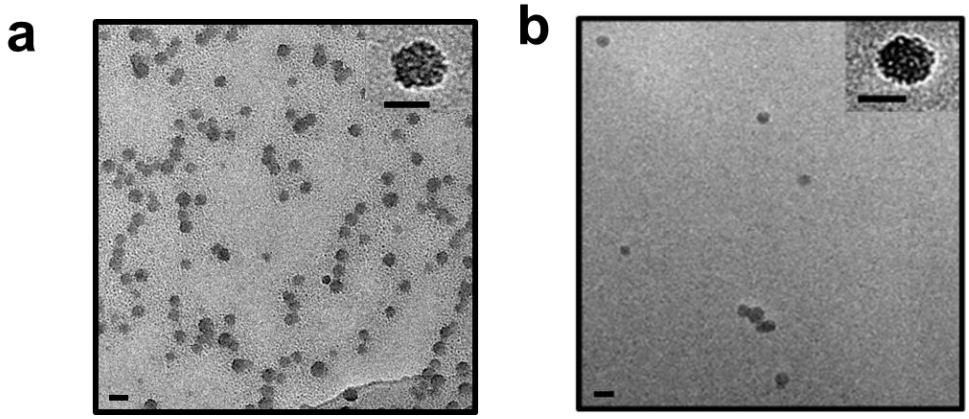

Figure 12. TEM image of a) PcNP, and b) PcNP@Drug. scale bar = 50 nm. Inset: magnified image of an individual PcNP, scale bar = 20 nm.

The synthesized PcNP was monodisperse as observed by TEM in Figure 12a with a diameter of 33 ± 4 nm (n = 30). After drug loading, PcNP@Drug showed the diameter of 34 ± 5 nm (n = 30, Figure 12b). These results mean that

there was no visible aggregation after drug loading, implying that there were no residue drugs coated on the surface of the nanoparticle and were all in the pores.

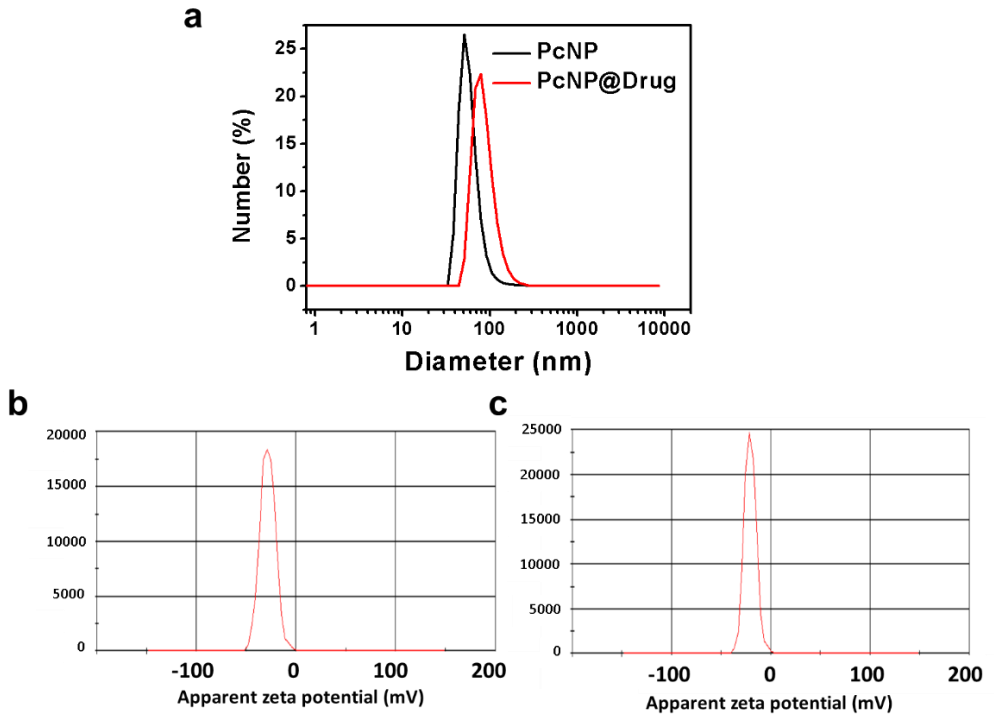

Figure 13. a) DLS measurement of purified PcNP and final PcNP@Drug. zeta potential of b) PcNP and c) PcNP@Drug

The hydrodynamic diameter was measured to be 50 nm and 78 nm for PcNP and PcNP@Drug respectively, as determined by DLS and presented in Figure 13a. This slight increase in hydrodynamic diameter can be attributed to the change of light refraction index of PcNP after drug loading[254], and not due to nanoparticle aggregation as was observed in the TEM images.

The zeta potential of PcNP was measured to be -21.3 ± 0.8 mV, and after drug loading for PcNP@Drug, it was -28.7 ± 0.4 mV (Figure 13b,c). This zeta potential falls within the range of "moderately stable", which gives it steric stabilization in aqueous solutions. It is widely known that highly negative zeta

potential of the nanoparticles confers great electrostatic stabilization and dispersibility in solution.[255]

4.3 Absorbance and fluorescence behaviour of PcNP

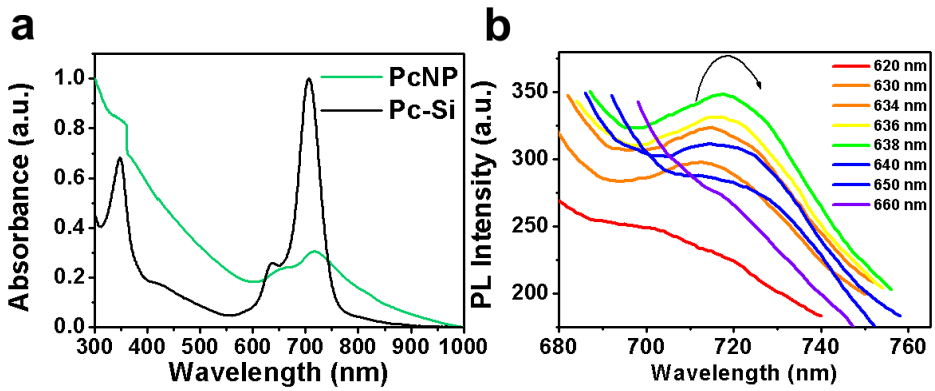

Figure 14. a) Absorbance curve of Pc-Si and PcNP. b) Excitation-dependent luminescence of PcNP displaying a peak fluorescence at excitation of 638 nm.

Absorbance spectra of PcNP

The absorption spectra (Figure 14a) indicate that Pc was successfully incorporated into the framework. This is seen from the Q-band at 707 nm present in the spectrum of Pc-Si in DMSO. The Q-band for PcNP in water red-shifted to 718 nm. The shoulder peak of Pc-Si at 636 nm displayed a similar red-shift to 649 nm in PcNP. This redshift behavior is a typical indication of the interaction between Si groups of Pc-Si and TMOS, due to the changes in the medium environment and the conformation of Pc when conjugated with silica in a 3D structure.[256]

Excitation-dependent fluorescence spectra

The excitation-dependent fluorescence behavior was studied and PcNP was shown to have an emission peak at 718 nm when excited at 638 nm (Figure 14b) due to Stokes shift. The emitted fluorescence was not strong, seen from the

rounded peak, which proves that a large portion of the photon energy received was not converted to fluorescence. However, this slight fluorescence was sufficient for cell imaging purposes.

4.4 XPS spectra analysis

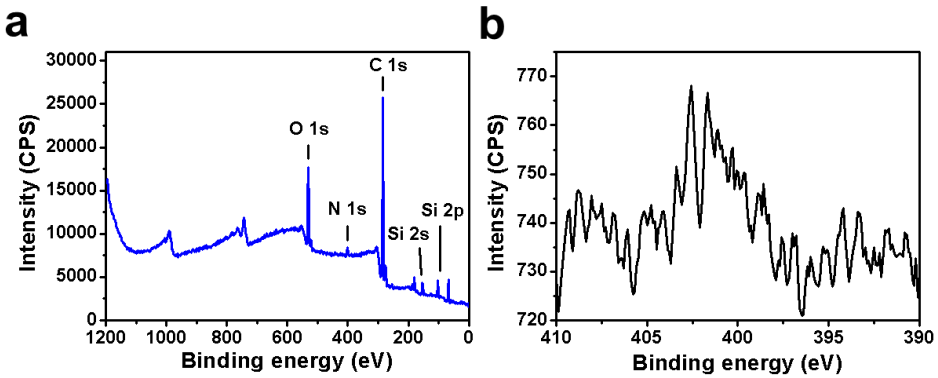

Figure 15. a) XPS spectrum of PcNP, indicating O, N, C and Si peaks from PcNP. b) High resolution scan of nitrogen binding energy for PcNP.

The XPS survey spectrum (Figure 15a) indicates the presence of oxygen at 531.6 eV, originated from TMOS. Relatively high carbon 1s peak at 284.5 eV was due to the framework carbon contributed mainly by the carbon in TMOS. The silicon 2s and 2p peaks at 153.6 eV and 67.5 eV respectively were contributed by silicon in TMOS and Pc-Si. In addition, a peak was observed at 401.7 eV (Figure 15a), which can be attributed to the nitrogen 1s peak of Pc, indicating that Pc was successfully incorporated into the nanoparticles. The low intensity of the nitrogen 1s peak is due to the relatively low incorporation of Pc in PcNP (1.19% by weight of nitrogen as measured by elemental analysis in section 4.1 Optimisation of silica precursor ratio (TMOS:Pc)). The high-resolution scan in the range of 410 – 390 eV where nitrogen's binding energy falls in, shows more clearly the presence of nitrogen in PcNP (Figure 15b).

4.5 Fourier Transform Infrared (FTIR) spectroscopy

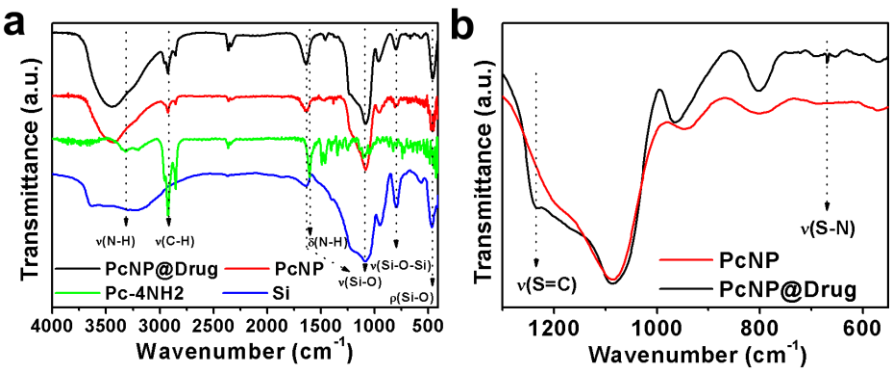

Figure 16. FTIR spectrum of a) Si, PcNP-4NH$_2$, PcNP and PcNP@Drug and b) close up of PcNP@Drug and PcNP in the range of 1300 –650 cm^{-1}.

In pure Si (pristine mesoporous silica nanoparticles), peaks at 1085, 800 and 470 cm^{-1} were presented and can be assigned to the asymmetric stretch of Si-O (ν_{Si-O}), stretching of Si-O bond (ν_{Si-O}) and rocking of Si-O bond (ρ_{Si-O}). These Si-O peaks were not present in Pc-4NH$_2$ but were present in PcNP and PcNP@Drug. Pc-4NH$_2$ presented peaks at 3326 and 3202 cm^{-1} corresponding to the N-H stretch of the 1^o amine (ν_{N-H}). Peaks at 2924 and 2845 cm^{-1} were due to the aliphatic C-H stretch (ν_{C-H}), 1599 cm^{-1} was due to the N-H bend (δ_{N-H}). The C-H bend (δ_{C-H}) gave peaks at 1493 and 1459 cm^{-1}. The aromatic ring structure of Pc also gave rise to the peaks in the region of 1535 - 1180 cm^{-1}.

These aromatic ring structures were also present in both PcNP (1515 – 1310 cm^{-1}) and PcNP@Drug (1488 – 1331 cm^{-1}). PcNP and PcNP@Drug also displayed the aliphatic C-H stretching (ν_{C-H}) at 2924 and 2845 cm^{-1} for both.

In addition, there was a slight S=C stretch ($\nu_{S=C}$) detected in PcNP@Drug at 1235 cm^{-1}. This can be attributed to the S=C bond present in Dabrafenib. The S-N stretch (ν_{S-N}) in Dabrafenib can also be detected at 670 cm^{-1}, further

confirming the presence of the drugs loaded in PcNP@Drug. These are denoted in the magnified range of 1300 – 650 cm^{-1} in Figure 16. FTIR spectrum of a) Si, PcNP-4NH_2, PcNP and PcNP@Drug and b) close up of PcNP@Drug and PcNP in the range of 1300 – 650 cm^{-1}.

4.6 Singlet oxygen quantum yield (ϕ_Δ) calculations

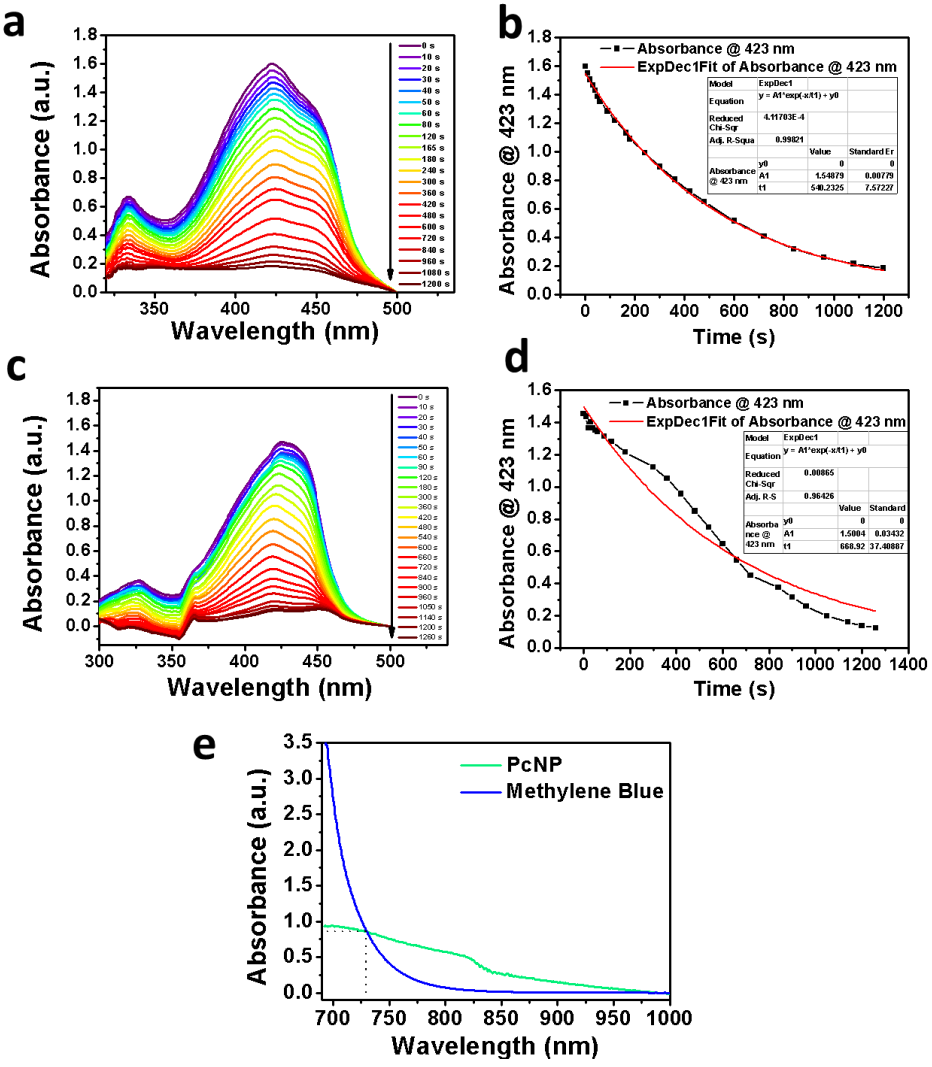

Figure 17. Quenching of DPBF when a) methylene blue and c) PcNP was mixed with a similar optical density of DPBF. Irradiation conditions were 730 nm 1 W/cm^2 laser. b, d) First order exponential fitting of absorbance of DPBF at 423 nm, for methylene blue and PcNP respectively. e) Absorbance curves of PcNP and MB between 700 – 1000 nm.

Singlet oxygen generation quantum yield (ϕ_Δ) of a material is described as the measurement relating to the efficiency in which photosensitizers are able to absorb light and convert oxygen in the ground state to an excited singlet state referred to as singlet oxygen. The ϕ_Δ of PcNP ($\phi_{\Delta(\text{PcNP})}$) was calculated by indirect chemical means using 1,3-diphenylisobenzofuran (DPBF). One of the most well-known is compound 1,3-diphenylisobenzofuran (DPBF). Its sensitized oxygenation forms o-dibenzoylbenzene when reacted with singlet oxygen.[257] The quenching of DPBF and the formation of the product o-dibenzoylbenzene can be checked spectroscopically. It is a good detector of PDT as it only reacts with $^1O_2$ rapidly, without reacting with ground state oxygen or O^{2-}.[257] Methylene Blue (MB) was used as the standard as it is water soluble, has some absorption around the 730 nm range, and its ϕ_Δ is well documented in various literatures.[258,259]

Firstly, the optical density at 730 nm for PcNP and MB was ensured to be similar as shown in Figure 17e. The absorbance curves at various time intervals were recorded in Figure 17a and c respectively for MB and PcNP respectively. Subsequently, the absorbance values at 423 nm were plotted against time and the trend was fitted using first order exponential decay to obtain the time to decay for MB and PcNP (Figure 17b,d). The time to decay for MB (t_{MB}) was analysed to be 540 seconds whereas that for PcNP (t_{PcNP}) was anlaysed to be 668 seconds. The calculations for $\phi_{\Delta(\text{PcNP})}$ according to eq (4) are presented as follows:

$$\phi_{\Delta(\text{PcNP})} = \phi_{MB}\left(\frac{t_{MB}}{t_{PcNP}}\right)$$

$$\phi_{\Delta(\text{PcNP})} = 0.52\left(\frac{540.2325}{668.96221}\right)$$

$$\phi_{\Delta(\text{PcNP})} = 0.42$$

$\phi_{\Delta(PcNP)}$ of PcNP was thus calculated to be 0.42, remarkably high for a synthesized organic photosensitizer in aqueous solution.

4.7 Nitrogen adsorption/desorption and pore diameter analysis

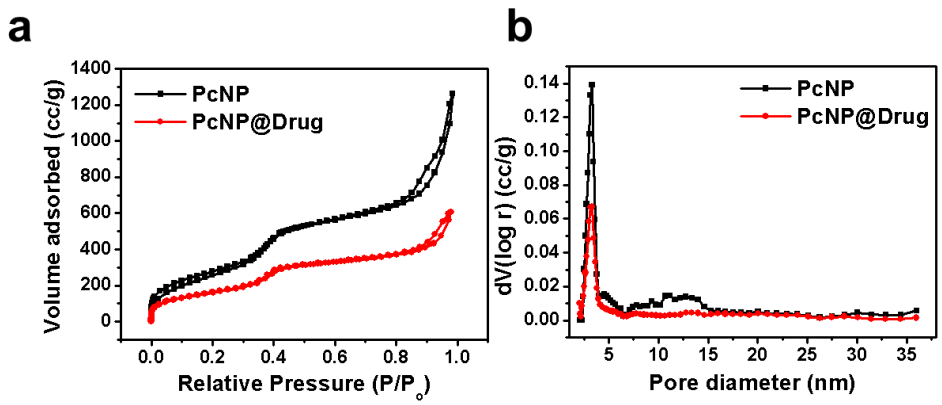

Figure 18. a) N_2 adsorption/desorption curves measured from p/p_0 = 0.05 - 0.2 and b) Pore size distributions of PcNP and PcNP@Drug measured by DFT analysis.

Brunauer–Emmett–Teller (BET) theory is a technique used to analyse physisorption of gas molecules on a solid surface. It is one of the main methods of analysing specific surface area of materials. It is an extension of the Langmuir monolayer theory to explain multilayer adsorption.

A type IV isotherm was obtained by N_2 adsorption/desorption analysis for both PcNP and PcNP@Drug, displaying a pore-condensation step located around p/p_0 = 0.35−0.45 and another one at higher relative pressures of p/p_0 = 0.8−1.0, indicative of uniform mesoporosity with strong interaction between sample surface and nitrogen. (p_0 is the saturation pressure of the adsorptive at measurement temperature).

In type IV adsorption isotherms, there is hysteresis detected in both adsorption and desorption. The shape of the hysteresis loops differs with the shape of mesopores detected. Hysteresis occurs whenever there is capillary

condensation of gas molecules in the mesopore, but the difference in the gas meniscus exists between adsorption and desorption processes. This causes the equilibrium amount of desorption to be larger than the one at adsorption.

The type H1 hysteresis observed at around p/p_0 = 0.8−1.0 is evident of textural mesoporous characteristics of PcNP (Figure 18a).[260] The Brunauer–Emmett–Teller (BET) surface areas were estimated to be 1036 and 597 m^2/g for PcNP and PcNP@Drug, respectively. The high surface areas of the nanoparticles, even after drug loading, could be attributed to their small particle size.

The pore size revealed narrow distributions, peaking at 3.2 nm for both PcNP and PcNP@Drug (Figure 18b). The sorption isotherms retained a similar shape after drug loading, implying no changes in the pore structure during the drug loading. The pore volumes of PcNP and PcNP@Drug were 1.763 and 0.851 cm^3/g respectively, which of PcNP@Drug was lower as a result of the drug occupation. The reduction in the intensity of $d_V/(\log r)$ from 0.14 to 0.06 after the drug loading also indicates that drugs were successfully loaded into the mesopores of PcNP.

4.8 Photostability studies

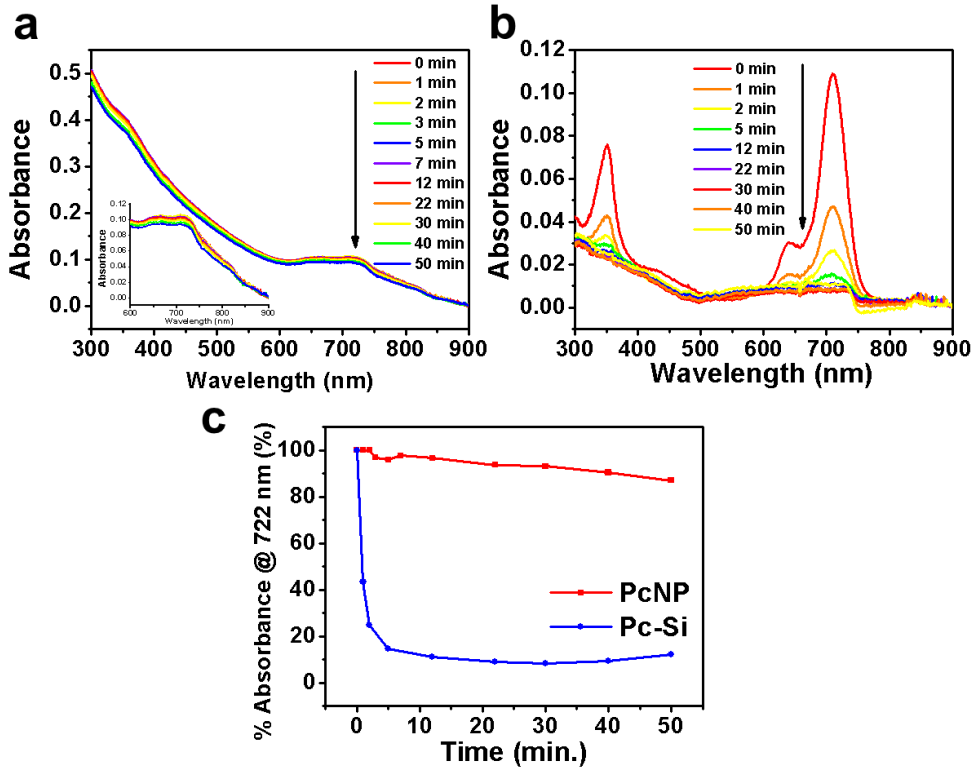

Figure 19. Absorbance curves of a) PcNP and b) Pc-Si upon laser irradiation, reflecting the photostability of PcNP. Inset of a) Absorbance curves of PcNP between 600 – 900 nm. c) Percentage absorbance at 722 nm against irradiation time for PcNP and Pc-Si.

The photostability of photosensitizer is important because PDT is often repeated after a certain time interval. The photosensitizer should be able to retain its PDT properties throughout the whole treatment duration without having to reapply the photosensitizer. One way to test the photostability is through absorbance curves. When photosensitizers photobleach, it is often because of aggregation, which will lower its absorbance profile.

Thus, the photostability of PcNP was investigated by irradiating PcNP and Pc-Si in water was for 50 minutes by 730 nm laser at 1 W/cm^2. The absorbance curves of PcNP and Pc-Si were recorded regularly throughout the irradiation process. The absorbance of PcNP barely quenched even after 50 minutes of

irradiation (Figure 19a). In contrast, the curve for Pc-Si was almost completely quenched, with a huge decrease of 85.3% within the first 5 minutes of irradiation (Figure 19b). The relative absorbance at 722 nm throughout the course of laser irradiation was plotted (Figure 19c), proving that when Pc was incorporated into the framework, its stability was preserved.

4.9 Photothermal behaviour

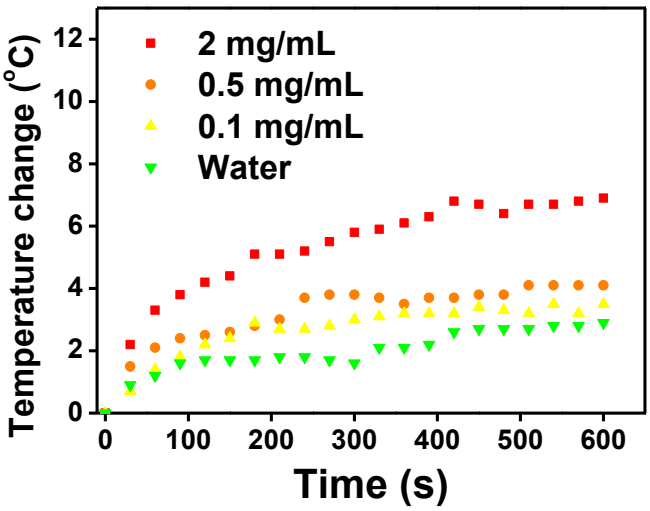

Figure 20. Photothermal behavior of PcNP at 2, 0.5, 0.1 and 0 mg/mL concentrations upon 730 nm, 1 W/cm^2 laser irradiation.

When a material is excited by light energy, the electron gets excited to the S_1 state. After which, the electron can relax back to the ground state via different mechanisms. One of which is fluorescence as discussed in section 4.3 Absorbance and fluorescence behaviour of PcNP. Another way of losing the energy is via radiative heat transfer. A good photosensitizer should produce more singlet oxygen than heat or fluorescence. As discussed earlier, PcNP did not give strong fluorescence, and in this part, the other mode of energy relaxation i.e. photothermal energy, was investigated.

PcNP in aqueous solutions at a series of different concentrations (2, 0.5, 0.1 mg/mL) was tested and corresponding temperature changes were recorded at various time intervals (Figure 20). After 10 minutes of irradiation, the temperature of water was enhanced by 2.9 ^{o}C, and that of 0.1, 0.5 and 2 mg/mL PcNP solutions was only increased by 3.5, 4.1 and 6.9 ^{o}C respectively. However, only a weight concentration of about 0.15 mg/mL of final PcNP or PcNP@Drug was used for cellular experiments. Upon irradiation, this concentration did not give any appreciable temperature rise that would have otherwise been sufficient to cause photothermal damage. Therefore, this observation confirms rather poor photothermal performance of PcNP. Hence, its photodynamic capability was further emphasized.

4.10 Drug loading capacity, encapsulation efficiency and cumulative drug release behaviour

The ratio of Dabrafenib and Trametinib that was loaded in the pores of PcNP was determined by means of the overall cytotoxicity to the targeted mutant melanoma cells as will be described in section 5.1.2 Optimisation of Dabrafenib to Trametinib ratio

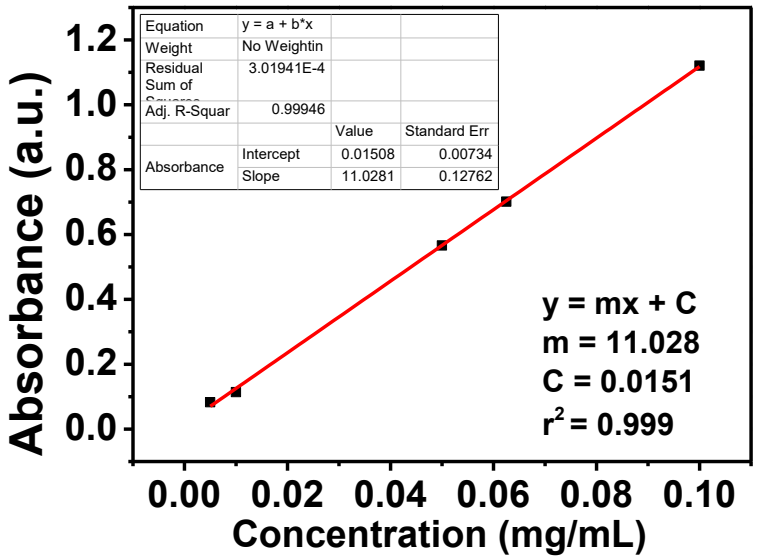

Figure 21. Calibration curve of Dabrafenib and Trametinib mixture.

Determination of DLC and EE

The DLC and EE of PcNP@Drug were calculated against the calibration curve of Dabrafenib and Trametinib which was taken at 334 nm readings (Figure 21). The DLC and EE values were calculated to be 16.2 ± 1.1% and 41.0 ± 1.6%, respectively. The calculations are presented in C0 = concentration of initial drug loading solution (mg/mL)

Table 6.

The gradient of the calibration curve was calculated to be 11.028 and the intercept to be 0.0151 by means of linear fitting. The absorbance readings of Dabrafenib and Trametinib in supernatant and the initial drug loading solution were measured. DLC and EE were calculated according to eq (2) and (3) respectively and the values were tabulated in Table 6 and plotted in Figure 22. Drug loading capacity (DLC) and encapsulation efficiency (EE) of a) Dabrafenib, b) Trametinib and c) Dabrafenib + Trametinib combination, into PcNP.

C_0 = concentration of initial drug loading solution (mg/mL)

Table 6. Tabulation of DLC and EE for different loading concentrations.

C_0	Dabrafenib		Trametinib		Dabrafenib + Trametinib	
	DLC	EE	DLC	EE	DLC	EE
1.0	20.6 ± 1.3%	48.9 ± 1.6%	5.0 ± 1.9%	11.3 ± 0.5%	16.2 ± 1.1%	41.0 ± 1.6%
2.0	22.8 ± 4.7%	31.6 ± 7.1%	8.6 ± 3.0%	16.2 ± 1.3%	19.3 ± 1.9%	24.7 ± 1.5%
5.0	40.6 ± 4.0%	24.9 ± 4.4%	22.9 ± 3.3%	16.8 ± 0.6%	20.8 ± 4.9%	10.9 ± 3.2%
10.0	48.1 ± 2.2%	19.0 ± 1.7%	41.6 ± 2.8%	17.3 ± 1.8%	36.9 ± 7.8%	11.9 ± 3.5%

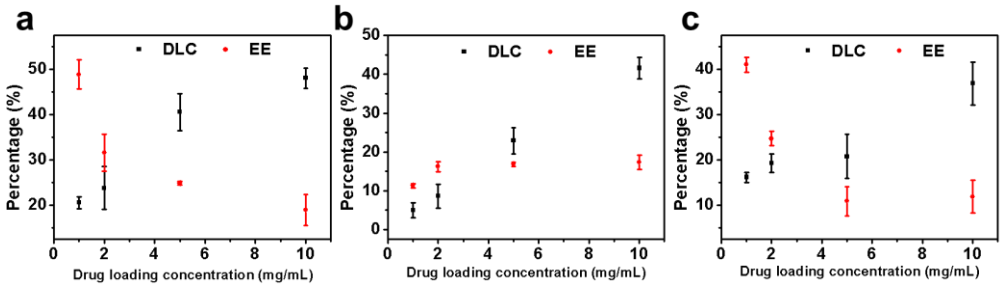

Figure 22. Drug loading capacity (DLC) and encapsulation efficiency (EE) of a) Dabrafenib, b) Trametinib and c) Dabrafenib + Trametinib combination, into PcNP.

For dabrafenib, at 1 mg/mL, the DLC and EE obtained were 20.6 ± 1.3% and 48.9 ± 1.6% respectively. At 10 mg/mL drug loading concentration, the DLC and EE were 48.1 ± 2.2% and 19.0 ± 1.7% respectively. The drug loading appeared to saturate at higher concentrations as the space in the pores were taken up already by drugs. The DLC and EE for Trametinib at 1 mg/mL was 5.0 ± 1.9%

and 11.3 ± 0.5% at 1 mg/mL, and 41.6 ± 2.8% and 17.3 ± 1.8% at 10 mg/mL (Figure 22a,b). These values for trametinib were lower than that for dabrafenib due to its lower solubility in DMSO. When Dabrafenib and Trametinib were loaded in combination, at 1 mg/mL, the DLC and EE were 16.2 ± 1.1% and 41.0 ± 1.63% respectively, and at 10 mg/mL, the values were 36.9 ± 7.8% and 11.9 ± 3.5% (Figure 22c). This drug loading behaviour was a mixture of Dabrafenib and Trametinib loading behaviour.

Determination of molar weight of photosensitizer incorporated in PcNP

A nitrogen weight percentage of 1.19 wt% was derived from elemental analysis results, and the corresponding Pc content in PcNP was calculated to be 53.2 μmol/mg. The calculations are as follows:

Number of N atoms in Pc =16

Atomic number of N = 14

Weight percent of N in PcNP = 1.192%

Initial mass of PcNP = 1 mg

Mass of N = 1 $mg\ x\ 1.192\% = 0.01192\ mg$

Number of moles of N $= \frac{0.01192}{14} = 0.000851429\ mol$

Number of moles Pc in 1 mg PcNP $= \frac{0.000851429}{16} = 5.32143\ x\ 10^{-5}\ mol$

$= 53.2\ \mu mol/mg$

Cumulative drug release behavior

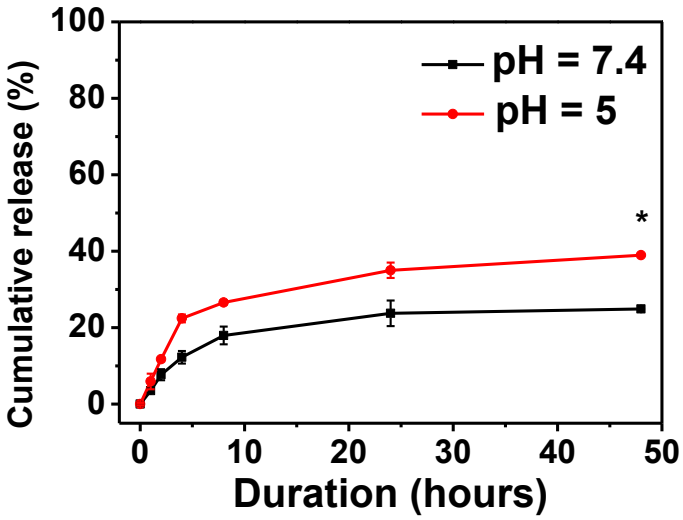

*Figure 23. Cumulative drug release kinetics of PcNP@Drug at pH 7.4 and 5, *p < 0.05.*

As PcNP@Drug is meant to be topically applied, it is essential to know whether there will be any burst release of Dabrafenib and Trametinib from the pores as they may be prematurely released when PcNP@Drug is still on the skin surface, preventing them from reaching the targeted melanoma site. On the other hand, Dabrafenib and Trametinib are very hydrophobic drugs, and there is a possibility that not all the drugs will be released.

The cumulative drug release kinetics of the inhibitors inside PcNP@Drug at different pH levels. At pH 7.4, PcNP@Drug released 3.5% of its payload in the first hour before tapering off to a total of 24.9% after 48 hours. At pH 5, PcNP@Drug released 5.9% in the first hour and a total of 38.9% after 48 hours (Figure 23). This sustained release means that the loaded drugs are not prematurely released in the epidermis of the skin, and PcNP@Drug would be accumulated to a large extent at the malignant sites before the drugs are released to their maximum. Furthermore, the increased drug release at acidic pH is beneficial, as endosome escape can be hastened.

Chapter 5. Cell Culture Experiments

5.1 2D Cell Culture Experiments

5.1.1 Biocompatibility of PcNP as a vehicle

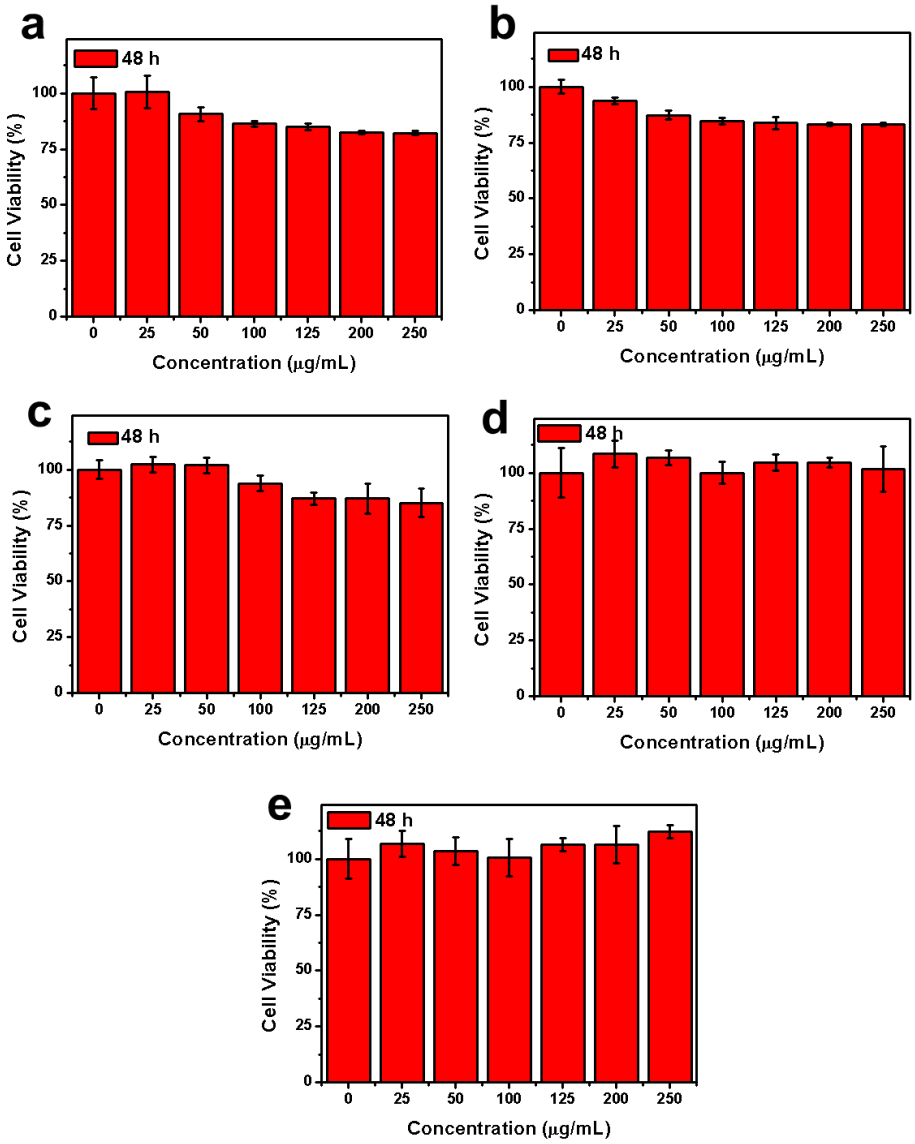

Figure 24. Biocompatibility of PcNP nanoplatform at various concentrations over 48 hours tested on a) A375, b) B16-F10, c) SKMEL-28, d) HDF and e) HEK cell lines.

A good drug delivery system requires the system to only elicit toxicity when allowed to. This means that the delivery vehicle (PcNP) itself has to have

no cytotoxicity in the absence of Dabrafenib, Trametinib, and irradiation. This should last for extended durations and at as high concentrations as possible.

In order to do this, the cell viability of 5 different cell lines were tested 48 hours after the addition of PcNP at various concentrations (Figure 24). The cells used were a mixture of the targeted $BRAF^{V600E}$ mutant A375 and SKMEL-28, $BRAF^{wt}$ B16F10, and the healthy HDF and HEK. This experiment was carried out in the absence of Dabrafenib, Trametinib and in the dark. After 48 hours of incubation, the cells survived well, proving low dark cytotoxicity of PcNP even at high concentrations of up to 250 µg/mL.

5.1.2 Optimisation of Dabrafenib to Trametinib ratio

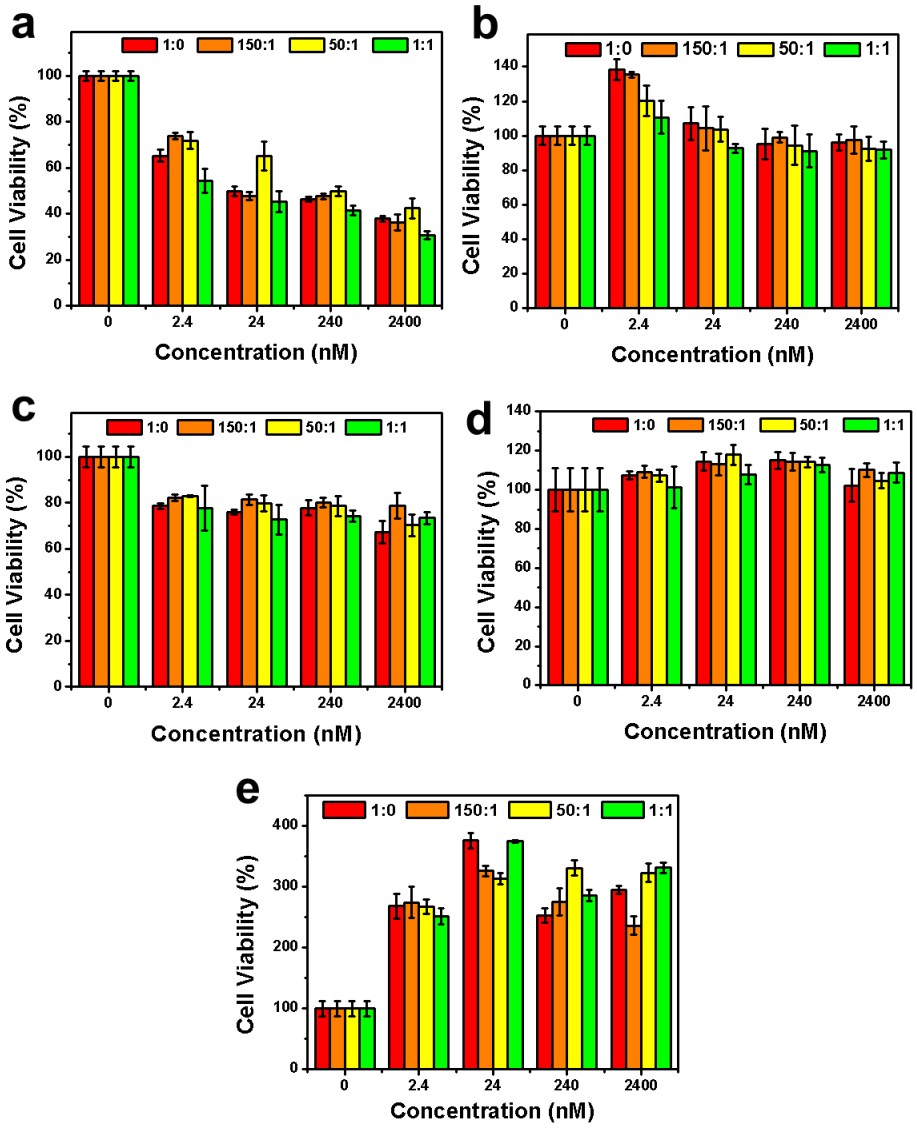

Figure 25. In vitro dosage optimisation results. The various ratios of Dabrafenib to Trametinib (1:0, 150:1, 50:1, 1:1) tested on a) SKMEL-28, b) B16-F10, c) A375, d) HDF and e) HEK cell.

The loading ratio of Dabrafenib to Trametinib into PcNP was decided based on its therapeutic efficacy in the targeted mutant cell line versus its effect on healthy human cells. Clinically, Dabrafenib and Trametinib are administered in a 150:1 ratio daily. Since this ratio was hard to control, we explored different ratios for the best therapeutic efficacy *in vitro*. The drugs were effective in the $BRAF^{V600E}$ mutant cells (SKMEL-28 and A375) (Figure 25a,c), and to a much

lesser extent in $BRAF^{wt}$ cell line B16F10 (Figure 25b). Healthy cells (HDF and HEK) showed no obvious toxicity (Figure 25d,e).

For the B16F10 cell line, at low concentrations of drugs (2.4 nM), the cells slightly proliferated till 138% for 1:0 ratio and 110% for 1:1 ratio (Figure 25b). Subsequently, when increasing the drug concentration, the cell viability remained constant at original value, indicating the specificity of Dabrafenib and Trametinib only to BRAF mutant cells. For HDF (Figure 25d), the cells proliferated only to a much lesser extent than B16F10. Interestingly, for HEK (Figure 25e), the cells proliferated by up to 3.7-folds at a concentration of 24 nM for ratios of 1:0 and 1:1. This interesting behavior was explained by a previous study that low concentrations of BRAF inhibitors can lead to the proliferation of keratinocytes[261] and they helped in wound healing too.[262]

This study indicates the specificity of Dabrafenib and Trametinib only to BRAF mutant cells. For all cell lines, the therapeutic efficacy was not vastly different when the ratio of Dabrafenib to Trametinib was varied. As such, a ratio of 1:1 was used for subsequent *in vitro* experiments.

5.1.3 Time-dependent intracellular internalization of nanovehicles

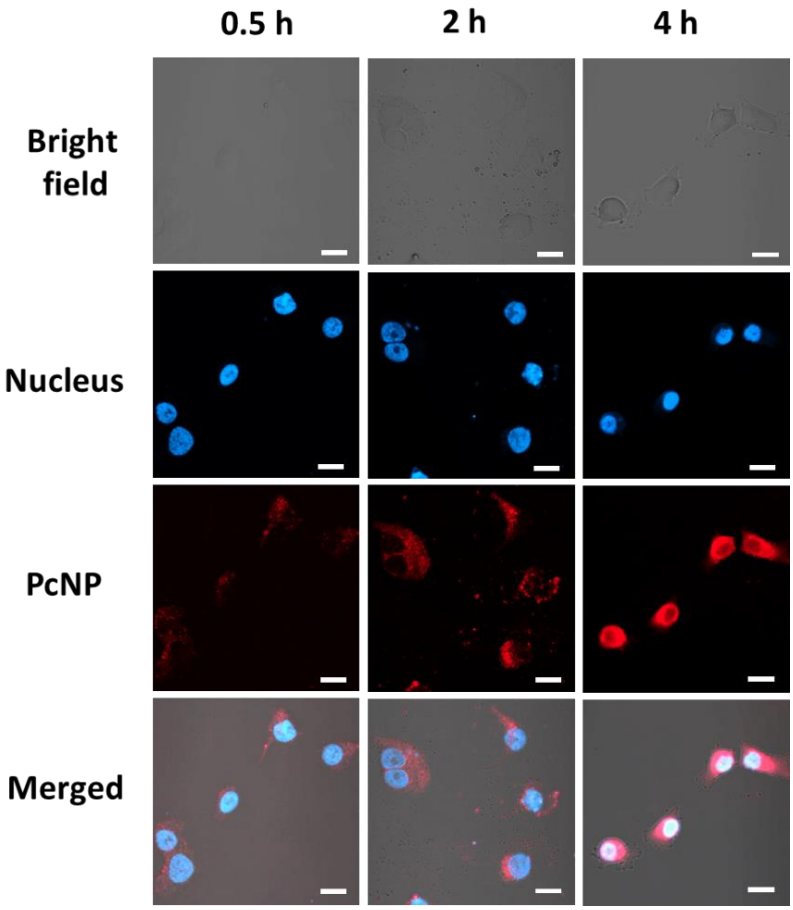

Figure 26.Time-dependent cellular internalization of PcNP in A375 cells after incubation for 0.5h, 2h, and 4h. Blue channel: Hoechst 33342 filter indicating nucleus location. Red channel: nanovehicle location. λex: 488 and 561 nm, λem: 565 – 700 nm. Scale bar = 20 µm

Next, the time-dependent internalization of PcNP was conducted to find out if PcNP will enter melanoma cells and also how long it will take. Thus, the experiment was conducted on A375 cells and imaged using CLSM. The red fluorescence detected was from the weak innate fluorescence of the pthalocyanine photosensitizer incorporated in PcNP. The blue fluorescence is attributed to Hoechst 33342, the cell nuclei dye.

The results in Figure 26 showed that PcNP was internalized into the cytoplasm of the cells as quick as within 0.5 hour as observed from the red

fluorescence surrounding the blue nucleus and overlaying the cell cytoplasm in the merged image. The cells also showed a gradual uptake increase over time, as evidenced by gradual stronger red fluorescence in the PcNP channel at 2 hours compared to 0.5 hours. Within 4 hours, the red fluorescence in cell cytoplasm was the strongest and interestingly, PcNP were observed to translocate into the nuclear region. Previous studies have shown that silica-based nanovehicles of similar charge and size could undergo clathrin-mediated endocytosis,[263,264] and are capable of entering the nucleus.[263]

5.1.4 Cell viability studies

Table 7. Summary table of treatment names and their descriptions.

Treatment name	**Description**		**Intended effect**
	Irradiation	Dabrafenib/Trametinib	
PcNP -hv	✗	✗	No toxicity
PcNP +hv	✓	✗	PDT
PcNP@Drug -hv	✗	✓	Targeted therapy
PcNP@Drug +hv	✓	✓	PDT & Targeted therapy

Table 7 summarises the treatment names, the conditions of treatment as well as the intended effect which will be used for *in vitro* and *in vivo* experiments subsequently.

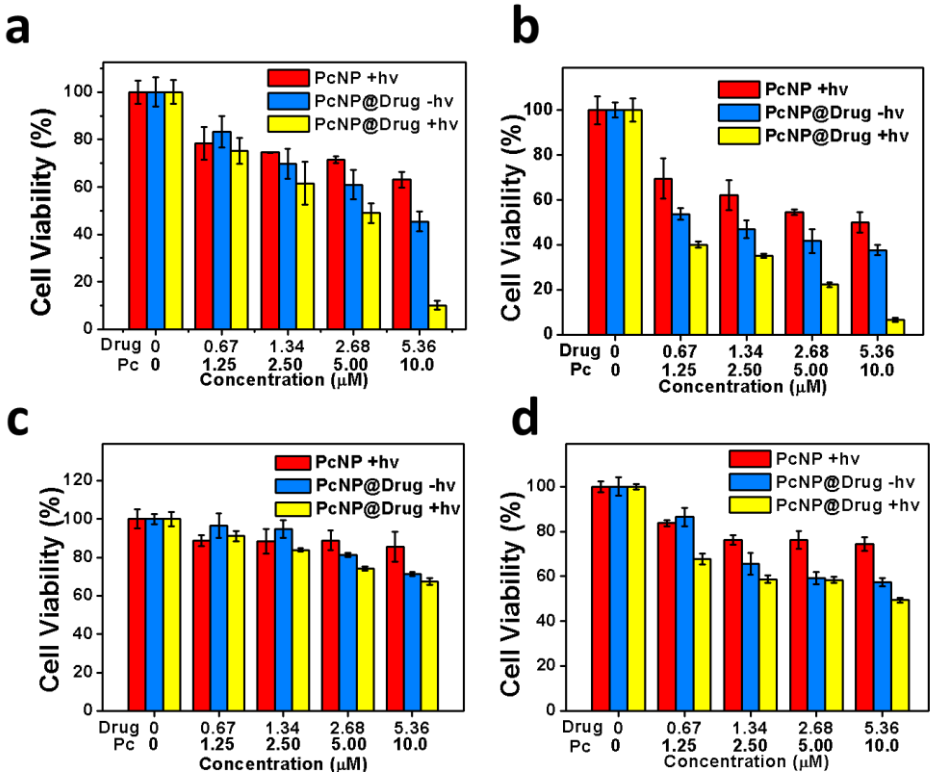

Figure 27. Cell viability of a) A375, b) SKMEL-28, c) HDF, and d) B16F10 cell lines. Incubation time: 16 hours, irradiation of 8 min/well.

The therapeutic effect on different cell lines by PcNP@Drug was tested using A375, SKMEL-28, B16F10 and HDF cell lines, of which A375 and SKMEL-28 are the targeted BRAF mutant cell lines, and B16F10 is wild-type melanoma. Combinational therapeutic effect of PcNP@Drug +hv was compared against single treatment of PDT (PcNP +hv) or targeted therapy (PcNP@Drug -hv) alone. In both SKMEL-28 and A375 cell lines at all concentrations, the combination treatment was able to kill more cells than single treatment (Figure 27b,a). This therapeutic effect was more pronounced at higher concentrations, where the cell viability decreased to 10.0% and 6.2% for A375 and SKMEL-28 cells respectively, corresponding to 5.36 μM drug and 10.0 μM Pc. The effect on B16F10 was rather limited as well due to the non-specificity of Dabrafenib and Trametinib to $BRAF^{wt}$ (Figure 27d). The effect of single PcNP +hv treatment was

limited as observed by the plateau effect even increasing the concentration. HDF cells were rather resistant to the treatment, only showing a slight decrease to 67.5% cell viability at the highest concentration (Figure 27c). This observation proves that topical treatment of PcNP@Drug would not affect the dermis layer of the skin as compared to the targeted melanoma cells, should it penetrate deeply. The combination treatment showed a synergistic effect (combination index = 0.79 for A375 at IC35, and 0.51 for SKMEL-28 at IC50) as calculated by the Chou-Talalay method, indicating an efficient therapy for the targeted cells. The synergistic effect was detected in A375 with treatment equivalent to at least 1.25 µM Pc and 0.67 µM drug, whereas it was efficient for SKMEL-28 under all concentrations used. The combination index plots are presented in Figure 28 below. The combination index plots for B16F10, HEK and HDF were not shown as IC50 was not achieved.

It was also observed that the ROS generation from PcNP +hv in the combination treatment was toxic toward HEK cells (data not shown), similar to other studies.[265,266] As such, we minimized the nanovehicle accumulation in the epidermis with the help of an MN patch as will be discussed later.

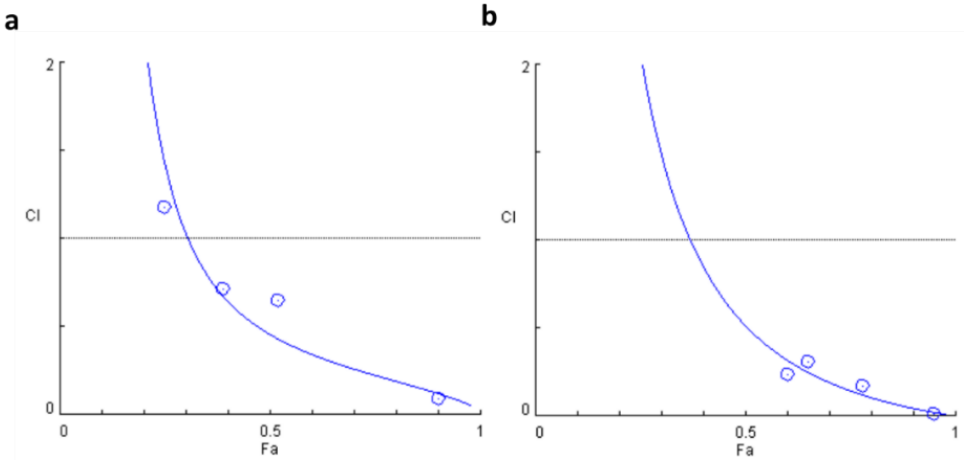

Figure 28. Combination Index plots for a) A375 and b) SKMEL-28 cell lines.

5.1.5 Live/dead confocal assay

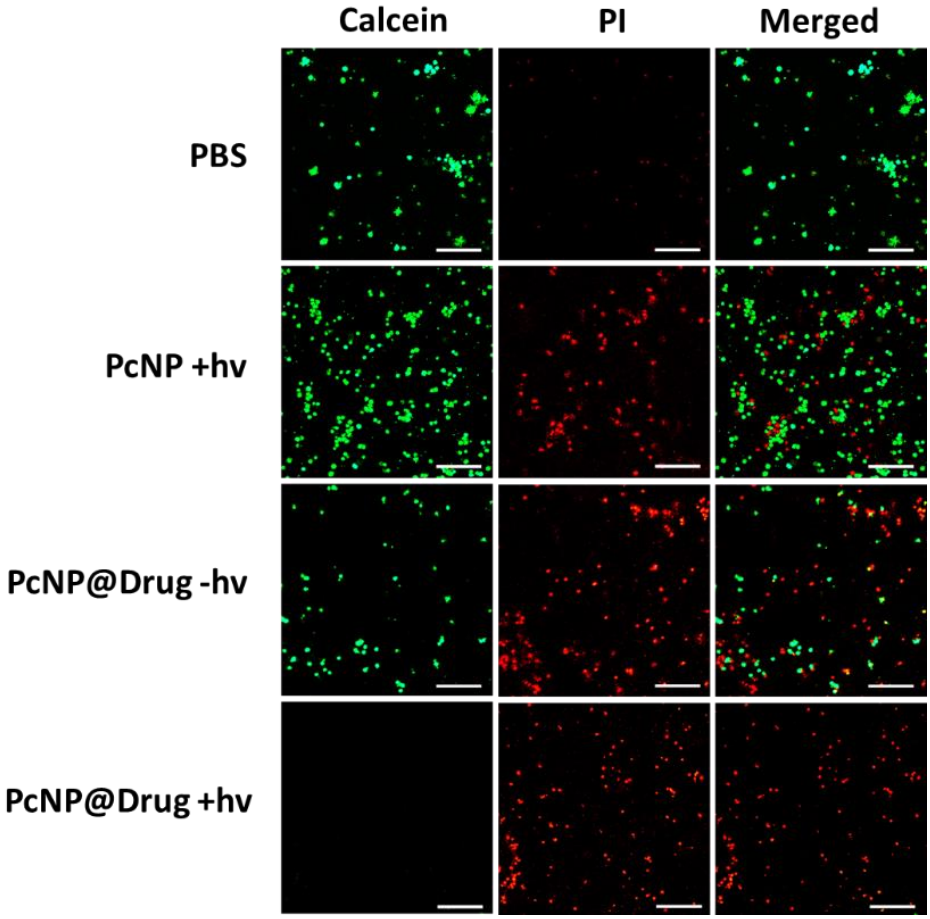

Figure 29. Live/dead cellular imaging of SKMEL-28 cell line for PcNP +hv (PDT), PcNP@Drug-hv (targeted therapy), and PcNP@Drug +hv (combinational treatment). Cells were incubated with PcNP or PcNP@Drug for 4 hours. Irradiation: 730 nm, 0.5 W/cm^2 laser for 15 minutes. λ_{ex}: 640 nm, λ_{em}: 650 – 700 nm. Scale bar = 200 µm.

To give a more visual representation of cell death upon treatment of PcNP or PcNP@Drug, the live/dead cellular assay was conducted and analysed using CLSM and the results reported in Figure 29. The green fluorescence is generated when intracellular esterase activity is detected. Calcein AM is a non-fluorescent molecule that can permeate through cell membranes and the intracellular esterases will remove ester groups and make the molecule fluoresce (reduced to calcein). PI on the other hand, does not permeate through healthy cell membranes

but will cause any cell with damaged cell membranes to be stained red. It binds strongly to DNA and causes the fluorescence to increase by >30-fold. So, green fluorescence indicates live cells and red fluorescence is indicative of dead cells.

Negative PBS control showed no visible presence of dead cells with no obvious red fluorescence in both the PI and merged channel. PcNP with irradiation (PcNP +hv) and PcNP@Drug without irradiation (PcNP@Drug -hv) showed some red fluorescence in the PI channel, but also green fluorescence was still detected in the Calcein channel, hence depicting some but not total cell death, as seen in the merged channel. However, in the case of PcNP@Drug with irradiation (PcNP@Drug +hv), there was no green fluorescence but a strong red fluorescence in the PI and merged channel, suggesting complete cell death.

5.1.6 *In vitro* oxidative stress confocal assay

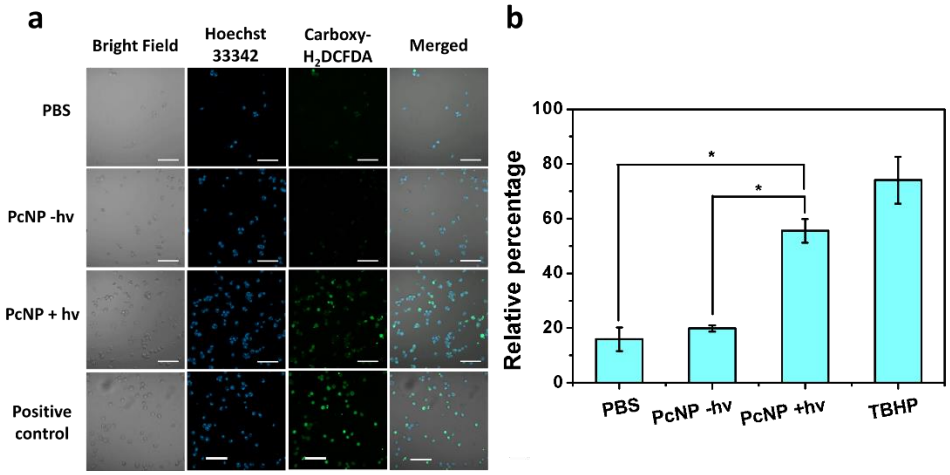

Figure 30. Mechanisms of cell deaths. a) In vitro cellular oxidative stress imaging of SKMEL-28 cell line for PcNP in the absence and presence of NIR light. Hoechst 33342 = nucleus location, and carboxy-H_2DCFDA = oxidative stress. Scale bar = 200 µm. b): Quantitative measurement of the oxidatively-stressed cells vs number of cells present (n=3).

Next, it is important to know if the cell deaths were caused by PDT, or in other words, if the photosensitizer incorporated inside PcNP produced any ROS

and whether it occurred in the presence or absence of light (Figure 30a). 6-carboxy-2',7'-dichlorodihydrofluorescein diacetate (carboxy-H_2DCFDA) is a reduced form of fluorescein used to detect *in vitro* ROS. When this non-fluorescent molecule has its acetate groups removed by intracellular esterases and after oxidation by *in vitro* ROS, it immediately becomes fluorescent. Therefore, green fluorescence in the carboxy-H_2DCFDA channel indicates that oxidative stress was detected. The cell nuclei were stained with Hoechst 33342, a cell nucleus dye. In the PBS control and PcNP in the absence of light (PcNP –hv), no observable green fluorescence was detected, suggesting low dark toxicity of PcNP. When PcNP was added and irradiated by NIR light (PcNP +hv), green fluorescence was observed in the cytosol, which merged well with the location of each cell due to overlap with the blue fluorescence arising from cell nuclei. This observation was similar to the positive control experiment done using tert-Butyl hydroperoxide (TBHP) that induces oxidative stress chemically *in vitro*.

Quantitative assessment (Figure 30b) shows that, in the PBS and PcNP -hv groups, only about 15% and 19% cells exhibited visible green fluorescence in the green channel, respectively. Significantly, a huge increment to 55% cells became oxidatively stressed after the irradiation, conforming that Pc in PcNP was only activated in the presence of light and responsible for producing the reactive oxygen species. The TBHP positive control displayed 74% of cells that were oxidatively stressed.

5.1.7 Caspase 3 activity assay

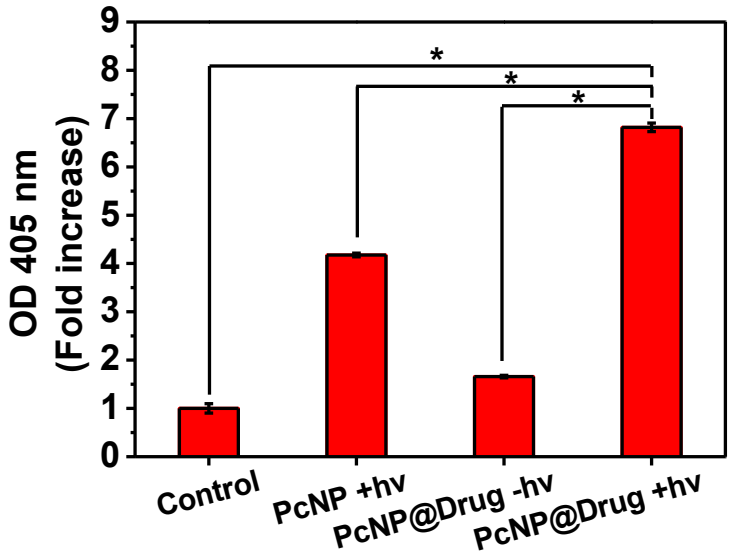

*Figure 31. Detection of caspase 3 activity in A375 cells upon various nanovehicle treatments. (n=3), *p < 0.005.*

Next, the mode of cell death was investigated. It is hypothesized that the main cell death mechanism is apoptosis as it is widely accepted according to section 2.2.1 Mechanism of PDTApoptosis is initiated by proteases known as caspases. These caspases cleave specific substrates in the cell, which leads to the propagation of pro-apoptosis signals. Caspases are detected in the cell lysate once apoptosis is initiated. The caspase 3 assay is developed because hydrolysis of the substrate acetyl-Asp-Glu-ValAsp p-nitroanilide (Ac-DEVD-pNA) by caspase 3 releases p-nitroaniline (pNA), which absorbs strongly between 400 – 405 nm. The amount of the released pNA can be derived using optical densities at 400 or 405 nm.[267]

The activity of crucial caspase 3 protein was then determined to test the apoptotic activity of cells upon different treatments (Figure 31). Under PcNP +hv treatment, the cells displayed a 4.1-fold increase in caspase 3 protease. When

treated with PcNP@Drug -hv, this increase was 1.6-fold. Upon PcNP@Drug+hv treatment, the caspase 3 protease increased by 6.8-fold over the control, further indicating effective combination treatment and also apoptosis being a mechanism of cell death.

5.2 3D cell culture

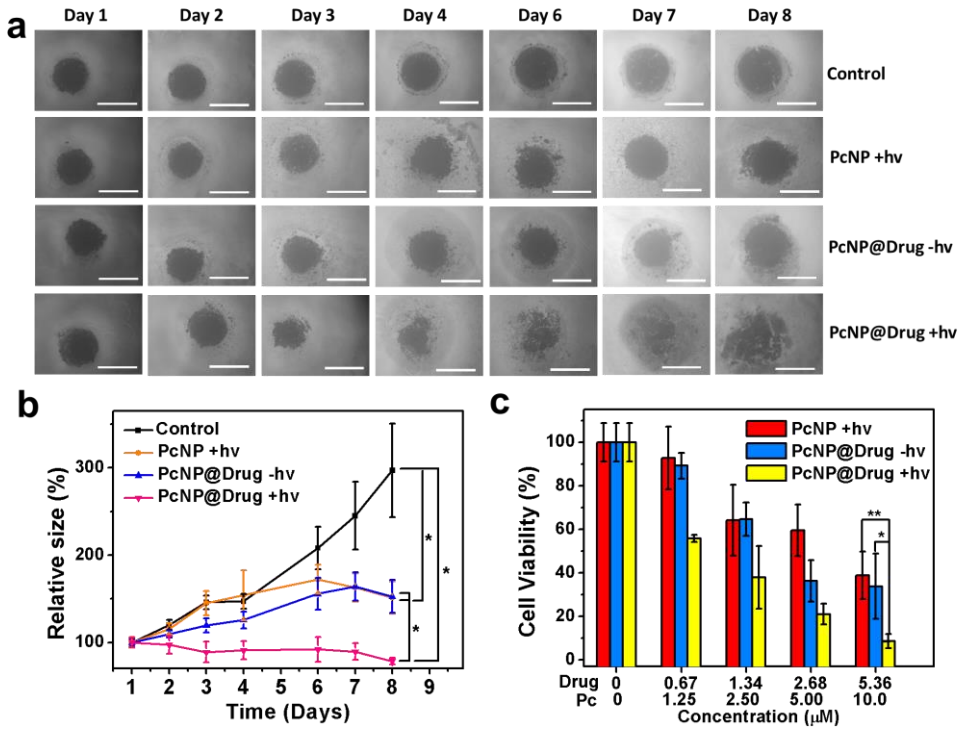

*Figure 32. Efficacy of PcNP on 3D tumour spheroids. a) Microscopic images of representative tumour spheroids receiving different treatments upon time. Scale bar = 500 μm. b) Relative tumour size chart. Error bar represents standard error of mean, *p < 0.05 (n = 5). c) Viability of tumour spheroids conducted using acid phosphatase assay. Error bar represents standard deviation, *p < 0.05, **p < 0.001 (n = 5).*

To show that the synthesized nanosystem is not only effective on 2D cell culture but has prospects to treat solid tumours, 3D spheroids were cultured to mimic the microenvironment of tumours. The spheroids were cultured using 8000 cells per droplet in 1% Matrigel by hanging drop method and left to grow

for 3 weeks. When the spheroids reached a diameter of about 400 μm, treatment commenced.

The digital photographs indicate that the control group of spheroids without any treatment increased in size steadily from 470 μm to 670 μm (Figure 32a). The spheroids receiving single treatment of either PcNP +hv or PcNP@Drug -hv grew slightly in size. The spheroids receiving the combination PcNP@Drug +hv treatment presented the best performance, with their size shrinking from day 3 of treatment and disaggregating from day 4 onwards. The radius of the spheroids shrank from an average of 502 μm to 452 μm over 8 days. The corresponding volumes of the spheroids were calculated according to eq (5) and their relative sizes were plotted (Figure 32b). At the end of the treatment, the combinational PcNP@Drug +hv was significantly more effective than single treatments and control group ($p < 0.05$). The cell viabilities of the spheroids were also analyzed using an acid phosphatase assay, as reported in several studies.[268,269] Across all concentrations, the combination PcNP@Drug +hv treatment was shown to have much better cell-killing efficacy than PcNP +hv or PcNP@Drug -hv alone. At the highest concentration, the cell viability of the spheroids receiving single treatment dropped to 39% and 33%, respectively. Conversely, the cell viability of the combination treatment was much lower at 8% (Figure 32c).

Chapter 6. Skin penetration studies

6.1 *Ex vivo* skin permeation top-view analysis

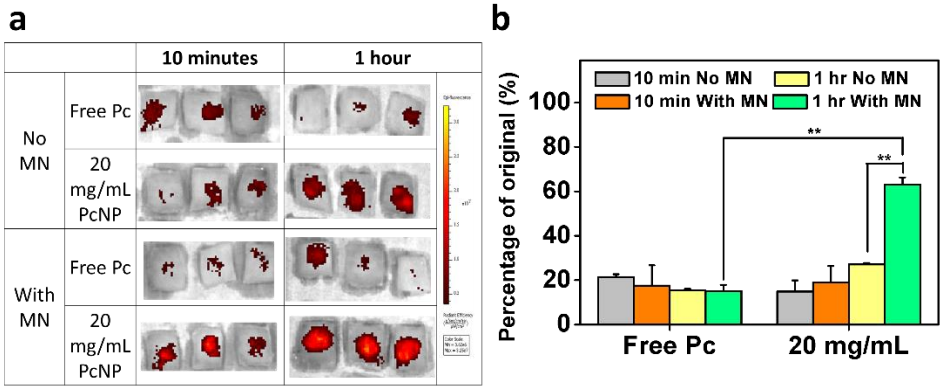

*Figure 33. Topical penetration of PcNP on porcine skin. a) Fluorescence of permeated PcNP (20 mg/mL) versus free Pc on fresh porcine skin for 10-minute and 1-hour durations with and without the MN assistance. λex: 620nm. λem: 640–700 nm. b) Intensity of the luminescence on the porcine skin tabulated into a graph. **p < 0.01.*

Microneedle (MN) patch was used to improve the penetration of PcNP into the stratum basale to bypass the keratinocytes, where PDT was found to be cytotoxic. MN patch was chosen as its penetration depth can be controlled by means of the needle length. The surface area of coverage and number of pores formed can also be controlled by the design before fabrication. MN can also be chosen to be solid/hollow/dissolving or stainless steel/polymer depending on the application required. Physical penetration methods would be preferred as chemicals may react with the drug/nanovehicle and could even work against it. Amongst the various physical penetration enhancing methods presented in section 2.6.3.2 Physical penetration methods, MN presents the simplest method of physical penetration without damaging the skin and has been tested to be pain-free compared to hypodermic needles. The MN patch used is commercially available and made of stainless steel.

In order to test the improvement in penetration by using MN patches, full-thickness porcine skin was used as a model for human skin as it is known to be the closest substitute to human skin.[71,270] The penetration depth and amount of PcNP was measured by means of IVIS imaging for the top-down measurement and CLSM for cross-section analysis. The penetration of PcNP was tested against free Pc, with and without the help of MN patch.

Following the topical application of PcNP or Pc with or without the help of MN patches, IVIS *ex vivo* imaging (Figure 33a) and histological analysis of the skin samples was carried out. At 10 minutes, there was no significant difference of particle signals between the untreated and MN-treated skin samples (Figure 33a,b). However, 1 hour later, the signal on MN-treated samples increased dramatically. The amount permeated was 27.2% and 63.1% without and with an MN, respectively. We did not observe significant change of NP penetration when there was no MN treatment. This indicates that it took 1 hour for PcNP to penetrate and distribute in the skin layers. Interestingly, there was minimal skin penetration of free Pc, regardless of the MN treatment. This should be due to the hydrophobicity of the drug, which can't diffuse in the skin layers.

6.2 *Ex vivo* porcine skin cross-section analysis

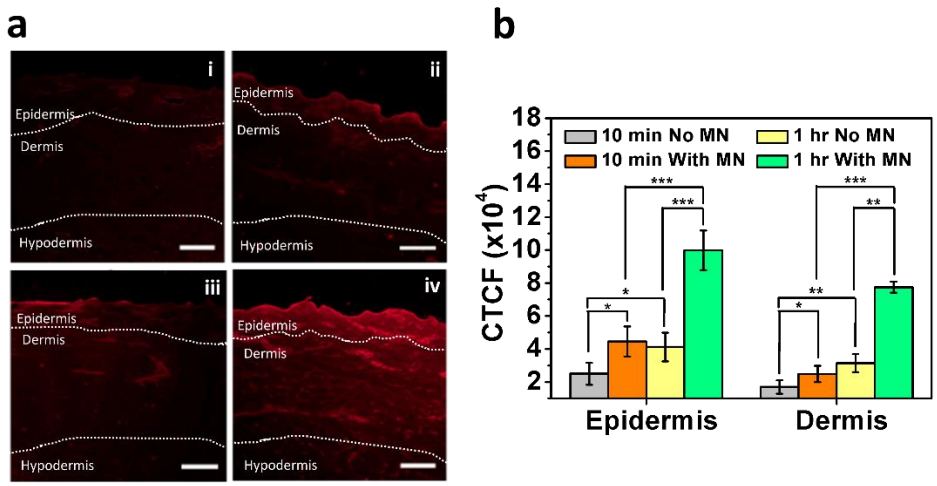

*Figure 34. a) Cross-section images of porcine skin permeated with PcNP (20 mg/mL) for (i) 10 mins without MN, ii) 10 mins with MN, iii) 1 hour without MN, and iv) 1 hour with MN. Scale bar = 200 µm. b) Fluorescence intensity of skin permeated with PcNP (20 mg/mL) for 10 minutes/1 hour, with/without MN. *p < 0.05, **p< 0.01, ***p< 0.005.*

As it is already established that free Pc was unable to penetrate through the skin, the skin that was already treated with the different PcNP, with and without microneedle for 10 minutes and 1-hour durations were fixed and sectioned. We then proceeded to examine the histological samples of the treated skin by its cross section by using confocal imaging (Figure 34a). As shown in Figure 34a(i), there was barely any signal from NPs in skin after the 10-minute topical application of the formulation. This is expected as 10 minutes is too short a time for most materials to pass through. As time for penetration increased to 1 hour, this signal in the epidermis layer increased a bit, as observed from the red fluorescence present in the epidermis in Figure 34a(iii). However, the signal in the dermis layer remained visually unchanged. This indicates that PcNP cannot get into the dermis layer no matter how long they stayed on the skin up till 1-hour duration.

However, when the skin was pre-treated with MNs, the particle signal in the epidermis layer was stronger after 10 minutes (Figure 34a(ii)) as compared to without the MN pre-treatment (Figure 34a(i)). And after 1 hour of treatment, the enhanced fluorescence signal in both epidermis and dermis layers was observed in Figure 34(iv). Interestingly, the signal distributes evenly through each layer, which suggests that PcNP penetrated in the skin through diffusion.

The CTCF in the porcine skin was quantified by taking the average of 4 regions in both the epidermis and dermis of the skin (Figure 34b) and calculated according to eq (6). Initially at 10 minutes and without MN pretreatment, there was not much signal throughout the skin. But with time, a 64% increase in the epidermis and an 85% increase in the dermis was detected. When the skin was pre-treated with MN, the fluorescence signal increased in both the epidermis (78%) and dermis (46%) after 10 minutes. After 1 hour of application, the increase was more prominent in both the epidermis (142%) and the dermis (152%). With time, the signal in the epidermis also increased by 112% and 368% in the dermis when pre-treated with MN. This result positively demonstrates the benefit of using MN in aiding the permeation of the PcNP nanovehicle.

Chapter 7. *In vivo* pilot studies

7.1 Tumour growth chart and tumour growth inhibition

Given the promising potential of the PcNP@Drug nanosystem in both 2D and 3D *in vitro* as well as its penetrating ability through the skin, animal studies were conducted to assess the nanosystem's overall therapeutic ability to treat melanoma. As the targeted cells are of human origin, CrTac:NCr-Foxn1nu mice were chosen as they are immunocompromised "nude" mice, reducing the rejection rate of subcutaneous xenografts. 4-week old mice were separated into 4 groups: control, PcNP +hv, PcNP@Drug -hv and PcNP@Drug +hv.

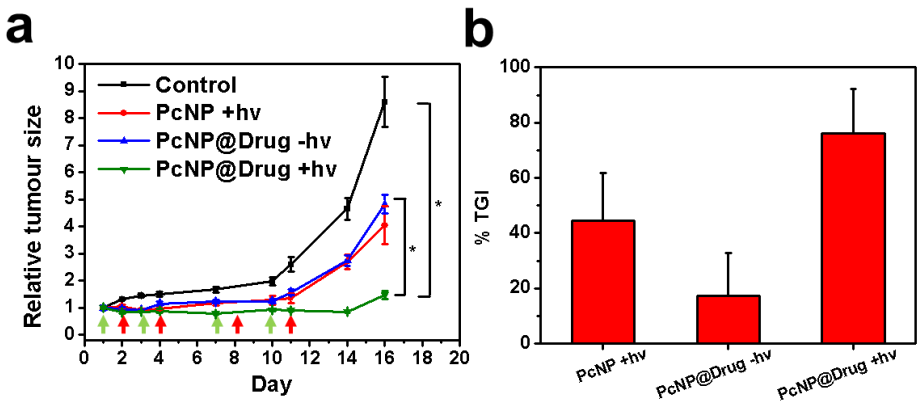

*Figure 35. In vivo antitumoural efficacy of PcNP. a) Relative tumour size growth chart for control, PcNP+hv, PcNP@Drug-hv, and PcNP@Drug+hv combination treatments. Green arrow: nanovehicle treatment, red arrow: laser treatment. *p < 0.05. b) Tumour growth inhibition (TGI) of PcNP +hv, PcNP@Drug -hv and PcNP@Drug +hv treatment groups.*

Using a xenografted tumour mouse model, we examined the anti-tumour efficacy of the drug-loaded nanovehicle (PcNP@Drug) through the combination treatment comprising of PDT, targeted therapy and MNs. The tumour model was established with subcutaneous injection of A375 cells into flanks of 4-week-old homozygous female CrTac:NCr-Foxn1nu mice.[271] When tumours reached a size

of about 5 mm in diameter, MN-assisted nanovehicle (PcNP or PcNP@Drug) treatment was conducted twice weekly for two consecutive weeks (as indicated by green arrow in Figure 35a), followed by laser treatment (as indicated by red arrow in Figure 35a). As shown in the tumour growth curve (Figure 35a), the control group exhibited exponential growth of tumours, while either PcNP+hv or PcNP@Drug-hv treatment alone showed modest inhibition of tumour growth. In comparison, the PcNP@Drug+hv treatment led to significant tumour regression as compared to PBS control or PcNP@Drug-hv alone ($P < 0.05$). In addition, the PcNP+hv and PcNP@Drug-hv groups gave tumour growth inhibition (TGI) values of 44.4% and 17.2% respectively, whereas the PcNP@Drug+hv combination group showed a TGI value of 76.0% (Figure 35b). This was calculated according to eq (7). Since a TGI > 50% is considered meaningful,[272] these data conclude excellent anti-tumour efficacy of the PcNP@Drug nanovehicle.

7.2 Tumour size monitoring

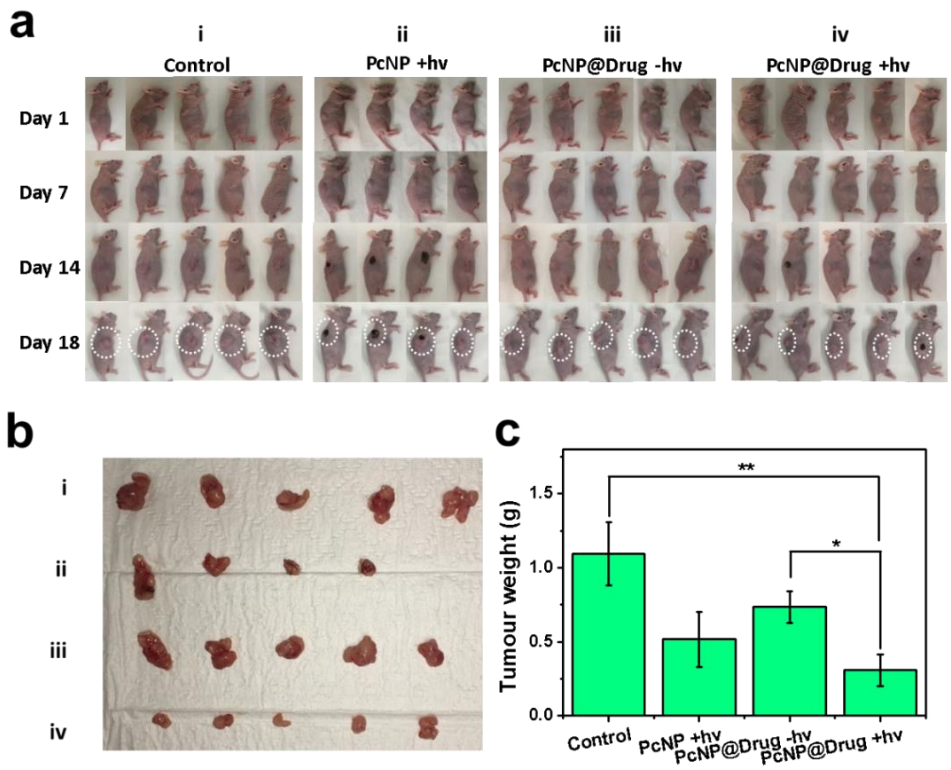

*Figure 36. a) Photographs of mice in the different experimental groups over duration of treatment. b) Photographs of excised tumours (circled in white) showing relative sizes of each group. c) Weights of tumours excised from the mice in different groups. *p < 0.05, **p < 0.01. e) H&E stained images of tumour cross-sections indicating cell nuclei density. (i) Control, (ii) PcNP +hv, (iii) PcNP@Drug -hv and (iv) PcNP@Drug +hv.*

In the control group, tumour sizes enlarged over the whole treatment duration. whereas the tumour sizes significantly shrunk for the PcNP@Drug +hv group (Figure 36a). Three out of the four mice in the group receiving PcNP +hv treatment also showed significant necrosis on the skin covering the tumour. After the course of the study, the mice were sacrificed and tumours were excised and photographed in Figure 36b. The tumours from the PcNP@Drug+hv group were smaller in size than other groups. The tumour weights in the PcNP@Drug+hv group were also significantly lighter than other groups (Figure 36c).

7.3 Hematoxylin and Eosin staining of tumour cross-sections

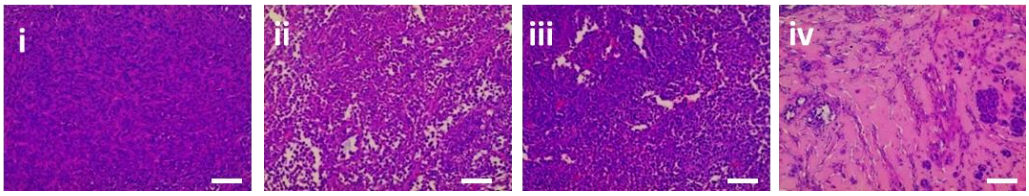

Figure 37. H&E stained images of tumour cross-sections indicating cell nuclei density. (i) Control, (ii) PcNP +hv, (iii) PcNP@Drug -hv and (iv) PcNP@Drug +hv. Scale bar = 50 µm.

H&E staining of tumour sections obtained from the various treatment groups of mice showed severe destruction of cancerous cells in the combination treatment group (PcNP@Drug+hv). The images obtained from single therapy groups (PcNP+hv or PcNP@Drug) displayed only slight damage. This observation confirms the tumour inhibition data and further demonstrates superior efficacy of the combination therapy.

7.4 Body weight of mice

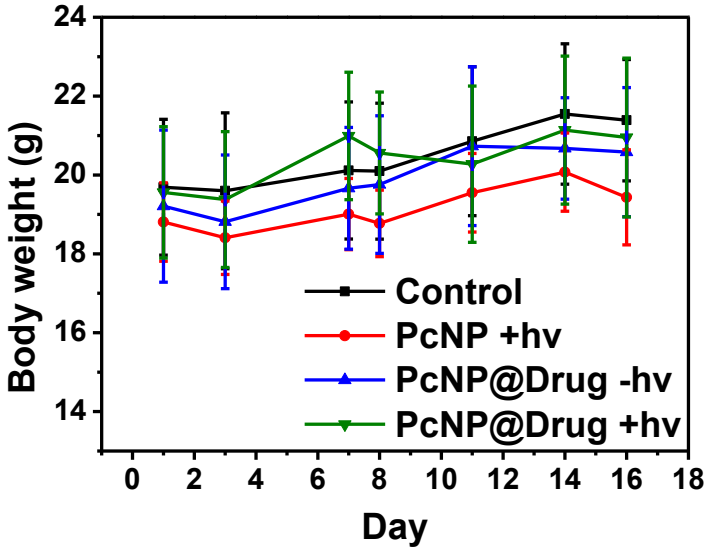

Figure 38. Body weights of mice throughout the duration of treatments. Error bar = standard deviation.

The mice were weighed regularly to ensure that they were healthy and the chart presented in Figure 38. A gradual weight loss could mean that the mice are not coping well and the treatment is too much for them to handle. Overall, the mice displayed a gradual gain in weight across all experimental groups. This can be attributed to the fact that the mice were only 4 weeks old when treatment started and have not reached full size yet. This observation means that all the treatment groups (PcNP +hv, PcNP@Drug -hv and PcNP@Drug +hv) were not detrimental to the overall health of the mice.

Chapter 8. Conclusions and Recommendations

8.1 Conclusions

This chapter summarizes chapters 4, 5, 6 and 7 in sections 8.1.1 Nanoparticle Characterisation, 8.1.2 Cell Culture Experiments, 8.1.3 Skin Penetration Studies, respectively. Section 8.1.5 Overall conclusionsconcludes the entire project with relation to the objectives and hypothesis that the work aimed to address at the start.

Finally, the recommendations and the future outlook are mentioned in section 8.2 Recommendations the future outlook

8.1.1 Nanoparticle Characterisation

In chapter 4, the nanoparticle's composition was optimised by synthesizing a range of different ratios of the 2 silica precursors and testing their ROS generating ability. The best ratio was used for further synthesis of the nanoparticle. Subsequently, the synthesized PcNP and PcNP@Drug were characterised according to various materials characterisations techniques such as absorbance and fluorescence spectra, TEM, DLS, FTIR, XPS, N_2 adsorption/desorption. Its DLC, EE and drug release kinetics were also calculated. Its photostability, photothermal efficiency and finally singlet oxygen quantum yield was also tested.

8.1.2 Cell Culture Experiments

In chapter 5, the biocompatibility of the bare nanoparticles in the absence of Dabrafenib and Trametinib and light irradiation was tested for 48 hours at up to concentrations of 250 µg/mL and were proven to be non-cytotoxic. The

optimisation of the Dabrafenib to Trametinib ratio was also tested by means of cell viability to obtain the best loading ratio to obtain PcNP@Drug.

The time-dependent internalisation of PcNP was also done using CLSM. The cell viability after treatment with PcNP and PcNP@Drug with various controls were done using MTT assays to prove its therapeutic efficacy compared to normal human epidermal keratinocytes and dermal fibroblasts. Live/dead assay was also conducted to prove the therapeutic efficacy. CLSM was also used to detect ROS generated *in vitro* to prove that PDT effect was taking place. Finally, a caspase 3 assay was done to find out the possible mode of death.

Following which, 3D spheroids were cultured to mimic a solid tumour microenvironment in the human body. The 3D spheroids were allowed to stabilise and treatment was started. The efficacy of the treatment was tested by measuring the volume of the spheroids and also by means of acid phosphatase activity. It was proven that the combinational PcNP@Drug +hv was superior to singular treatment of PDT (PcNP +hv) and targeted therapy (PcNP@Drug -hv).

A possible mechanism of action for the death of melanoma cells is depicted in Scheme 1 whereby once PcNP@Drug enters the cell, it starts to release Dabrafenib and Trametinib, which will inhibit the BRAF and MEK pathway respectively. Meanwhile, PcNP releases ROS when shone with NIR light. Both these processes contribute to apoptosis and eventually, cell death.

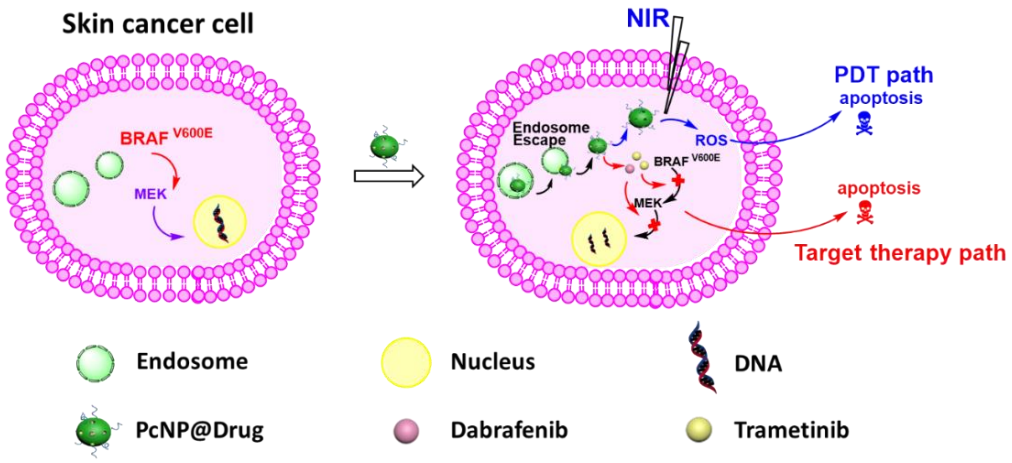

Scheme 5. Possible schematic for the cellular mechanism for the action of PcNP@Drug.

8.1.3 Skin Penetration Studies

Skin penetration studies were also conducted on full-thickness porcine skin, the closest model of human skin, to prove the benefit of using MN and encapsulating photosensitizer in our nanoparticle. The penetration was analysed in two directions: top-down and cross-section. The top-down analysis was done using the IVIS system and the remaining fluorescence was calculated. The cross-section analysis was carried out by sectioning and mounting and the fluorescence was detected by CLSM. We have proved that encapsulating the photosensitizer in the PcNP improved the penetration as compared to free Pc due to its aqueous stability. Also, MN was found to improve the penetration through human skin and possible to reach the dermis region. This means that there would be no problem reaching the melanoma site, which is present at the stratum basale.

8.1.4 *In vivo* pilot studies

Encouraged by the results of the 2D and 3D *in vitro* experiments and the porcine skin topical penetration results, *in vivo* pilot studies were explored. A375 subcutaneous tumours were cultivated in NCr mice and when the tumour size

reached about 100 mm^3, treatment was started using the same experimental groups. A treatment protocol of alternating PcNP/PcNP@Drug treatment and laser irradiation was carried out, and the tumour volumes were measured frequently. Treatment was stopped when the tumour size of the control group exceeded 2000 mm^3. Tumour weight was measured and imaged using H&E staining after sectioning. The *in vivo* studies have shown that the combinational PcNP@Drug +hv treatment was most superior, consistent with the *in vitro* 2D and 3D experiments.

8.1.5 Overall conclusions

In this work, we have synthesized organosilica nanoparticles with Pc covalently incorporated within the framework. The porous photodynamically-active nanoparticles were capable of incorporating inhibitor drugs to enhance therapeutic efficacy. Its small size enables the permeation through skin efficiently, especially with the assistance of a microneedle patch *in vivo*. We have established that the drug loaded PcNP@Drug nanovehicle could successfully deliver a mixture of inhibitors into cancer cells, while it was non-toxic to non-BRAF mutant cells. We have also demonstrated that the nanovehicle aided by MN patch was able to penetrate into skin through the stratum corneum layer and epidermal barrier, as evidenced by the porcine skin permeation experiments and *in vivo* results. *In vivo* studies have proven that the developed PcNP@Drug+hv treatment had exemplary anti-tumour ability, being able to impede the tumour growth when irradiated with 730 nm laser. Therefore, this work presents excellent validation of applying the PcNP@Drug platform against the deadly melanoma disease. This technology platform could be applicable to encapsulate other types of inhibitors or drugs to be released topically. The organic moiety within the platform could

also be replaced with other photosensitizers that absorb at desirable light wavelengths to suit their applications.

To address the objectives stated in section 1.3 Objectives

The first objective was to develop a drug-containing mesoporous organosilica nanocarrier that is pre-conjugated with large molecular weight photosensitizer (i.e. phthalocyanine) and load it with the two inhibitors (Dabrafenib and Trametinib). In Chapter 4. **Nanoparticle Characterisation**, the precursor ratio of TMOS to Pc-Si was optimized, and the subsequent PcNP was synthesized. Pc was proven to be conjugated within the framework of PcNP. The ratio of Dabrafenib to Trametinib was optimized in section 5.1.2 Optimisation of Dabrafenib to Trametinib ratio by MTT assays and the best one was chosen as the drug loading concentration.

The second objective was to test its therapeutic efficacy on $BRAF^{V600E}$ melanoma versus $BRAF^{wt}$ as well as non-cancerous cell lines in the skin. This was achieved as explained and proven in section 5.1.4 Cell viability studies, that PcNP@Drug was effective only on BRAF mutant melanoma cells and to a much lesser extent for the wildtype and HDF. The PDT effect was, however, toxic towards keratinocytes, for which we utilized MN to bypass this top layer.

The third objective was to test its penetration through skin. This was demonstrated in Chapter 6. **Skin penetration studies** and it was also further proven that MN patch was able to enhance this penetration through skin.

And finally, the last objective was to bring this nanoplatform to an *in vivo* platform, and test if it is capable of treating melanoma that is in a living body. This was achieved in

Chapter 7. *In vivo* pilot studies, where topical administration of PcNP@Drug and PcNP were used to treat melanoma in the mice and the therapeutic efficacy of PcNP@Drug +hv was proven to be the most effective.

Thus, the hypothesis to prove that the topically applied nanoparticle can enhance targeted photodynamic therapy to treat mutant melanoma was achieved.

8.1.6 Novelty of project

The novelty of this project is listed here:

1) The first sub-50 nm organic-inorganic mesoporous silica hybrid functionalized with large molecular-weight Pc capable of PDT was synthesized.
2) It is the first time that the topical application of an organic-inorganic mesoporous hybrid nanomaterial has been carried out and proven to be able to treat skin cancer.
3) This system overcomes some of the issues preventing the clinical use of PDT, by enhancing efficacy and skin penetration, as well as selectivity against cancerous tissue.
4) This nanosystem has made a hydrophobic high molecular weight photosensitizer stable in aqueous solutions while maintaining its monomeric state, solving the hydrophobicity-induced aggregation of most photosensitizers which have hindered their implementation in topical treatment of melanoma.

8.2 Recommendations the future outlook

There are a few directions that this project can be extended to. This chapter divides it into three broad areas: (1) nanoparticle synthesis, (2) biological/cellular and (3) application.

8.2.1 Nanoparticle synthesis perspective

8.2.1.1 Silica precursors

In this project, silylated pthalocyanine was used as the photosensitizer to due to its high quantum yield, and also to demonstrate that a high molecular weight photosensitizer can be used in topical treatment of skin cancer, as an alternative to the 5-ALA and MAL used currently in clinics. However, it would be interesting to see if other forms of high molecular weight silylated photosensitizers can be incorporated in the organic-inorganic hybrid's framework. This will produce different quantum yields of the final synthesized products. The size of the nanoparticle product may also differ, affecting the depth of penetration through skin. Also, the wavelength of light required to activate PDT will also differ, which can somewhat be used to control the depth of activation under the skin. Moreover, it would also be interesting to see how the degree of silylation of the photosensitizer will affect the morphology of the final synthesized project. In this project, the photosensitizer Pc-Si had 4 silica end groups to react with TMOS to form PcNP.

8.2.1.2 Dabrafenib and Trametinib

In this project, Dabrafenib and Trametinib were used as the small molecular inhibitors to treat the $BRAF^{V600E}$ melanoma cells. But other forms of inhibitors can be loaded inside PcNP as well. For example, the chemotherapeutic drugs

used in melanoma treatment (fluorouracil, temozolomide or dacarbazine) can actually be loaded inside PcNP. Then the drug-loaded nanoparticle can be administered in the same MN-pretreated way to enhance their topical permeation for an enhanced PDT plus chemotherapy treatment.

Moreover, the outer surface of PcNP can be decorated with antibodies such as ipilimumab (human IgG1 anti-CTLA4 antibody) or lambrolizumab (anti-PD-1 humanised IgG4 antibody) to further improve the targeting ability of the nanovehicle to melanoma cells. This also will stimulate T-cells to the melanoma region to help combat the cancerous cells. The PD-L1ligand upregulated on the surface of antigen presenting cells can also be targeted. CSPG4 overexpressed on 80 – 85% of melanoma lesions can also be targeted.

8.2.2 Biological/cellular perspective

In this project, the $BRAF^{V600E}$ cells used were A375 and SKMEL-28. CLSM was done to test the time-dependent uptake, live/dead assay and ROS-generation ability of PcNP@Drug and PcNP.

8.2.2.1 Cell death mechanism

Caspase 3 assay was done to find out the mode of cell death. However, it can be investigated further if necrosis is one possible mode of death. This can be done by flow cytometry using live cell/apoptosis/necrotic kits.

8.2.2.2 Cell internalization mode

Furthermore, this project has concluded that the nanoparticles were able to enter melanoma cells in a short period of time of half an hour and increased with time. However, more can be done to elucidate the mode of internalization. Literature has proven that nanoparticles of similar size and charge will enter cells

via clathrin-mediated endocytosis[263,264], however it would be good to prove the exact mode pertaining to PcNP using various endocytosis blockers.

8.2.2.3 In vivo studies

The work in this project only covered pilot studies of the nanoparticle's application *in vivo*. Basic tumour growth curves and H&E staining were conducted only. While these were sufficient to prove that PcNP@Drug was sufficient to treat melanoma by topical application, more in-depth studies can be conducted. For example, the various other controls such as PcNP -hv, free Pc, free Dabrafenib + Trametinib, or individually Dabrafenib and Trametinib can be included in the study. Various other parameters can also be varied, such as the duration and intensity of laser irradiation, concentration of nanoparticle solution used, frequency of application or drug-to-light interval.

Furthermore, other modes of administration can also be conducted, such as intratumoural injection or intravenous injection. As Dabrafenib and Trametinib are clinically given orally, it may be beneficial if these inhibitors be allowed to flow in the bloodstream to catch any metastasized cells. Furthermore, due to the existence of EPR effect in intravenous applications, PcNP can locate itself at malignant sites. More in-depth *in vivo* studies can also be studied. For example, it would be interesting to know if PcNP will permeate through the dermis and into the bloodstream. Other tests such as the blood retention time or clearance route of the nanoparticles could be investigated as well. *In vivo* fluorescence imaging of the tumour and the other organs or the whole mouse can also be done.

8.2.3 Applications perspective

8.2.3.1 Optimisaton of topical treatment formulation

It would be advantageous if the synthesized nanoparticles could be optimally formulated in a way ready for direct treatment, such as in creams or gels. The formulation is essential as it helps stabilize the nanoparticles, preventing aggregation, can also increase permeation through the skin and also maintain a steady flux into the skin. Various skin-protection chemicals can also be included within the formulation to help the skin heal after treatment.

8.2.3.2 Integration of MN patch

In this project, it is a three-step treatment, whereby the skin is first pre-treated with MN, secondly, the nanoparticle mixture is added and allowed to permeate. Third and lastly, laser is shone on the tumour site to activate the photosensitizer. It would be more convenient if this treatment can be streamlined into one or two steps. For example, MN can be coated with the nanoparticle formulation and dried. The nanoparticle formulation can also be added into the reservoir of hollow MN patches. And then the nanoparticle-coated MN patch can directly be applied on the skin, saving time and effort and reducing room for error.

In this project, the MN patch used was obtained commercially. In future, different parameters of MN patches can be explored. For example, microneedle arrays of different gap size and length can be tested out to find the optimum penetration efficiency to the malignant site. Polymer MN patches can also be used as a disposable applicator in clinics.

References

(1) Organisation, W. H. Cancer http://www.who.int/cancer/en/ (accessed Mar 29, 2018).

(2) Organisation, W. H. Cancer Fact Sheet http://www.who.int/mediacentre/factsheets/fs297/en/.

(3) Health, M. of. Principal Causes of Death https://www.moh.gov.sg/content/moh_web/home/statistics/Health_Facts_Singapore/Principal_Causes_of_Death.html.

(4) Health Promotion Board, N. R. of D. O. (N.). *Singapore Cancer Registry Annual Registry Report 2015*; 2017.

(5) Lens, M. B.; Dawes, M. Global Perspectives of Contemporary Epidemiological Trends of Cutaneous Malignant Melanoma. *Br J Dermatol* **2004**, *150*, 179–185.

(6) Simões, M. C. F.; Sousa, J. J. S.; Pais, A. A. C. C. Skin Cancer and New Treatment Perspectives: A Review. *Cancer Lett.* **2015**, *357*, 8–42.

(7) *Cancer Facts & Figures*; 2017.

(8) Jorg, R. Sunlight, Vitamin D and Skin Cancer. In *Advances in Experimental Medicine and Biology*; Jorg, R., Ed.; Springer Science+Business Media, Inc, 2008.

(9) Baldea, I.; Filip, A. G. Photodynamic Therapy in Melanoma--an Update. *J. Physiol. Pharmacol.* **2012**, *63*, 109–118.

(10) Welsh, S. J.; Corrie, P. G. Management of BRAF and MEK Inhibitor Toxicities in Patients with Metastatic Melanoma. *Ther. Adv. Med. Oncol.* **2015**, *7*, 122–136.

(11) Zhao, Baozhong; He, Y. Y. Recent Advances in the Prevention and Treatment of Skin Cancer Using Photodynamic Therapy. *Expert Rev Anticancer Ther.* **2010**, *10*, 1797–1809.

(12) Davies, H.; Bignell, G. R.; Cox, C.; Stephens, P.; Edkins, S.; Clegg, S.; Teague, J.; Woffendin, H.; Garnett, M. J.; Bottomley, W.; *et al.* Mutations of the BRAF Gene in Human Cancer. *Nature* **2002**, *417*, 949–954.

(13) Box, N. F.; Vukmer, T. O.; Terzian, T. Targeting P53 in Melanoma. *Pigment Cell Melanoma Res.* **2014**, *27*, 8–10.

(14) Robert, C.; Schachter, J.; Long, G. V.; Arance, A.; Grob, J. J.; Mortier, L.; Daud, A.; Carlino, M. S.; McNeil, C.; Lotem, M.; *et al.* Pembrolizumab versus Ipilimumab in Advanced Melanoma. *N. Engl. J. Med.* **2015**, *372*, 2521–2532.

(15) Long, G. V; Stroyakovskiy, D.; Gogas, H.; Levchenko, E.; de Braud, F.; Larkin, J.; Garbe, C.; Jouary, T.; Hauschild, A.; Grob, J.-J.; *et al.* Dabrafenib and Trametinib versus Dabrafenib and Placebo for Val600 BRAF-Mutant Melanoma: A Multicentre, Double-Blind, Phase 3 Randomised Controlled Trial. *Lancet* **2015**, *6736*, 1–8.

(16) Luke, J. J.; Hodi, F. S. Ipilimumab, Vemurafenib, Dabrafenib, and Trametinib: Synergistic Competitors in the Clinical Management of BRAF Mutant Malignant Melanoma. *Oncologist* **2013**, *18*, 717–725.

(17) Robert, C.; Karaszewska, B.; Schachter, J.; Rutkowski, P.; Mackiewicz, A.; Stroiakovski, D.; Lichinitser, M.; Dummer, R.; Grange, F.; Mortier, L.; *et al.* Improved Overall Survival in Melanoma with Combined Dabrafenib and Trametinib. *N. Engl. J. Med.* **2015**, *372*, 30–39.

(18) Rheault, T. R.; Stellwagen, J. C.; Adjabeng, G. M.; Hornberger, K. R.; Petrov, K. G.; Waterson, A. G.; Dickerson, S. H.; Mook, R. A.; Laquerre, S. G.; King, A. J.; *et al.* Discovery of Dabrafenib: A Selective Inhibitor of Raf Kinases with Antitumor Activity against B-Raf-Driven Tumors. *ACS Med. Chem. Lett.* **2013**, *4*, 358–362.

(19) Hauschild, A.; Grob, J.-J.; Demidov, L. V.; Jouary, T.; Gutzmer, R.; Millward, M.; Rutkowski, P.; Blank, C. U.; Miller Jr, W. H.; Kaempgen, E.; *et al.* Dabrafenib In< I> BRAF</i>-Mutated Metastatic Melanoma: A Multicentre, Open-Label, Phase 3 Randomised Controlled Trial. *Lancet* **2012**, *380*, 358–365.

(20) Croissant, J.; Maynadier, M.; Mongin, O.; Hugues, V.; Blanchard-Desce, M.; Chaix, A.; Cattoën, X.; Wong Chi Man, M.; Gallud, A.; Gary-Bobo, M.; *et al.* Enhanced Two-Photon Fluorescence Imaging and Therapy of Cancer Cells via Gold@Bridged Silsesquioxane Nanoparticles. *Small* **2015**, *11*, 295–299.

(21) Ma, X.; Sreejith, S.; Zhao, Y. Spacer Intercalated Disassembly and Photodynamic Activity of Zinc Phthalocyanine inside Nanochannels of Mesoporous Silica Nanoparticles. *ACS Appl. Mater. Interfaces* **2013**, *5*, 12860–12868.

(22) Slowing, I. I.; Trewyn, B. G.; Giri, S.; Lin, V. S. Mesoporous Silica Nanoparticles for Drug Delivery and Biosensing Applications. *Adv. Funct. Mater.* **2007**, *17*, 1225–1236.

(23) Campos, P. M.; Bentley, M. V. L. B.; Torchilin, V. P. Nanopreparations for Skin Cancer Therapy. In *Nanobiomaterials in Cancer Therapy: Applications of Nanobiomaterials*; 2016; pp. 1–28.

(24) National Cancer Institute. Skin Cancer Treatment (PDQ®)–Health Professional Version https://www.cancer.gov/types/skin/hp/skin-treatment-pdq/ (accessed Apr 30, 2018).

(25) National cancer Centre Singapore. Skin Cancer https://www.singhealth.com.sg/PatientCare/ConditionsAndTreatments/Pages/Skin-cancer.aspx (accessed Apr 9, 2018).

(26) Gloster, H. M.; Brodland, D. G. The Epidemiology of Skin Cancer. *Br. J. Dermatol.* **2002**, *146*, 217–226.

(27) Chandra, A. M. Skin Cancer: Types And Symptoms https://www.healthxchange.sg/cancer/skin-cancer/skin-cancer-types-symptoms.

(28) Akbani, R.; Akdemir, K. C.; Aksoy, B. A.; Albert, M.; Ally, A.; Amin, S. B.; Arachchi, H.; Arora, A.; Auman, J. T.; Ayala, B.; *et al.* Genomic Classification of Cutaneous Melanoma. *Cell* **2015**, *161*, 1681–1696.

(29) Society, A. C. What Is Merkel Cell Carcinoma? https://www.cancer.org/cancer/merkel-cell-skin-cancer/about/what-is-merkel-cell-carcinoma.html (accessed Apr 26, 2018).

(30) Jakob, L.; Metzler, G.; Chen, K.-M.; Garbe, C. Non-AIDS Associated Kaposi's Sarcoma: Clinical Features and Treatment Outcome. *PLoS One* **2011**, *6*.

(31) Radu, O.; Pantanowitz, L. Kaposi Sarcoma. *Arch. Pathol. Lab. Med.* **2013**, *137*, 289–294.

(32) Foundation, C. lymphoma. About Cutaneous Lymphoma | Cutaneous Lymphoma Foundation https://www.clfoundation.org/ (accessed Apr 30, 2018).

(33) Maira, F.; Catania, A.; Candido, S.; Erika Russo, A.; A. McCubrey, J.; Libra, M.; Malaponte, G.; Fenga, C. Molecular Targeted Therapy in Melanoma: A Way to Reverse Resistance to Conventional Drugs. *Curr. Drug Deliv.* **2012**, *9*, 17–29.

(34) Eggermont, A. M. M. Advances in Systemic Treatment of Melanoma. *Ann. Oncol.* **2010**, *21*, vii339-vii344.

(35) Uribe, P.; Gonzalez, S. Epidermal Growth Factor Receptor (EGFR) and Squamous Cell Carcinoma of the Skin: Molecular Bases for EGFR-Targeted Therapy. *Pathol. - Res. Pract.* **2011**, *207*, 337–342.

(36) Oikonomou, E.; Koustas, E.; Goulielmaki, M.; Pintzas, A. BRAF vs RAS Oncogenes: Are Mutations of the Same Pathway Equal? Differential Signalling and Therapeutic Implications. *Oncotarget* **2014**, *5*.

(37) Lovly, C. M.; Dahlman, K. B.; Fohn, L. E.; Su, Z.; Dias-Santagata, D.; Hicks, D. J.;

Hucks, D.; Berry, E.; Terry, C.; Duke, M.; *et al.* Routine Multiplex Mutational Profiling of Melanomas Enables Enrollment in Genotype-Driven Therapeutic Trials. *PLoS One* **2012**, *7*, e35309.

(38) Rubinstein, J. C.; Sznol, M.; Pavlick, A. C.; Ariyan, S.; Cheng, E.; Bacchiocchi, A.; Kluger, H. M.; Narayan, D.; Halaban, R. Incidence of the V600K Mutation among Melanoma Patients with BRAF Mutations, and Potential Therapeutic Response to the Specific BRAF Inhibitor PLX4032. *J. Transl. Med.* **2010**, *8*, 67.

(39) Gray-Schopfer, V. C.; Dias, S. da R.; Marais, R. The Role of B-RAF in Melanoma. *Cancer Metastasis Rev.* **2005**, *24*, 165–183.

(40) Brose, M. S.; Volpe, P.; Feldman, M.; Kumar, M.; Rishi, I.; Gerrero, R.; Einhorn, E.; Herlyn, M.; Minna, J.; Nicholson, A.; *et al.* Mutant V599EB-Raf Regulates Growth and Vascular Development of Malignant Melanoma Tumors. *Cancer Res.* **2005**, *65*, 6997–7000.

(41) Christine M. Lovly; Pao, W.; Sosman, J. BRAF c.1799T>A (V600E) Mutation in Melanoma - My Cancer Genome https://www.mycancergenome.org/content/disease/melanoma/braf/54/ (accessed Apr 10, 2018).

(42) Rushworth, L. K.; Hindley, A. D.; Neill, E. O. '; Kolch, W. Regulation and Role of Raf-1/B-Raf Heterodimerization. *Mol. Cell. Biol.* **2006**, *26*, 2262–2272.

(43) Li, J.; Wang, Y.; Liang, R.; An, X.; Wang, K.; Shen, G.; Tu, Y.; Zhu, J.; Tao, J. Recent Advances in Targeted Nanoparticles Drug Delivery to Melanoma. *Nanomedicine* **2015**, *11*, 769–794.

(44) America, C. T. C. of. Skin Cancer Surgery: Procedures https://www.cancercenter.com/skin-cancer/surgery/ (accessed Apr 27, 2018).

(45) Motley, R.; Kersey, P.; Lawrence, C. Multiprofessional Guidelines for the Management of the Patient with Primary Cutaneous Squamous Cell Carcinoma. *Br. J. Dermatol.* **2002**, *146*, 18–25.

(46) Lovett, R. D.; Perez, C. A.; Shapiro, S. J.; Garcia, D. M. External Irradiation of Epithelial Skin Cancer. *Int. J. Radiat. Oncol.* **1990**, *19*, 235–242.

(47) Gutman, H.; Hess, K. R.; Kokotsakis, J. A.; Ross, M. I.; Guinee, V. F.; Balch, C. M. Surgery for Abdominal Metastases of Cutaneous Melanoma. *World J. Surg.* **2001**, *25*, 750–758.

(48) Leo, F.; Cagini, L.; Rocmans, P.; Cappello, M.; Geel, A. N. Van; Maggi, G.; Goldstraw, P.; Pastorino, U. Lung Metastases from Melanoma: When Is Surgical Treatment Warranted? *Br. J. Cancer* **2000**, *83*, 569–572.

(49) Master, A.; Livingston, M.; Sen, A. Photodynamic Nanomedicine in the Treatment of Solid Tumors : Perspectives and Challenges. *J. Control. Release* **2013**, *168*, 88–102.

(50) Alibakhshi, A.; Abarghooi Kahaki, F.; Ahangarzadeh, S.; Yaghoobi, H.; Yarian, F.; Arezumand, R.; Ranjbari, J.; Mokhtarzadeh, A.; de la Guardia, M. Targeted Cancer Therapy through Antibody Fragments-Decorated Nanomedicines. *J. Control. Release* **2017**, *268*, 323–334.

(51) Rofstad, E. K.; Halsør, E. F. Vascular Endothelial Growth Factor, Interleukin 8, Platelet-Derived Endothelial Cell Growth Factor, and Basic Fibroblast Growth Factor Promote Angiogenesis and Metastasis in Human Melanoma Xenografts. *CANCER Res.* **2000**, *60*, 4932–4938.

(52) Gray-Schopfer, V.; Wellbrock, C.; Marais, R. Melanoma Biology and New Targeted Therapy. *Nature* **2007**, *445*, 851–857.

(53) Manson, G.; Norwood, J.; Marabelle, A.; Kohrt, H.; Houot, R. Biomarkers Associated with Checkpoint Inhibitors. *Ann. Oncol.* **2016**, *27*, 1199–1206.

(54) National Cancer Institute. Drugs Approved for Melanoma https://www.cancer.gov/about-cancer/treatment/drugs/melanoma (accessed Mar 27, 2018).

(55) Pardoll, D. M. The Blockade of Immune Checkpoints in Cancer Immunotherapy. *Nat. Rev. Cancer* **2012**, *12*, 252–264.

(56) Selby, M. J.; Engelhardt, J. J.; Quigley, M.; Henning, K. A.; Chen, T.; Srinivasan, M.; Korman, A. J. Anti-CTLA-4 Antibodies of IgG2a Isotype Enhance Antitumor Activity through Reduction of Intratumoral Regulatory T Cells. *Cancer Immunol. Res.* **2013**, *1*, 32–42.

(57) Robert, C.; Thomas, L.; Bondarenko, I.; O'Day, S.; M D, J. W.; Garbe, C.; Lebbe, C.; Baurain, J.-F.; Testori, A.; Grob, J.-J.; *et al.* Ipilimumab plus Dacarbazine for Previously Untreated Metastatic Melanoma. *N. Engl. J. Med.* **2011**, *364*, 2517–2526.

(58) Sosman, J. A.; Haanen, J. B.; Gonzalez, R.; Robert, C.; Ph, D.; Schadendorf, D.; Hassel, J. C.; Akerley, W.; Eertwegh, A. J. M. Van Den; Ph, D.; *et al.* Improved Survival with Ipilimumab in Patients with Metastatic Melanoma. *N. Engl. J. Med.* **2010**, *363*, 711–723.

(59) Keilholz, U.; Goey, S. H.; Punt, C. J.; Proebstle, T. M.; Salzmann, R.; Scheibenbogen, C.; Schadendorf, D.; Liénard, D.; Enk, A.; Dummer, R.; *et al.* Interferon Alfa-2a and Interleukin-2 with or without Cisplatin in Metastatic Melanoma: A Randomized Trial of the European Organization for Research and Treatment of Cancer Melanoma Cooperative Group. *J. Clin. Oncol.* **1997**, *15*, 2579–2588.

(60) Society, A. C. Local Treatments Other than Surgery for Basal and Squamous Cell Skin Cancers https://www.cancer.org/cancer/basal-and-squamous-cell-skin-cancer/treating/other-than-surgery.html (accessed Apr 26, 2018).

(61) Phase 3 Study of Nivolumab or Nivolumab Plus Ipilimumab Versus Ipilimumab Alone in Previously Untreated Advanced Melanoma (CheckMate 067) - NCT01844505 - National Cancer Institute https://www.cancer.gov/about-cancer/treatment/clinical-trials/search/v?id=NCT01844505&r=1 (accessed Apr 30, 2018).

(62) Dharmadhikari, N.; Mehnert, J. M.; Kaufman, H. L. Oncolytic Virus Immunotherapy for Melanoma. *Curr. Treat. Options in Oncol* **2015**, *16*.

(63) Medicine, N. U. S. N. L. of. Efficacy and Safety Study of Talimogene Laherparepvec Compared to Granulocyte Macrophage Colony Stimulating Factor (GM-CSF) in Melanoma https://clinicaltrials.gov/ct2/show/NCT00769704.

(64) Sadek, H.; Azli, N.; Wendling, J. L.; Cvitkovic, E.; Rahal, M.; Mamelle, G.; Guillaume, J. C.; Armand, J. P.; Avril, M. F. Treatment of Advanced Squamous Cell Carcinoma of the Skin with Cisplatin, 5-Fluorouracil, and Bleomycin. *Cancer* **1990**, *66*, 1692–1696.

(65) Luxenberg, M. N.; Guthrie, T. H. Chemotherapy of Basal Cell and Squamous Cell Carcinoma of the Eyelids and Periorbital Tissues. *Ophthalmology* **1986**, *93*, 504–510.

(66) Khandekar, J. D. Complete Response of Metastatic Basal Cell Carcinoma to Cisplatin Chemotherapy: A Report on Two Patients. *Arch. Dermatol.* **1990**, *126*, 1660.

(67) Boogerd, W.; de Gast, G. C.; Dalesio, O. Temozolomide in Advanced Malignant Melanoma with Small Brain Metastases. *Cancer* **2007**, *109*, 306–312.

(68) Wong, S. L.; Balch, C. M.; Hurley, P.; Agarwala, S. S.; Akhurst, T. J.; Cochran, A.; Cormier, J. N.; Gorman, M.; Kim, T. Y.; McMasters, K. M.; *et al.* Sentinel Lymph Node Biopsy for Melanoma: American Society of Clinical Oncology and Society of Surgical Oncology Joint Clinical Practice Guideline. *J. Clin. Oncol.* **2012**, *30*, 2912–2918.

(69) Shen, P.; Wanek, L. A.; Morton, D. L. Is Adjuvant Radiotherapy Necessary after Positive Lymph Node Dissection in Head and Neck Melanomas? *Ann. Surg. Oncol.* **2000**, *7*, 554-9; discussion 560-1.

(70) Medicine, N. U. S. N. L. of. Multicenter Selective Lymphadenectomy Trial II (MSLT-II) https://clinicaltrials.gov/ct2/show/NCT00297895.

(71) Muizzuddin, N.; Marenus, K. D.; Schnittger, S. F.; Sullivan, M.; Maes, D. H. Topical and Transdermal Drug Delivery: Principles and Practice. In *Journal of cosmetic science*; 2005; Vol. 56, pp. 311–321.

(72) Love, W. E.; Bernhard, J. D.; Bordeaux, J. S. Topical Imiquimod or Fluorouracil Therapy for Basal and Squamous Cell Carcinoma. *Arch. Dermatol.* **2009**, *145*, 1431–1438.

(73) Peikert, J. M. Prospective Trial of Curettage and Cryosurgery in the Management of Non-Facial, Superficial, and Minimally Invasive Basal and Squamous Cell Carcinoma. *Int. J. Dermatol.* **2011**, *50*, 1135–1138.

(74) Agostinis, P.; Berg, K.; Cengel, K. a; Foster, T. H.; Girotti, A. W.; Gollnick, S. O.; Hahn, S. M.; Hamblin, M. R.; Juzeniene, A.; Kessel, D.; *et al.* Photodynamic Therapy of Cancer : An Update. *Am. Cancer Soc.* **2011**, *61*, 250–281.

(75) Fan, W.; Huang, P.; Chen, X. Overcoming the Achilles' Heel of Photodynamic Therapy. *Chem. Soc. Rev.* **2016**.

(76) Silva, Z. S.; Bussadori, S. K.; Fernandes, K. P. S.; Huang, Y.-Y.; Hamblin, M. R. Animal Models for Photodynamic Therapy (PDT). *Biosci. Rep.* **2015**, *35*, e00265.

(77) Garland, M. J.; Cassidy, C. M.; Woolfson, D.; Donnelly, R. F. Designing Photosensitizers for Photodynamic Therapy: Strategies, Challenges and Promising Developments. *Future Med. Chem.* **2009**, *1*, 667–691.

(78) Jaque, D.; Maestro, L. M.; Rosal, B. Del; Haro-Gonzalez, P.; Benayas, A.; Plaza, J. L.; Rodríguez, E. M.; Solé, J. G. Nanoparticles for Photothermal Therapies. *Nanoscale* **2014**, *6*, 9494–9530.

(79) Abrahamse, H.; Hamblin, M. R. New Photosensitizers for Photodynamic Therapy. *J. Biochem.* **2016**, *473*, 347–364.

(80) Chen, B.; Roskams, T.; de Witte, P. a M. Antivascular Tumor Eradication by Hypericin-Mediated Photodynamic Therapy. *Photochem. Photobiol.* **2002**, *76*, 509–513.

(81) Oliveira, C. S.; Turchiello, R.; Kowaltowski, A. J.; Indig, G. L.; Baptista, M. S. Major Determinants of Photoinduced Cell Death: Subcellular Localization versus Photosensitization Efficiency. *Free Radic. Biol. Med.* **2011**, *51*, 824–833.

(82) Garg, A. D.; Nowis, D.; Golab, J.; Vandenabeele, P.; Krysko, D. V.; Agostinis, P. Immunogenic Cell Death, DAMPs and Anticancer Therapeutics: An Emerging Amalgamation. *Biochim. Biophys. Acta - Rev. Cancer* **2010**, *1805*, 53–71.

(83) Chatterjee, D. K.; Fong, L. S.; Zhang, Y. Nanoparticles in Photodynamic Therapy: An Emerging Paradigm. *Adv. Drug Deliv. Rev.* **2008**, *60*, 1627–1637.

(84) Dolmans, D. E. J. G. J.; Dai, F.; Rakesh K., J. Photodynamic Therapy for Cancer. *Nat. Rev. Cancer* **2003**, *3*, 380–387.

(85) Triesscheijn, M.; Baas, P.; Schellens, J. H. M.; Stewart, F. a. Photodynamic Therapy in Oncology. *Oncologist* **2006**, *11*, 1034–1044.

(86) Josefsen, L. B.; Boyle, R. W. Unique Diagnostic and Therapeutic Roles of Porphyrins and Phthalocyanines in Photodynamic Therapy, Imaging and Theranostics. *Theranostics* **2012**, *2*, 916–966.

(87) Dougherty, T. J.; Gomer, C. J.; Henderson, B. W.; Jori, G.; Kessel, D.; Korbelik, M.; Moan, J.; Peng, Q. Photodynamic Therapy. *J. Natl. Cancer Inst.* **1998**, *90*, 889–905.

(88) Wilson, B. C. Photodynamic Therapy for Cancer: Principles. *Can. J. Gastroenterol.* **2002**, *16*, 393–396.

(89) Bonnett, R. Photosensitizers of the Porphyrin and Phthalocyanine Series for Photodynamic Therapy. *Chem. Soc. Rev.* **1995**, 19–33.

(90) Castano, A. P.; Mroz, P.; Hamblin, M. R. Photodynamic Therapy and Anti-Tumour Immunity. *Nat. Rev. Cancer* **2006**, *6*, 535–545.

(91) Jaggi Rao; Robert Bissonnette. Photodynamic Therapy for the Dermatologist https://emedicine.medscape.com/article/1121517-overview#a2 (accessed Mar 28, 2018).

(92) Juarranz, Á.; Jaén, P.; Sanz-Rodríguez, F.; Cuevas, J.; González, S. Photodynamic Therapy of Cancer. Basic Principles and Applications. *Clin. Transl. Oncol.* **2008**, *10*, 148–154.

(93) Vrouenraets, M. B.; Visser, G. W. M.; Snow, G. B.; van Dongen, G. A. M. S. Basic Principles, Applications in Oncology and Improved Selectivity of Photodynamic Therapy. *Anticancer Res.* **2003**, *23*, 505–522.

(94) Capella, M. A. M.; Capella, L. S. A Light in Multidrug Resistance: Photodynamic Treatment of Multidrug-Resistant Tumors. *J. Biomed. Sci.* **2003**, *10*, 361–366.

(95) Zhang, Y.; Lovell, J. F. Porphyrins as Theranostic Agents from Prehistoric to Modern Times. *Theranostics* **2012**, *2*, 905–915.

(96) G. Steven Martin. Cell Signaling and Cancer. *Cancer Cell* **2003**, *4*, 167–174.

(97) Di Malta, C.; Siciliano, D.; Calcagni, A.; Monfregola, J.; Punzi, S.; Pastore, N.; Eastes, A. N.; Davis, O.; De Cegli, R.; Zampelli, A.; *et al.* Transcriptional Activation of RagD GTPase Controls MTORC1 and Promotes Cancer Growth. *Science* **2017**, *356*, 1188–1192.

(98) Siena, S.; Sartore-Bianchi, A.; Di Nicolantonio, F.; Balfour, J.; Bardelli, A. Biomarkers Predicting Clinical Outcome of Epidermal Growth Factor Receptor-Targeted Therapy in Metastatic Colorectal Cancer. *J. Natl. Cancer Inst.* **2009**, *101*, 1308–1324.

(99) Gerber, D. Targeted Therapies: A New Generation of Cancer Treatments https://www.aafp.org/afp/2008/0201/p311.pdf (accessed Mar 26, 2018).

(100) Sliwkowski, M. X.; Mellman, I. Antibody Therapeutics in Cancer. *Science (80-.).* **2013**, *341*, 1192–1198.

(101) Malas, S.; Harrasser, M.; Lacy, K. E.; Karagiannis, S. N. Antibody Therapies for Melanoma: New and Emerging, Opportunities to Activate Immunity (Review). *Oncol. Rep.* **2014**, *32*, 875–886.

(102) Zhang, J.; Yang, P. L.; Gray, N. S. Targeting Cancer with Small Molecule Kinase Inhibitors. *Nat. Rev. Cancer* **2009**, *9*, 28–39.

(103) Cohen, P. Protein Kinases--the Major Drug Targets of the Twenty-First Century? *Nat. Rev. Drug Discov.* **2002**, *1*, 309–315.

(104) Weinstein, I. B.; Joe, A. K. Mechanisms of Disease: Oncogene Addiction—a Rationale for Molecular Targeting in Cancer Therapy. *Nat. Clin. Pract. Oncol.* **2006**, *3*, 448–457.

(105) Weinstein, I. B.; Begemann, M.; Zhou, P.; Han, E. K.; Sgambato, A.; Doki, Y.; Arber, N.; Ciaparrone, M.; Yamamoto, H. Disorders in Cell Circuitry Associated with Multistage Carcinogenesis: Exploitable Targets for Cancer Prevention and Therapy. *Clin. Cancer Res.* **1997**, *3*, 2696–2702.

(106) Davies, S. P.; Reddy, H.; Caivano, M.; Cohen, P. Specificity and Mechanism of Action of Some Commonly Used Protein Kinase Inhibitors. *Biochem. J* **2000**, *351*, 95–105.

(107) Da Silva, C. G.; Godefridus, ·; Peters, J.; Ferry Ossendorp, ·; Cruz, L. J. The Potential of Multi-compound Nanoparticles to Bypass Drug Resistance in Cancer. *Cancer Chemother. Pharmacol.* **2017**, *80*, 881–894.

(108) Shah, N. P. Overriding Imatinib Resistance with a Novel ABL Kinase Inhibitor. *Science (80-.).* **2004**, *305*, 399–401.

(109) Louis J. Lombardo,* Francis Y. Lee, P. C.; Derek Norris, Joel C. Barrish, K. B.; Stephen Castaneda, L. A. M. C.; Jagabandhu Das, A. M. D.; Craig Fairchild, John T. Hunt, I. I.; Kathy Johnston, Amrita Kamath, D. K.; Herbert Klei, Punit Marathe, S. P.; Russell Peterson, Sidney Pitt, G. L. S.; Robert J. Schmidt, John Tokarski, M.-L. W.; John Wityak, and R. M. B. Discovery of N-(2-Chloro-6-Methylphenyl)-2-(6-(4-(2-Hydroxyethyl)- Piperazin-1-Yl)-2-Methylpyrimidin-4- Ylamino)Thiazole-5-Carboxamide (BMS-354825), a Dual Src/Abl Kinase Inhibitor with Potent Antitumor Activity in Preclinical Assays. *J. Med. Chem.* **2004**, *47*, 6658–6661.

(110) O'Brien, S. G.; Guilhot, F.; Larson, R. A.; Gathmann, I.; Baccarani, M.; Cervantes, F.; Cornelissen, J. J.; Fischer, T.; Hochhaus, A.; Hughes, T.; *et al.* Imatinib Compared with Interferon and Low-Dose Cytarabine for Newly Diagnosed Chronic-Phase Chronic Myeloid Leukemia. *N. Engl. J. Med.* **2003**, *348*, 994–1004.

(111) Forbes, S.; Clements, J.; Dawson, E.; Bamford, S.; Webb, T.; Dogan, A.; Flanagan, A.; Teague, J.; Wooster, R.; Futreal, P.; *et al.* COSMIC 2005. *Br. J. Cancer* **2006**, *94*, 318–322.

(112) Futreal, P. A.; Coin, L.; Marshall, M.; Down, T.; Hubbard, T.; Wooster, R.; Rahman, N.; Stratton, M. R. A Census of Human Cancer Genes. *Nat. Rev. Cancer* **2004**, *4*, 177–183.

(113) Velu, T.; Beguinot, L.; Vass, W.; Willingham, M.; Merlino, G.; Pastan, I.; Lowy, D.; Bridges, A. Epidermal-Growth-Factor-Dependent Transformation by a Human EGF Receptor Proto-Oncogene. *Science (80-.).* **1987**, *238*, 1408–1410.

(114) Osherov, N.; Levitzki, A. Epidermal-Growth-Factor-Dependent Activation of the Src-Family Kinases. *Eur. J. Biochem.* **1994**, *225*, 1047–1053.

(115) Ward, W. H. J.; Cook, P. N.; Slater, A. M.; Davies, D. H.; Holdgate, G. A.; Green, L. R. Epidermal Growth Factor Receptor Tyrosine Kinase: Investigation of Catalytic Mechanism, Structure-Based Searching and Discovery of a Potent Inhibitor. *Biochem. Pharmacol.* **1994**, *48*, 659–666.

(116) Wahid, M.; Jawed, A.; Mandal, R. K.; Dar, S. A.; Khan, S.; Akhter, N.; Haque, S. Vismodegib, Itraconazole and Sonidegib as Hedgehog Pathway Inhibitors and Their Relative Competencies in the Treatment of Basal Cell Carcinomas. *Crit. Rev. Oncol. Hematol.* **2016**, *98*, 235–241.

(117) Medicine, N. U. S. N. L. of. A Study of the BRAF Inhibitor Dabrafenib in Combination With the MEK Inhibitor Trametinib in the Adjuvant Treatment of High-risk BRAF V600 Mutation-positive Melanoma After Surgical Resection. (COMBI-AD) https://clinicaltrials.gov/ct2/show/NCT01682083.

(118) Long, G. V.; Hauschild, A.; Santinami, M.; Atkinson, V.; Mandalà, M.; Chiarion-Sileni, V.; Larkin, J.; Nyakas, M.; Dutriaux, C.; Haydon, A.; *et al.* Adjuvant Dabrafenib plus Trametinib in Stage III *BRAF* -Mutated Melanoma. *N. Engl. J. Med.* **2017**, *377*, 1813–1823.

(119) Xue, Y.; Martelotto, L.; Baslan, T.; Vides, A.; Solomon, M.; Mai, T. T.; Chaudhary, N.; Riely, G. J.; Li, B. T.; Scott, K.; *et al.* An Approach to Suppress the Evolution of Resistance in BRAFV600E-Mutant Cancer. *Nat. Med.* **2017**, *23*.

(120) Palka, K. T.; Lebow, R. L.; Weaver, K. D.; Kressin, M. K. Major Response to Imatinib Mesylate in KIT-Mutated Melanoma. *J. Clin. Oncol.* **2008**, *26*, 2042–2046.

(121) Guo, J.; Si, L.; Kong, Y.; Flaherty, K. T.; Xu, X.; Zhu, Y.; Corless, C. L.; Li, L.; Li, H.; Sheng, X.; *et al.* Phase II, Open-Label, Single-Arm Trial of Imatinib Mesylate in Patients with Metastatic Melanoma Harboring c-Kit Mutation or Amplification. *J. Clin. Oncol.* **2011**, *29*, 2904–2909.

(122) Carvajal, R. D. KIT as a Therapeutic Target in Metastatic Melanoma. *Jama* **2011**, *305*, 2327.

(123) Flaherty, K. T.; Lee, S. J.; Zhao, F.; Schuchter, L. M.; Flaherty, L.; Kefford, R.; Atkins, M. B.; Leming, P.; Kirkwood, J. M. Phase III Trial of Carboplatin and Paclitaxel with or without Sorafenib in Metastatic Melanoma. *J. Clin. Oncol.* **2013**, *31*, 373–379.

(124) Kerbel, R. S. Tumor Angiogenesis. *N. Engl. J. Med.* **2008**, *358*, 2039–2049.

(125) Susman, E. Novel Agent Extends Breast Cancer Time to Progression https://www.medpagetoday.com/MeetingCoverage/SABCS/36306 (accessed May 2, 2018).

(126) Novartis. Novartis Kisqali® (ribociclib, LEE011) receives FDA approval as first-line treatment for HR+/HER2- metastatic breast cancer in combination with any aromatase inhibitor https://www.novartis.com/news/media-releases/novartis-kisqalir-ribociclib-lee011-receives-fda-approval-first-line-treatment (accessed May 2, 2018).

(127) Administration, U. S. F. and D. Press Announcements - FDA Approves New Treatment for Certain Advanced or Metastatic Breast Cancers. *FDA News Release* **2017**.

(128) Ashton, S.; Song, Y. H.; Nolan, J.; Cadogan, E.; Murray, J.; Odedra, R.; Foster, J.; Hall, P. A.; Low, S.; Taylor, P.; *et al.* Aurora Kinase Inhibitor Nanoparticles Target Tumors with Favorable Therapeutic Index in Vivo. *Sci. Transl. Med.* **2016**, *8*, 1–11.

(129) Wang, S.; Gao, R.; Zhou, F.; Selke, M. Nanomaterials and Singlet Oxygen Photosensitizers: Potential Applications in Photodynamic Therapy. *J. Mater. Chem.* **2004**, *14*, 487.

(130) Chen, T.; Shukoor, M. I.; Wang, R.; Zhao, Z.; Yuan, Q.; Bamrungsap, S.; Xiong, X.; Tan, W. Smart Multifunctional Nanostructure for Targeted Cancer Chemotherapy and Magnetic Resonance Imaging. *ACS Nano* **2011**, *5*, 7866–7873.

(131) Lim, E. K.; Jang, E.; Lee, K.; Haam, S.; Huh, Y. M. Delivery of Cancer Therapeutics Using Nanotechnology. *Pharmaceutics* **2013**, *5*, 294–317.

(132) Shoseyov, O.; Levy, I. *Nanobiotechnology: BioInspired Devices and Materials of the Future*; Humana Press: Totowa, New Jersey, 2008.

(133) Sun, T.; Zhang, Y. S.; Pang, B.; Hyun, D. C.; Yang, M.; Xia, Y. Engineered Nanoparticles for Drug Delivery in Cancer Therapy. *Angew. Chemie - Int. Ed.* **2014**, *53*, 12320–12364.

(134) Bechet, D.; Couleaud, P.; Frochot, C.; Viriot, M.-L.; Guillemin, F.; Barberi-Heyob, M. Nanoparticles as Vehicles for Delivery of Photodynamic Therapy Agents. *Trends Biotechnol.* **2008**, *26*, 612–621.

(135) van Straten, D.; Mashayekhi, V.; de Bruijn, H. S.; Oliveira, S.; Robinson, D. J. Oncologic Photodynamic Therapy: Basic Principles, Current Clinical Status and Future Directions. *Cancers (Basel).* **2017**, *9*, 1–54.

(136) Prow, T. W.; Grice, J. E.; Lin, L. L.; Faye, R.; Butler, M.; Becker, W.; Wurm, E. M. T.; Yoong, C.; Robertson, T. A.; Soyer, H. P.; *et al.* Nanoparticles and Microparticles for Skin Drug Delivery. *Adv. Drug Deliv. Rev.* **2011**, *63*, 470–491.

(137) New Zealand Datasheet-METVIX™.

(138) Chu, P. K.; Liu, X. *Biomaterials Fabrication and Processing Handbook*; CRC Press, 2008.

(139) Rosenholm, J.; Sahlgren, C.; Lindén, M. Cancer-Cell Targeting and Cell-Specific Delivery by Mesoporous Silica Nanoparticles. *J. Mater. Chem.* **2010**, *20*, 2707.

(140) He, Q.; Shi, J. MSN Anti-Cancer Nanomedicines: Chemotherapy Enhancement, Overcoming of Drug Resistance, and Metastasis Inhibition. *Adv. Mater.* **2014**, *26*, 391–411.

(141) Ma, X.; Qu, Q.; Zhao, Y. Targeted Delivery of 5-Aminolevulinic Acid by Multifunctional Hollow Mesoporous Silica Nanoparticles for Photodynamic Skin Cancer Therapy. *ACS Appl. Mater. Interfaces* **2015**, *7*, 10671–10676.

(142) Rizzi, M.; Tonello, S.; Estevão, B. M.; Gianotti, E.; Marchese, L.; Renò, F. Verteporfin Based Silica Nanoparticle for in Vitro Selective Inhibition of Human Highly Invasive Melanoma Cell Proliferation. *J. Photochem. Photobiol. B Biol.* **2017**, *167*, 1–6.

(143) Hoffmann, F.; Cornelius, M.; Morell, J.; Fröba, M. Silica-Based Mesoporous Organic-Inorganic Hybrid Materials. *Angew. Chemie - Int. Ed.* **2006**, *45*, 3216–3251.

(144) croissant, jonas; Cattoën, X.; Durand, J.-O.; Wong Chi Man, M.; Khashab, N. M. Organosilica Hybrid Nanomaterials with High Organic Content: Syntheses and Applications of Silsesquioxanes. *Nanoscale* **2016**, *8*, 19945–19972.

(145) Croissant, J.; Salles, D.; Maynadier, M.; Mongin, O.; Hugues, V.; Blanchard-desce, M.; Cattoe, X.; Wong, M.; Man, C.; Gallud, A.; *et al.* Mixed Periodic Mesoporous Organosilica Nanoparticles and Core − Shell Systems , Application to in Vitro Two-Photon Imaging , Therapy , and Drug Delivery. *Chem. Mater.* **2014**, *26*, 7214–7220.

(146) Mauriello-Jimenez, C.; Knezevic, N.; Galan-Rubio, Y.; Szunerits, S.; Boukherroub, R.; Teodorescu, F.; Croissant, J. G.; Hocine, O.; Seric, M.; Raehm, L.; *et al.* Core-Shell Nanodiamonds-Periodic Mesoporous Organosilica Nanoparticles for Two-Photon Imaging, Photodynamic Therapy and Synergistic PH-Responsive Drug Delivery. *J. Mater. Chem. B* **2016**.

(147) Danhier, F.; Feron, O.; Préat, V. To Exploit the Tumor Microenvironment: Passive and Active Tumor Targeting of Nanocarriers for Anti-Cancer Drug Delivery. *J. Control. Release* **2010**, *148*, 135–146.

(148) Záruba, K.; Králová, J.; Řezanka, P.; Poučková, P.; Veverková, L.; Král, V. Modified Porphyrin–brucine Conjugated to Gold Nanoparticles and Their Application in Photodynamic Therapy. *Org. Biomol. Chem.* **2010**, *8*, 3202.

(149) Haimov, E.; Weitman, H.; Polani, S.; Schori, H.; Zitoun, D.; Shefi, O. Meso-Tetrahydroxyphenylchlorin-Conjugated Gold Nanoparticles as a Tool To Improve Photodynamic Therapy. *ACS Appl. Mater. Interfaces* **2018**, *10*, 2319–2327.

(150) Tham, H. P.; Chen, H.; Tan, Y. H.; Qu, Q.; Sreejith, S.; Zhao, L.; Venkatraman, S. S.; Zhao, Y. Photosensitizer Anchored Gold Nanorods for Targeted Combinational Photothermal and Photodynamic Therapy. *Chem. Commun.* **2016**, *52*, 8854–8857.

(151) Vankayala, R.; Lin, C. C.; Kalluru, P.; Chiang, C. S.; Hwang, K. C. Gold Nanoshells-Mediated Bimodal Photodynamic and Photothermal Cancer Treatment Using Ultra-Low Doses of near Infra-Red Light. *Biomaterials* **2014**, *35*, 5527–5538.

(152) Gao, L.; Fei, J.; Zhao, J.; Li, H.; Cui, Y.; Li, J. Hypocrellin-Loaded Gold Nanocages with High Two-Photon Efficiency for Photothermal/Photodynamic Cancer Therapy in Vitro. *ACS Nano* **2012**, *6*, 8030–8040.

(153) Srivatsan, A.; Jenkins, S. V.; Jeon, M.; Wu, Z.; Kim, C.; Chen, J.; Pandey, R. K. Gold Nanocage-Photosensitizer Conjugates for Dual-Modal Image-Guided Enhanced Photodynamic Therapy. *Theranostics* **2014**, *4*, 163–174.

(154) Tada, D. B.; Vono, L. L. R.; Duarte, E. L.; Itri, R.; Kiyohara, P. K.; Baptista, S.; Rossi, L. M.; March, R. V; Final, I.; May, F. Methylene Blue-Containing Silica-Coated Magnetic Particles : A Potential Magnetic Carrier for Photodynamic Therapy. *Langmuir* **2007**, 8194–8199.

(155) Wang, D.; Fei, B.; Halig, L. V; Qin, X.; Hu, Z.; Xu, H.; Andrew Wang, Y.; Chen, Z.; Kim, S.; Shin, D. M.; *et al.* Targeted Iron-Oxide Nanoparticle for Photodynamic Therapy and Imaging of Head and Neck Cancer. *ACS Nano* **2014**, *8*, 6620–6632.

(156) Choi, K.-H.; Nam, K.; Kim, U.-H.; Cho, G.; Jung, J.-S.; Park, B. Optimized Photodynamic Therapy with Multifunctional Cobalt Magnetic Nanoparticles.

Nanomaterials **2017**, *7*, 144.

(157) Cui, S.; Yin, D.; Chen, Y.; Di, Y.; Chen, H.; Ma, Y.; Achilefu, S.; Gu, Y. In Vivo Targeted Deep-Tissue Photodynamic Therapy Based on near-Infrared Light Triggered Upconversion Nanoconstruct. *ACS Nano* **2013**, *7*, 676–688.

(158) Idris, N. M.; Gnanasammandhan, M. K.; Zhang, J.; Ho, P. C.; Mahendran, R.; Zhang, Y. In Vivo Photodynamic Therapy Using Upconversion Nanoparticles as Remote-Controlled Nanotransducers. *Nat. Med.* **2012**, *18*, 1580–1585.

(159) Punjabi, A.; Wu, X.; Tokatli-apollon, A.; El-rifai, M.; Lee, H. Amplifying the Red-Emission of Upconverting Nanoparticles for Biocompatible Clinically Used. *ACS Nano* **2014**, *8*, 10621–10630.

(160) Clapp, A. R.; Pons, T.; Medintz, I. L.; Delehanty, J. B.; Melinger, J. S.; Tiefenbrunn, T.; Dawson, P. E.; Fisher, B. R.; O'Rourke, B.; Mattoussi, H. Two-Photon Excitation of Quantum-Dot-Based Fluorescence Resonance Energy Transfer and Its Applications. *Adv. Mater.* **2007**, *19*, 1921–1926.

(161) and, C. Z.; Johnson*, L. W. Quantifying RNA−Peptide Interaction by Single-Quantum Dot-Based Nanosensor: An Approach for Drug Screening. *Anal. Chem.* **2007**, *79*, 7775–7781.

(162) Samia, A. C. S.; Dayal, S.; Burda, C. Quantum Dot-Based Energy Transfer: Perspectives and Potential for Applications in Photodynamic Therapy. *Photochem. Photobiol.* **2006**, *82*, 617.

(163) and, S. D.; Burda*, C. Semiconductor Quantum Dots as Two-Photon Sensitizers. *J. Am. Chem. Soc.* **2008**, *130*, 2890–2891.

(164) Samia, A. C. S.; Chen, X.; Burda, C. Semiconductor Quantum Dots for Photodynamic Therapy. *J. Am. Chem. Soc.* **2003**, *125*, 15736–15737.

(165) Tsay, J. M.; Trzoss, M.; Shi, L.; Kong, X.; Selke, M.; Jung, M. E.; Weiss, S. Singlet Oxygen Production by Peptide-Coated Quantum Dot-Photosensitizer Conjugates. *J. Am. Chem. Soc.* **2007**, *129*, 6865–6871.

(166) Hsieh, J.-M.; Ho, M.-L.; Wu, P.-W.; Chou, P.-T.; Tsai, T.-T.; Chi, Y. Iridium-Complex Modified CdSe/ZnS Quantum Dots; a Conceptual Design for Bi-Functionality toward Imaging and Photosensitization. *Chem. Commun. (Camb).* **2006**, *1*, 615–617.

(167) Shi, L.; Hernandez, B.; Selke, M. Singlet Oxygen Generation from Water-Soluble Quantum Dot − Organic Dye Nanocomposites Singlet Oxygen Generation from Water-Soluble Quantum Dot-Organic Dye. *J. Am. Chem. Soc. Commun.* **2006**, 9–11.

(168) de la Fuente, J. M.; Grazu, V. *Nanobiotechnology Inorganic Nanoparticles vs Organic Nanoparticles*; Jesus M. de la Fuente, V. G., Ed.; 2012.

(169) Konan, Y. N.; Cerny, R.; Favet, J.; Berton, M.; Gurny, R.; Allemann, E. Preparation and Characterization of Sterile Sub-200 Nm Meso-Tetra(4-Hydroxylphenyl)Porphyrin-Loaded Nanoparticles for Photodynamic Therapy. *Eur. J. Pharm. Biopharm.* **2003**, *55*, 115–124.

(170) Ricci-Júnior, E.; Marchetti, J. M. Preparation, Characterization, Photocytotoxicity Assay of PLGA Nanoparticles Containing Zinc (II) Phthalocyanine for Photodynamic Therapy Use. *J. Microencapsul.* **2006**, *23*, 523–538.

(171) Saxena, V.; Sadoqi, M.; Shao, J. Polymeric Nanoparticulate Delivery System for Indocyanine Green: Biodistribution in Healthy Mice. *Int. J. Pharm.* **2006**, *308*, 200–204.

(172) Zeisser-Labouèbe, M.; Lange, N.; Gurny, R.; Delie, F. Hypericin-Loaded Nanoparticles for the Photodynamic Treatment of Ovarian Cancer. *Int. J. Pharm.* **2006**, *326*, 174–181.

(173) Rijcken, C. J. F.; Hofman, J.-W.; Zeeland, F. Van; Hennink, W. E.; Van Nostrum, C. F.

Photosensitiser-Loaded Biodegradable Polymeric Micelles: Preparation, Characterisation and in Vitro PDT Efficacy. *J. Control. Release* **2007**, *124*, 144–153.

(174) Gibot, L.; Lemelle, A.; Till, U.; Moukarzel, B.; Oise Mingotaud, A.-F.; Pimienta, V.; Saint-Aguet, P.; Rols, M.-P.; Gaucher, M.; Violleau, F.; *et al.* Polymeric Micelles Encapsulating Photosensitizer: Structure/ Photodynamic Therapy Efficiency Relation. *Biomacromolecules* **2014**, *15*, 1443–1455.

(175) Yuan, A.; Tang, X.; Qiu, X.; Jiang, K.; Wu, J.; Hu, Y. Activatable Photodynamic Destruction of Cancer Cells by NIR Dye/Photosensitizer Loaded Liposomes. *Chem. Commun.* **2015**, *51*, 3340–3342.

(176) Liu, L.-H.; Zhang, Y.-H.; Qiu, W.-X.; Zhang, L.; Gao, F.; Li, B.; Xu, L.; Fan, J.-X.; Li, Z.-H.; Zhang, X.-Z. Dual-Stage Light Amplified Photodynamic Therapy against Hypoxic Tumor Based on an O_2 Self-Sufficient Nanoplatform. *Small* **2017**, 1701621.

(177) Huang, Z.; Huang, L.; Huang, Y.; He, Y.; Sun, X.; Fu, X.; Xu, X.; Wei, G.; Chen, D.; Zhao, C. Phthalocyanine-Based Coordination Polymer Nanoparticles for Enhanced Photodynamic Therapy. *Nanoscale* **2017**, *9*, 15883–15894.

(178) Kim, J.; Santos, O. A.; Park, J. H. Selective Photosensitizer Delivery into Plasma Membrane for Effective Photodynamic Therapy. *J. Control. Release* **2014**, *191*, 98–104.

(179) Pierre, M. B. R.; Tedesco, A. C.; Marchetti, J. M.; Bentley, M. V. L. Stratum Corneum Lipids Liposomes for the Topical Delivery of 5-Aminolevulinic Acid in Photodynamic Therapy of Skin Cancer: Preparation and in Vitro Permeation Study. *BMC Dermatol.* **2001**, *1*, 1.

(180) Oh, E. K.; Jin, S. E.; Kim, J. K.; Park, J. S.; Park, Y.; Kim, C. K. Retained Topical Delivery of 5-Aminolevulinic Acid Using Cationic Ultradeformable Liposomes for Photodynamic Therapy. *Eur. J. Pharm. Sci.* **2011**, *44*, 149–157.

(181) KOTLA, N. G.; Chandrasekar, B.; Rooney, P.; Gandhi, S.; Larrañaga, A.; Kanala, V. K.; Pandit, A.; Rochev, Y. A. Biomimetic Lipid-Based Nanosystems for Enhanced Dermal Delivery of Drugs and Bioactive Agents. *ACS Biomater. Sci. Eng.* **2017**, acsbiomaterials.6b00681.

(182) Klajnert, B.; Rozanek, M.; Bryszewska, M. Dendrimers in Photodynamic Therapy. *Curr. Med. Chem.* **2012**, *19*, 4903–4912.

(183) Taratula, O.; Schumann, C.; Naleway, M. A.; Pang, A. J.; Chon, K. J.; Taratula, O. A Multifunctional Theranostic Platform Based on Phthalocyanine- Loaded Dendrimer for Image-Guided Drug Delivery and Photodynamic Therapy. *Mol. Pharm.* **2013**, *10*, 3946−3958.

(184) Taratula, O.; Schumann, C.; Duong, T.; Taylor, K. L.; Taratula, O. Dendrimer-Encapsulated Naphthalocyanine as a Single Agent-Based Theranostic Nanoplatform for near-Infrared Fluorescence Imaging and Combinatorial Anticancer Phototherapy. *Nanoscale* **2015**, 3888–3902.

(185) Jang, W.-D.; Nakagishi, Y.; Nishiyama, N.; Kawauchi, S.; Morimoto, Y.; Kikuchi, M.; Kataoka, K. Polyion Complex Micelles for Photodynamic Therapy: Incorporation of Dendritic Photosensitizer Excitable at Long Wavelength Relevant to Improved Tissue-Penetrating Property. *J. Control. Release* **2006**, *12*, 73–79.

(186) Gluth, M. B.; Kaufmann, Y. C.; Dornhoffer, J. L.; Ferguson, S. Immunotargeted Photodynamic Therapy for Cholesteatoma. *Otol. Neurotol.* **2014**, *36*, 1.

(187) Bae, B. chan; Na, K. Self-Quenching Polysaccharide-Based Nanogels of Pullulan/Folate-Photosensitizer Conjugates for Photodynamic Therapy. *Biomaterials* **2010**, *31*, 6325–6335.

(188) Yadav, S. C.; Kumari, A.; Yadav, R. Development of Peptide and Protein Nanotherapeutics by Nanoencapsulation and Nanobioconjugation. *Peptides* **2011**, *32*,

173–187.

(189) Grainger, D. W. Controlled-Release and Local Delivery of Therapeutic Antibodies. *Expert Opin. Biol. Ther.* **2004**, *4*, 1029–1044.

(190) Pérez-Martínez, D.; Tanaka, T.; Rabbitts, T. H. Intracellular Antibodies and Cancer: New Technologies Offer Therapeutic Opportunities. *BioEssays* **2010**, *32*, 589–598.

(191) Sousa, F.; Castro, P.; Fonte, P.; Kennedy, P. J.; Neves-Petersen, M. T.; Sarmento, B. Nanoparticles for the Delivery of Therapeutic Antibodies: Dogma or Promising Strategy? *Expert Opin. Drug Deliv.* **2017**, *14*, 1163–1176.

(192) Srinivasan, A. R.; Lakshmikuttyamma, A.; Shoyele, S. A. Investigation of the Stability and Cellular Uptake of Self-Associated Monoclonal Antibody (MAb) Nanoparticles by Non-Small Lung Cancer Cells. *Mol. Pharm.* **2013**, *10*, 3275−3284.

(193) Yildirimer, L.; Thanh, N. T. K.; Loizidou, M.; Seifalian, A. M. Toxicological Considerations of Clinically Applicable Nanoparticles. *Nano Today* **2011**, *6*, 585–607.

(194) Son, S.; Lee, W. R.; Joung, Y. K.; Kwon, M. H.; Kim, Y. S.; Park, K. D. Optimized Stability Retention of a Monoclonal Antibody in the PLGA Nanoparticles. *Int. J. Pharm.* **2009**, *368*, 178–185.

(195) Gao, L.; Han, L.; Ding, X.; Xu, J.; Wang, J.; Zhu, J.; Lu, W.; Sun, J.; Yu, L.; Yan, Z.; *et al.* An Effective Intracellular Delivery System of Monoclonal Antibody for Treatment of Tumors: Erythrocyte Membrane-Coated Self-Associated Antibody Nanoparticles. *Nanotechnology* **2017**, *28*.

(196) Cui, N.; Zhu, S.-H. Monoclonal Antibody-Tagged Polyethylenimine (PEI)/Poly(Lactide) (PLA) Nanoparticles for the Enhanced Delivery of Doxorubicin in HER-Positive Breast Cancers. *RSC Adv.* **2016**, *6*, 79822.

(197) Dinauer, N.; Balthasar, S.; Weber, C.; Kreuter, J.; Langer, K.; Briesen, H. von. Selective Targeting of Antibody-Conjugated Nanoparticles to Leukemic Cells and Primary T-Lymphocytes. *Biomaterials* **2005**, *26*, 5898–5906.

(198) Marslin, G.; Sheeba, C. J.; Kalaichelvan, V. K.; Manavalan, R.; Neelakanta Reddy, P.; Franklin, G. Poly(D,L-Lactic-Co-Glycolic Acid) Nanoencapsulation Reduces Erlotinib-Induced Subacute Toxicity in Rat. *J. Biomed. Nanotechnol.* **2009**, *5*, 464–471.

(199) Spring, B. Q.; Bryan Sears, R.; Zheng, L. Z.; Mai, Z.; Watanabe, R.; Sherwood, M. E.; Schoenfeld, D. A.; Pogue, B. W.; Pereira, S. P.; Villa, E.; *et al.* A Photoactivable Multi-Inhibitor Nanoliposome for Tumour Control and Simultaneous Inhibition of Treatment Escape Pathways. *Nat. Nanotechnol.* **2016**, *11*, 378–387.

(200) Kuruppu, A. I.; Zhang, L.; Collins, H.; Turyanska, L.; Thomas, N. R.; Bradshaw, T. D. An Apoferritin-Based Drug Delivery System for the Tyrosine Kinase Inhibitor Gefitinib. *Adv. Healthc. Mater.* **2015**, n/a-n/a.

(201) Trummer, B. J.; Iyer, V.; Balu-lyer, S. V.; O'Connor, R.; Straubinger, R. M. Physicochemical Properties of EGF Receptor Inhibitors and Development of a Nanoliposomal Formulation of Gefitinib. *J. Pharm. Sci.* **2012**, *101*, 2763–2776.

(202) Sarkar, S.; Konar, S.; Prasad, P. N.; Rajput, S.; Prashanth Kumar, B. N.; Rao, R. R.; Pathak, A.; Fisher, P. B.; Mandal, M. Micellear Gold Nanoparticles as Delivery Vehicles for Dual Tyrosine Kinase Inhibitor ZD6474 for Metastatic Breast Cancer Treatment. *Langmuir* **2017**, *33*, 7649–7659.

(203) Mizrachi, A.; Shamay, Y.; Shah, J.; Brook, S.; Soong, J.; Rajasekhar, V. K.; Humm, J. L.; Healey, J. H.; Powell, S. N.; Baselga, J.; *et al.* Tumour-Specific PI3K Inhibition via Nanoparticle- Targeted Delivery in Head and Neck Squamous Cell Carcinoma. *Nat. Commun.* **2017**, *8*, 14292.

(204) Candido G Da Silva, Richard J Honeywell, H. D. & G. J. P. Physicochemical Properties of Novel Protein Kinase Inhibitors in Relation to Their Substrate Specificity for Drug

Transporters. *Expert Opin. Drug Metab. Toxicol.* **2015**, *11*, 703–717.

(205) Au, K. M.; Min, Y.; Tian, X.; Zhang, L.; Perello, V.; Caster, J. M.; Wang, A. Z. Improving Cancer Chemoradiotherapy Treatment by Dual Controlled Release of Wortmannin and Docetaxel in Polymeric Nanoparticles. *ACS Nano* **2015**, *9*, 8976–8996.

(206) Morton, S. W.; Lee, M. J.; Deng, Z. J.; Dreaden, E. C.; Siouve, E.; Shopsowitz, K. E.; Shah, N. J.; Yaffe, M. B.; Hammond, P. T. A Nanoparticle-Based Combination Chemotherapy Delivery System for Enhanced Tumor Killing by Dynamic Rewiring of Signaling Pathways. *Sci. Signal.* **2014**, *7*, ra44-ra44.

(207) Wikipedia. Human skin https://en.wikipedia.org/wiki/Human_skin.

(208) D'Orazio, J.; Jarrett, S.; Amaro-Ortiz, A.; Scott, T. UV Radiation and the Skin. *Int. J. Mol. Sci.* **2013**, *14*, 12222–12248.

(209) Proksch, E.; Brandner, J. M.; Jensen, J.-M. The Skin: An Indispensable Barrier. *Exp. Dermatol.* **2008**, *17*, 1063–1072.

(210) Fuchs, E. Scratching the Surface of Skin Development. *Nature* **2007**, *445*, 834–842.

(211) Madison, K. C. Barrier Function of the Skin: "La Raison d'être" of the Epidermis. *J. Invest. Dermatol.* **2003**, *121*, 231–241.

(212) Elias, P. M.; Friend, D. S. The Permeability Barrier in Mammalian Epidermis. *J. Cell Biol.* **1975**, *19*, 180–191.

(213) Lademann, J.; Richter, H.; Teichmann, A.; Otberg, N.; Blume-Peytavi, U.; Luengo, J.; Weiß, B.; Schaefer, U. F.; Lehr, C. M.; Wepf, R.; *et al.* Nanoparticles - An Efficient Carrier for Drug Delivery into the Hair Follicles. *Eur. J. Pharm. Biopharm.* **2007**, *66*, 159–164.

(214) Bolzinger, M. A.; Briançon, S.; Pelletier, J.; Chevalier, Y. Penetration of Drugs through Skin, a Complex Rate-Controlling Membrane. *Curr. Opin. Colloid Interface Sci.* **2012**, *17*, 156–165.

(215) Alexander, A.; Dwivedi, S.; Giri, T. K.; Saraf, S.; Saraf, S.; Krishna, D. Approaches for Breaking the Barriers of Drug Permeation through Transdermal Drug Delivery. *J. Control. Release* **2012**, *164*, 26–40.

(216) Guy, R. H. Transdermal Drug Delivery. *Nat. Biotechnol.* **2010**, *26*, 399–410.

(217) Morton, C. A.; Braathen, L. R. Update on Topical Photodynamic Therapy for Skin Cancer. *Вестник дерматологии и венерологии* **2014**, 26–34.

(218) Dragicevic-Curic, N.; Gräfe, S.; Gitter, B.; Winter, S.; Fahr, A. Surface Charged Temoporfin-Loaded Flexible Vesicles: In Vitro Skin Penetration Studies and Stability. *Int. J. Pharm.* **2010**, *384*, 100–108.

(219) Fadel, M.; Samy, N.; Nasr, M.; Alyoussef, A. A. Topical Colloidal Indocyanine Green-Mediated Photodynamic Therapy for Treatment of Basal Cell Carcinoma. *Pharm. Dev. Technol.* **2016**, *7450*, 1–6.

(220) Bragagni, M.; Scozzafava, A.; Mastrolorenzo, A.; Supuran, C. T.; Mura, P. Development and Ex Vivo Evaluation of 5-Aminolevulinic Acid-Loaded Niosomal Formulations for Topical Photodynamic Therapy. *Int. J. Pharm.* **2015**, *494*, 258–263.

(221) Garg, B. J.; Garg, N. K.; Beg, S.; Singh, B.; Katare, O. P. Nanosized Ethosomes-Based Hydrogel Formulations of Methoxsalen for Enhanced Topical Delivery against Vitiligo: Formulation Optimization, *in Vitro* Evaluation and Preclinical Assessment. *J. Drug Target.* **2016**, *24*, 233–246.

(222) Zhang, Z.; Chen, Y.; Xu, H.; Wo, Y.; Zhang, Z.; Liu, Y.; Su, W.; Cui, D.; Zhang, Y. 5-Aminolevulinic Acid Loaded Ethosomal Vesicles with High Entrapment Efficiency for in Vitro Topical Transdermal Delivery and Photodynamic Therapy of Hypertrophic

Scars. *Nanoscale* **2016**.

(223) Silva Garcia Praca, F.; Silva Garcia Medina, W.; Petrilli, R.; Vitoria Lopes Badra Bentley, M. Liquid Crystal Nanodispersions Enable the Cutaneous Delivery of Photosensitizer for Topical PDT: Fluorescence Microscopy Study of Skin Penetration. *Curr. Nanosci.* **2012**, *8*, 535–540.

(224) Cristina Rossetti, F.; Biagini Lopes, L.; Regina Carollo, A. H.; Thomazini, J. A.; Cláudio Tedesco, A.; Vitória Lopes Badra Bentley, M. A Delivery System to Avoid Self-Aggregation and to Improve in Vitro and in Vivo Skin Delivery of a Phthalocyanine Derivative Used in the Photodynamic Therapy. *J. Control. Release* **2011**, *155*, 400–408.

(225) Shi, L.; Wang, X.; Zhao, F.; Luan, H.; Tu, Q.; Huang, Z.; Wang, H.; Wang, H. In Vitro Evaluation of 5-Aminolevulinic Acid (ALA) Loaded PLGA Nanoparticles. *Int. J. Nanomedicine* **2013**, *8*, 2669–2676.

(226) Fang, J.-Y.; Zhang, S. A.; Al-Suwayeh, C.-F.; Hung, C.-C.; Chen, J.-Y. Oil Components Modulate the Skin Delivery of 5-Aminolevulinic Acid and Its Ester Prodrug from Oil-in-Water and Water-in-Oil Nanoemulsions. *Int. J. Nanomedicine* **2011**, *6*, 693.

(227) Qidwai, A.; Khan, S.; Md, S.; Fazil, M.; Baboota, S.; Narang, J. K.; Ali, J. Nanostructured Lipid Carrier in Photodynamic Therapy for the Treatment of Basal-Cell Carcinoma. *Drug Deliv.* **2016**, *23*, 1071–7544.

(228) Beack, S.; Kong, W. H.; Jung, H. S.; Do, I. H.; Han, S.; Kim, H.; Kim, K. S.; Yun, S. H.; Hahn, S. K. Photodynamic Therapy of Melanoma Skin Cancer Using Carbon Dot â€“ Chlorin E6 â€“ Hyaluronate Conjugate. *Acta Biomater.* **2015**, *26*, 295–305.

(229) Bos, J. D.; Meinardi, M. M. H. M. The 500 Dalton Rule for the Skin Penetration of Chemical Compounds and Drugs. *Exp. Dermatol.* **2000**, *9*, 165–169.

(230) Santus, G. C.; Baker, R. W. Transdermal Enhancer Patent Literature. *J. Control. Release* **1993**, *25*, 1–20.

(231) Goates, C. Y.; Knutson, K. Enhanced Permeation of Polar Compounds through Human Epidermis. I. Permeability and Membrane Structural Changes in the Presence of Short Chain Alcohols. *Biochim. Biophys. Acta - Biomembr.* **1994**, *1195*, 169–179.

(232) Sugibayashi K; Nakayama S; Seki T; Hosoya K; Morimoto Y. Mechanism of Skin Penetration-Enhancing Effect by Laurocapram. *J. Pharm. Sci.* **1992**, *81*, 58–64.

(233) Kandimalla K; Kanikkannan N; Andega S; Singh M. Effect of Fatty Acids on the Permeation of Melatonin across Rat and Pig Skin In-Vitro and on the Transepidermal Water Loss in Rats in-Vivo. *J. Pharm. Pharmacol.* **1999**, *51*, 783–790.

(234) Parry GE; Bunge AL; Silcox GD; Pershing LK; Pershing DW. Percutaneous Absorption of Benzoic Acid across Human Skin. I. In Vitro Experiments and Mathematical Modeling. *Pharm. Res.* **1990**, *7*, 230–236.

(235) Cornwell, P. A.; Barry, B. W.; Bouwstra, J. A.; Gooris, G. S. Modes of Action of Terpene Penetration Enhancers in Human Skin; Differential Scanning Calorimetry, Small-Angle X-Ray Diffraction and Enhancer Uptake Studies. *Int. J. Pharm.* **1996**, *127*, 9–26.

(236) Yamane, M. A.; Williams, A. C.; Barry, B. W. Effects of Terpenes and Oleic Acid as Skin Penetration Enhancers towards 5-Fluorouracil as Assessed with Time; Permeation, Partitioning and Differential Scanning Calorimetry. *Int. J. Pharm.* **1995**, *116*, 237–251.

(237) Elias, P. M.; Tsai, J.; Menon, G. K.; Holleran, W. M.; Feingold, K. R. The Potential of Metabolic Interventions to Enhance Transdermal Drug Delivery. *J. Investig. Dermatology Symp. Proc.* **2002**, *7*, 79–85.

(238) Guy, R. Iontophoresis--Recent Developments. *J. Pharm. Pharmacol. Pharmacol.* **1998**,

50, 371–374.

(239) Mitragotri, S.; Edwards, D. A.; Blankschtein, D.; Hnger, R. A Mechanistic Study of Ultrasonically-Enhanced Transdermal Drug Delivery. *J. Pharm. Sci.* **1995**, *84*, 697–706.

(240) McAllister, D. V.; Allen, M. G.; Prausnitz, M. R. Microfabricated Microneedles for Gene and Drug Delivery. *Annu. Rev. Biomed. Eng.* **2000**, *2*, 289–313.

(241) Prausnitz, M. R. A Practical Assessment of Transdermal Drug Delivery by Skin Electroporation. *Adv. Drug Deliv. Rev.* **1999**, *35*, 61–76.

(242) Gill, H. S.; Denson, D. D.; Burris, B. A.; Prausnitz, M. R. Effect of Microneedle Design on Pain in Human Subjects. *Clin. J. Pain* **2008**, *24*, 585–594.

(243) Oberli, M. A.; Schoellhammer, C. M.; Langer, R.; Blankschtein, D. Ultrasound-Enhanced Transdermal Delivery: Recent Advances and Future Challenges Transdermal Drug Delivery.

(244) Khan, A.; Yasir, M.; Asif, M.; Chauhan, I.; Singh, A. P.; Sharma, R.; Singh, P.; Rai, S. Iontophoretic Drug Delivery: History and Applications. *J. Appl. Pharm. Sci.* **2011**, *01*, 11–24.

(245) Ita, K. Perspectives on Transdermal Electroporation. *Pharmaceutics* **2016**, *8*.

(246) Alzeer, J.; Roth, P. J. C.; Luedtke, N. W. An Efficient Two-Step Synthesis of Metal-Free Phthalocyanines Using a Zn(Ii) Template. *Chem. Commun.* **2009**, 1970.

(247) Chou, T.-C.; Talalay, P. Quantitative Analysis of Dose-Effect Relationships: The Combined Effects of Multiple Drugs or Enzyme Inhibitors. *Adv. Enzyme Regul.* **1984**, *22*, 27–55.

(248) Martin, N.; Chou, T.-C. CompuSyn software for drug combinations and for general dose-effect analysis, and user's guide http://www.combosyn.com/Content2012/Users Guide.pdf.

(249) Fujiwara, M.; Akiyama, M.; Hata, M.; Shiokawa, K.; Nomura, R. Photo Induced Acceleration of Effluent Rate of Developing Solvents in Azobenzene Tethered Silica Gel. *ACS Nano* **2008**, *2*, 1671–1681.

(250) Mizoshita, N.; Tani, T.; Inagaki, S. Syntheses, Properties and Applications of Periodic Mesoporous Organosilicas Prepared from Bridged Organosilane Precursors. *Chem. Soc. Rev.* **2011**, *40*, 789–800.

(251) Yamada, H.; Urata, C.; Aoyama, Y.; Osada, S.; Yamauchi, Y.; Kuroda, K. Preparation of Colloidal Mesoporous Silica Nanoparticles with Different Diameters and Their Unique Degradation Behavior in Static Aqueous Systems. *Chem. Mater.* **2012**, *24*, 1462–1471.

(252) Ali, H.; van Lier, J. E. Metal Complexes as Photo- and Radiosensitizers. *Chem. Rev.* **1999**, *99*, 2379–2450.

(253) Lindig, B. A.; Rodgers, M. A. J.; Schaap, A. P. Determination of the Lifetime of Singlet Oxygen in D20 Using 9,10-Anthracenedipropionic Acid, a Water-Soluble Probe. *J. Am. Chem. Soc.* **1980**, *102*, 5590–5593.

(254) Potenza, M. A. C.; Sanvito, T.; Argentiere, S.; Cella, C.; Paroli, B.; Lenardi, C.; Milani, P. Single Particle Optical Extinction and Scattering Allows Real Time Quantitative Characterization of Drug Payload and Degradation of Polymeric Nanoparticles. *Sci. Rep.* **2015**, *5*, 1–9.

(255) Bhattacharjee, S. Review Article DLS and Zeta Potential – What They Are and What They Are Not ? *J. Control. Release* **2016**, *235*, 337–351.

(256) Zhu, Y.-X.; Jia, H.-R.; Chen, Z.; Wu, F.-G. Photosensitizer (PS)/Polyhedral Oligomeric Silsesquioxane (POSS)-Crosslinked Nanohybrids for Enhanced Imaging-Guided

Photodynamic Cancer Therapy. *Nanoscale* **2017**.

(257) Amat-Guerri, F.; Lempe, E.; Lissi, E. A.; Rodriguez, F. J.; Trull, F. R. Water-Soluble 1,3-Diphenylisobenzofuran Derivatives. Synthesis and Evaluation as Singlet Molecular Oxygen Acceptors for Biological Systems. *J. Photochem. Photobiol. A Chem.* **1996**, *93*, 49–56.

(258) Nakamura, T.; Son, A.; Umehara, Y.; Ito, T.; Kurihara, R.; Ikemura, Y.; Tanabe, K. Confined Singlet Oxygen in Mesoporous Silica Nanoparticles: Selective Photochemical Oxidation of Small Molecules in Living Cells. *Bioconjug. Chem.* **2016**, *27*, 1058–1066.

(259) Hayashi, K.; Maruhashi, T.; Nakamura, M.; Sakamoto, W.; Yogo, T. One-Pot Synthesis of Dual Stimulus-Responsive Degradable Hollow Hybrid Nanoparticles for Image-Guided Trimodal Therapy. *Adv. Funct. Mater.* **2016**, *26*, 8613–8622.

(260) Pauly, T. R.; Liu, Y.; Pinnavaia, T. J.; Billinge, S. J. L.; Rieker, T. P. Textural Mesoporosity and the Catalytic Activity of Mesoporous Molecular Sieves with Wormhole Framework Structures. *J. Am. Chem. Soc.* **1999**, *121*, 8835–8842.

(261) Roh, M. R.; Kim, J. M.; Lee, S. H.; Jang, H. S.; Park, K. H.; Chung, K. Y.; Rha, S. Y. Low-Concentration Vemurafenib Induces the Proliferation and Invasion of Human HaCaT Keratinocytes through Mitogen-Activated Protein Kinase Pathway Activation. *J. Dermatol.* **2015**, *42*, 881–888.

(262) Chertok, B.; Langer, R.; Anderson, D. G. Cutaneous Wound Healing through Paradoxical MAPK Activation by BRAF Inhibitors. *Nat. Commun.* **2016**, *7*, 12348.

(263) Schübbe, S.; Schumann, C.; Cavelius, C.; Koch, M.; Müller, T.; Kraegeloh, A. Size-Dependent Localization and Quantitative Evaluation of the Intracellular Migration of Silica Nanoparticles in Caco-2 Cells. *Chem. Mater.* **2012**, *24*, 914–923.

(264) Shang, L.; Nienhaus, K.; Nienhaus, G. Engineered Nanoparticles Intercating With Cells: Size Matters. *J Nanobiotechnology* **2014**, *12*, 3155–3170.

(265) Liu, L.; Xie, H.; Chen, X.; Shi, W.; Xiao, X.; Lei, D.; Li, J. Differential Response of Normal Human Epidermal Keratinocytes and HaCaT Cells to Hydrogen Peroxide-Induced Oxidative Stress. *Clin. Exp. Dermatol.* **2012**, *37*, 772–780.

(266) Tapajós, E. C. C.; Longo, J. P.; Simioni, A. R.; Lacava, Z. G. M.; Santos, M. F. M. A.; Morais, P. C.; Tedesco, A. C.; Azevedo, R. B. In Vitro Photodynamic Therapy on Human Oral Keratinocytes Using Chloroaluminum-Phthalocyanine. *Oral Oncol.* **2008**, *44*, 1073–1079.

(267) Sigma-Aldrich, I. *Caspase 3 Assay Kit, Colorimetric*.

(268) Friedrich, J.; Eder, W.; Castaneda, J.; Doss, M.; Huber, E.; Ebner, R.; Kunz-Schughart, L. A. A Reliable Tool to Determine Cell Viability in Complex 3-d Culture: The Acid Phosphatase Assay. *J. Biomol. Screen.* **2007**, *12*, 925–937.

(269) Jin, S.; Ma, X.; Ma, H.; Zheng, K.; Liu, J.; Hou, S.; Meng, J.; Wang, P. C.; Wu, X.; Liang, X.-J. Surface Chemistry-Mediated Penetration and Gold Nanorod Thermotherapy in Multicellular Tumor Spheroids. *Nanoscale* **2013**, *5*, 143–146.

(270) Schmook, F. P.; Meingassner, J. G.; Billich, A. Comparison of Human Skin or Epidermis Models with Human and Animal Skin in in Vitro Percutaneous Absorption. *Int. J. Pharm.* **2001**, *215*, 51–56.

(271) Li, L.; Song, L.; Yang, X.; Li, X.; Wu, Y.; He, T.; Wang, N.; Yang, S.; Zeng, Y.; Yang, L.; *et al.* Multifunctional " Core-Shell " Nanoparticles-Based Gene Delivery for Treatment of Aggressive Melanoma. *Biomaterials* **2016**, *111*, 124–137.

(272) Franklin, M.; Wild, R. Combination Cancer Therapy Comprising Administration of an EGFR Inhibitor and an IGF-1R Inhibitor. US 2012/0064072 A1, 2012.